NASA Technical Paper 2506

AVSCOM Technical Report 85-B-3

1986

Aerodynamic Characteristics of Several Current Helicopter Tail Boom Cross Sections Including the Effect of Spoilers

John C. Wilson
and Henry L. Kelley

Aerostructures Directorate
USAARTA-AVSCOM
Langley Research Center
Hampton, Virginia

National Aeronautics
and Space Administration

Scientific and Technical Information Branch

Summary

Single-rotor helicopters experience significant aerodynamic loading on the tail boom in hovering and low-speed flight. Major sources of the boom loads are induced aerodynamic effects from the main and tail rotors and crosswinds. Complexity of the flow field has precluded satisfactory analytical models of the boom loads, and a scarcity of experimental aerodynamic data exists for cross-sectional shapes typical of helicopter tail booms. Consequently, a wind-tunnel investigation was conducted in the Langley 4- by 7-Meter Tunnel on three representative helicopter tail boom shapes (those of the AH-64, UH-60, and UH-1H). Two-dimensional aerodynamic forces and pressure distributions were obtained with large-scale models of the cross sections for a flow incidence range from $-45°$ to $90°$ and a dynamic pressure range from 1.5 to 50 psf. The effects of protuberances such as tail rotor drive-shaft covers and spoilers were investigated. Of the tail boom shapes tested, the circular cross section without the drive-shaft cover had the least aerodynamic side force. Addition of the shaft cover to each shape changed side-force and vertical-force characteristics significantly. The addition of spoilers to the booms at selected locations shifted the side force in a favorable direction over a wide range of flow angles. Consequently, there is a potential for reducing the amount of directional control required in hover and sideward flight through a reduction in tail rotor thrust required. Although the spoiler increases down load, the net effect is an improvement in helicopter performance.

Introduction

Helicopters experience significant aerodynamic loading on the tail assembly and fuselage during hovering and low-speed flight because of combinations of wind speed, maneuvers, and downwash from the main rotor (ref. 1). Aerodynamic loading on the tail boom is of particular interest because it is subjected to the highest rotor wake velocities and to varying flow angles. The down load must be offset by thrust from the main rotor and a corresponding reduction of payload. Sideward loading of the tail boom can increase the thrust required of the tail rotor in the direction which produces a yawing moment that adds to main rotor torque. Since the forces and moments from the tail boom loads must be balanced by tilting of the tip path plane of the main rotor and/or by additional tail rotor thrust, the result is a reduction in payload and yaw-control margin.

Little consideration is given for tail boom effects in the prediction of aerodynamic loads for low flight speeds, and there is a scarcity of two-dimensional data for typical tail boom cross sections to implement such analyses.

Previous investigations of two-dimensional cylinders of various cross sections have demonstrated the sensitivity of aerodynamic characteristics to viscous effects (as characterized by Reynolds number) and flow incidence (refs. 2 through 7). The effects have not been amenable to analytical definition, as was demonstrated in attempts to correlate theory with experiments (ref. 3). Current analytical techniques, such as vortex sheet representation (ref. 8) of helicopter fuselage shapes, still require development and correlation with experiments for the prediction of fuselage loads at low flight speeds. Experimental investigations have been conducted on many cross-sectional shapes typical of fixed-wing aircraft. None of these tests or analyses have dealt with the typical helicopter tail boom cross section that has a unique protuberance introduced by the tail rotor drive-shaft cover.

Since there are insufficient data available for the understanding of air loads on helicopter tail booms, an experimental study was undertaken of two-dimensional cross-sectional shapes of three typical current U.S. Army helicopter tail booms (those of the AH-64, UH-60, and UH-1H, which together constitute the bulk of the U.S. Army helicopter fleet). Air loads and pressure distributions were measured for the effects of shape (including tail rotor drive-shaft cover on and off, and spoilers on and off), flow incidence, and dynamic pressure. The investigation was made in the Langley 4- by 7-Meter Tunnel over a range of dynamic pressure from 1.5 to 50 psf and a range of flow incidence from $-45°$ to $90°$.

Symbols

The aerodynamic data and angle of flow incidence are referenced to the body axis system, as shown in figure 1. Section coefficients c_y and c_z and Reynolds number R are referenced to dimensions customarily used, as indicated in references 2 through 7.

b	maximum width of cylinder normal to flow at zero flow angle, ft
C_p	pressure coefficient, $\frac{\text{(Local static pressure)}-\text{(Free-stream static pressure)}}{q}$
c	maximum depth of cylinder parallel to flow at zero flow angle, ft
c_y	section side-force coefficient, $\frac{\text{Side force per unit length}}{bq}$
c_z	section drag-force coefficient, $\frac{\text{Longitudinal force per unit length}}{bq}$

q	dynamic pressure, $\rho V^2/2$, psf
R	Reynolds number, $\rho V c/\mu$
R_{mr}	radius of main rotor, ft
r	distance of fuselage station from main rotor hub, ft
V	free-stream velocity, ft/sec
y	cross-sectional lateral coordinate, in.
z	cross-sectional vertical coordinate, in.
μ	viscosity, slugs/ft-sec
ρ	free-stream air density, slugs/ft^3
ϕ	angle of flow incidence in plane normal to axis of two-dimensional cylinder, deg
ψ_1	pressure port location on tail boom, deg
ψ_2	pressure port location on tail rotor drive-shaft cover, deg

Abbreviations:

S	spoiler configuration (see table I)
TRSC	tail rotor drive-shaft cover

Models and Apparatus

Three two-dimensional models having cross-sectional shapes representative of the tail boom designs of a majority of current U.S. Army helicopters were tested. Included were the boom shapes of an attack helicopter (AH-64), a utility tactical transport helicopter (UH-60), and a utility helicopter (UH-1H). Each shape represented, at reduced size (approximately 50 percent for the UH-60 and AH-64 and 82 percent for the UH-1H), the cross section at a station approximately 80 percent of the rotor radius behind the main rotor shaft (the location where near-maximum rotor wake velocities are generally experienced in hover). The dimensions and shapes are described in figure 2 for each cross section. Table II provides the coordinates of the shapes. Comparisons of the relative size of the cross sections at model and full scale are given in figure 3. The AH-64 configuration is circular when the tail rotor drive-shaft cover is removed. The other two configurations are roughly oval with large corner radii and, though symmetric about the z-axis, are nonsymmetric about the y-axis even when the tail rotor drive-shaft covers are removed.

The models were constructed of aluminum sheet metal attached to aluminum bulkheads with flush screws. The shapes were held within ±0.08 in. of true contour. The contours and surface smoothness are representative of full-scale helicopter tail booms, though without the customary protruding rivet heads. Table I lists 1- and 2-in-high aluminum spoilers, attached as shown in figure 2, that were used for some tests. The spoilers were attached only when the tail rotor drive-shaft covers were installed. These spoilers were positioned by judgment based on pressure distribution data obtained in preliminary testing.

A photograph of the installation in the Langley 4- by 7-Meter Tunnel is shown in figure 4. The arrangement of cylindrical components and balance is described in figure 5. The upper and lower cylindrical segments were attached rigidly to a center strut. The middle segment was the metric component, and it was attached to a strain-gauge balance (measuring the force and moment), which in turn was attached to the center strut. The center strut was attached to a model mounting support below the tunnel floor that could be rotated to vary angle of flow incidence. Also, pressure-measuring ports were located on the surface of the metric component in a plane perpendicular to the cylinder axis. The locations of the ports are indicated by tick marks in figure 2.

Large-diameter (48 in.) end plates were attached to the top and bottom segments to help ensure that two-dimensional flow would be achieved on the metric section (fig. 5).

Tests

The cylinders were tested at constant flow incidence angles over a range of dynamic pressure; hence, data were obtained over a range of Reynolds number. Also, tests were made at constant dynamic pressure (i.e., approximately constant flow velocity and constant Reynolds number) for a range of flow incidence angles. Flow incidence was varied by rotating the cylinders about their longitudinal axes (i.e., vertical in the tunnel) through a range from $-45°$ to $90°$. The dynamic pressure range from 1.5 to 50 psf was selected to encompass the range of flow conditions characterized by Reynolds number that may be experienced by full-scale helicopter tail booms. An approximate rotor-wake velocity distribution is combined with the full-scale dimensions to show a typical Reynolds number distribution that may be experienced along the tail boom at full scale (fig. 6(a)). Figure 6(b) also shows the range of test Reynolds number related to the test dynamic pressures for the AH-64, UH-60, and UH-1H shapes. The large range of flow incidence covered the extreme flow angles that may be experienced by the tail boom. For example, the range included $90°$ that could occur in right

sideward flight, when the flight velocity is high enough that the rotor wake may be clear of the tail boom.

Since the maximum test Mach number was approximately 0.18, compressibility effects were considered to be negligible. Because of the large test section and relatively small volume of the test apparatus, the test data did not require correction for blockage effects.

Presentation of Data

The results are presented in coefficient form as vertical-force and side-force body axes coefficients. The coefficients are based on the dimension b, which is consistent with presentations of data in references 2 through 7. Pressure measurements are presented as standard pressure coefficients on polar coordinate graphs. Some distortion of apparent pressure distribution for the UH-60 and UH-1H shapes results because of their noncircular cross-sectional shapes.

The arrangement of data figures is as follows:

Discussion of Results

There are several factors that affect the pressure patterns experienced by cylindrical shapes in two-dimensional flow other than the shape itself, and an awareness of these factors can assist in the interpretation of the data presented herein. The influence of viscosity, for one, has been shown to be extreme (refs. 2 through 7). Reynolds number R provides a standard for judgment of these effects of viscosity by relating viscosity to flow velocity and cylinder size. Typically, drastic changes in pressure patterns and, therefore, air loads occur in the Reynolds number range from 0.3×10^6 to 0.7×10^6. For some shapes, such as square cylinders with relatively small corner radii, the changes can occur at higher Reynolds number (refs. 3 and 4). A second factor, surface finish of the contour, can be important (refs. 6 and 7). Typically, tests are conducted with highly polished cylinders implying contours fabricated within close tolerances. The cylinders used in the present test were fabricated with less stringent tolerances and are more representative of full-scale helicopter contours and surfaces.

The procedure for setting test conditions of dynamic pressure (i.e., wind speed) or flow incidence can also influence the results. A hysteresis effect can occur if, for example, dynamic pressure is increased to a desired test condition at one time; however at another time, the same test condition is approached by decreasing dynamic pressure. The hysteresis is essentially due to a change in the pattern of separated flow (and for these shapes there are always regions of separated flow) causing a change in pressure pattern and associated aerodynamic loads. The setting of flow incidence angle can also result in hysteresis effects if the flow incidence setting is approached from

.e negative side at one time, and then from the positive side at another time. To avoid or reduce these hysteresis effects in this investigation, the flow incidence and dynamic pressure were always set by approaching each condition from a lower value.

Yet another factor affecting the interpretation of data is the turbulence in the tunnel flow that causes a higher effective Reynolds number than that calculated for smooth flow conditions. Turbulence measurements made in the Langley 4- by 7-Meter Tunnel indicate that the tunnel has a turbulence factor of 1.3; that is, the effective Reynolds number is 30 percent higher than the value that would be obtained in absolutely "smooth" flow. Of course, helicopter tail booms can experience turbulence in the wake of the rotor and, therefore, experience a higher effective Reynolds number than would be determined from steady downwash velocities.

Comparison of Basic Configurations

The three shapes together (AH-64, UH-60, and UH-1H), each with a tail rotor drive-shaft cover (TRSC), are representative of a large percentage of single-rotor helicopter tail boom cross sections. There are significant differences between these shapes (see fig. 2), however, such as the ratio of depth to width c/b and the curvature of the "corners." (Compare the UH-60 with the UH-1H in fig. 3.) These differences result in different aerodynamic characteristics, as shown by the variations in coefficients c_y and c_z with flow incidence in figure 7. The AH-64 data show notable differences when compared with that of the other two shapes for the flow incidence range from $-20°$ to $20°$ for a c_z range from $-35°$ to $35°$ where the slopes of c_y plotted against ϕ for the UH-1H and UH-60 shapes are more than double that for the AH-64 shape. For $|\phi| > 20°$, the variation of c_z with ϕ for the UH-60 shape differs markedly from that for the AH-64 and UH-1H shapes.

A comparison of the variations of c_y and c_z with ϕ for the three shapes without the tail rotor drive-shaft covers is given in figure 8. These shapes are more like those described in references 2 through 7, except that in those references all shapes are symmetric about the y-axis whereas the UH-60 and UH-1H shapes are not. The variations of c_y and c_z with ϕ are similar for the UH-60 and UH-1H but significantly different from that of the AH-64 with the drive-shaft covers off as well as with them on. Of course, the tail rotor drive-shaft cover increases the asymmetry about the y-axis for the UH-1H and UH-60 shapes (and adds asymmetry to the AH-64 shape), resulting in significant effects on the patterns of c_y and c_z plotted against ϕ. (Compare fig. 8 with fig. 7.) These results suggest that a departure from a circular cross section has a major effect; whereas the details of noncircular shapes have relatively minor effects, and the addition of the tail rotor drive-shaft cover also affects the patterns of c_y and c_z plotted against ϕ.

Discussion of Characteristics of Each Shape

In the following discussion the force and pressure data acquired at various dynamic pressures are described for each shape individually. The sequence of presentation (AH-64, UH-60, and UH-1H) follows the order of testing. During this investigation, various spoiler configurations were tested in attempts to alter beneficially the characteristics of side-force coefficient of each shape. The beneficial effect desired is a positive increase in c_y, which implies a side air load to the right (if viewing the helicopter from the rear) that would result in a decrease of the thrust required of the tail rotor. For each shape, variations of c_y and c_z with ϕ for various dynamic pressures are presented along with supplementary data describing pressure patterns. The variations of c_z and c_y with dynamic pressure are shown to indicate the level of dynamic pressure at which the data are relatively free of variations due to R effects.

AH-64 Shape

The circular cross section of the AH-64 without the TRSC is the most extensively tested shape in aerodynamics, and thus its aerodynamic characteristics are well understood. The data obtained in this investigation are shown in figure 9 and correspond reasonably well with past experience. For example, in figure 9(b) the variation of c_z with dynamic pressure is similar to the variation of drag coefficient shown in figure 3 of reference 3. The differences between these data and those of reference 3 can probably be attributed to the greater irregularities in the contours of the models tested in the present investigation.

The installation of the TRSC and aluminum spoilers (S_1 and S_2) on the circular shape resulted in significantly different variations of the coefficients (figs. 10 through 13). The influence of viscosity on c_z and c_y plotted against ϕ is large for $|\phi| > 25°$ where, for example, c_z ranges from a minimum of less than 0 at $q = 45$ psf to a value approaching 1.0 at $q = 5$ psf for the TRSC installed as shown in figure 10. The effect of dynamic pressure (and therefore Reynolds number) on the variation of c_y with ϕ is also large throughout the range of ϕ tested.

The difference between the spoiler configurations was only in the height of the spoiler: S_1 was 1 in. high and S_2 was 2 in. high. (Full-scale values are 2

and 4 in., respectively.) The spoilers were attached at a location found from preliminary tests to alter the side-force (c_y) characteristics beneficially. The basic effect of both spoilers was to produce a positive c_y increment as shown in figure 13 for the range of ϕ from $-20°$ to $48°$. Such a range may well encompass the flow incidence felt by the AH-64 tail boom from hover (where wake swirl produces a small negative incidence) through a portion of right sideward flight (where $\phi > 0°$). The favorable shift in the side force indicates a potential for reducing power required for directional control in hover and sideward flight through a reduction in tail rotor thrust required. However, there is a penalty caused by the spoiler that is the positive increment of c_z, as shown in figure 13. That increment would result in a greater down load on a tail boom for the same range of ϕ from $-20°$ to $48°$. Some simple calculations made by using the present data show that the net effect, however, is an improvement in overall helicopter performance. This improvement is realized largely because the down load penalty is compensated for by the main rotor that is efficient in using the power saved by unloading the tail rotor.

UH-60 Shape

The UH-60 tail boom without the tail rotor driveshaft cover has a depth-to-width ratio of 1.64 and larger radii of curvature on the lower half than on the upper half; these features combine to contribute to a lower value of c_z at $\phi = 0°$ (fig. 19(a)) than that for the circular shape. The depth-to-width ratio for the UH-60 shape also results in a steep slope for the curve of c_y plotted against ϕ. The addition of the TRSC on the UH-60 shape does not change the slope significantly within the range of ϕ from $-5°$ to $5°$ (fig. 20(a)). It does, however, increase the positive and negative values of c_y out to $|\phi| = 15°$. Viscosity effects are evident also in figures 19 and 20.

Several spoiler configurations were investigated for the UH-60 shape, and the results are presented in figures 21 through 24. In figure 21, data for two different size spoilers (S_1 and S_2) attached at the upper "left" corner are presented. For $\phi > 0°$, the c_y variations with the two spoilers are practically identical. Compared with the basic shape with the TRSC on, there is a substantial beneficial increment in c_y between $\phi = 0°$ and $20°$ that diminishes to 0 at $\phi = 30°$. (Here, c_y for spoiler on is the same as c_y for spoiler off.) For $-12° < \phi < 0°$, the S_2 spoiler resulted in greater c_y than that for the S_1 spoiler. An airfoil-like stall occurred at $\phi \approx -8°$ for the S_2 spoiler and at $\phi \approx -2°$ for the S_1 spoiler. The increment in c_z (positive c_z represents a down load on the tail boom) for the larger spoiler (S_2) is greater than that of the smaller spoiler (S_1) for the range of ϕ from $-30°$ to $30°$. That may be an acceptable penalty if the greater increment in c_y for the range of ϕ from $-12°$ to $0°$ is desirable for reduced tail rotor thrust in hover.

In a limited effort to extend the range of increased c_y and reduce the penalty of increased c_z, two alternate spoiler configurations were tested. Spoilers of 1-in. and 2-in. were attached on the lower left side of the UH-60 shape (see fig. 2(b)) in combination with the 1-in. and 2-in. spoilers on the upper side. In figures 22, 23, and 24 it is evident that the increment in c_y was obtained for $\phi < -10°$, which may be beneficial for left sideward flight of the UH-60.

Pressure distribution data were not acquired for the UH-60 spoiler configurations. However, those distributions shown for the UH-60 shape without and with the TRSC (figs. 25 and 26, respectively) may provide some clues to other placements of spoiler configurations that could increase the positive range of ϕ (beyond $30°$) for positive increments of c_y.

UH-1H Shape

According to figure 6, the dynamic pressure that results in the most representative Reynolds number of the full-scale UH-1H shape is approximately 10 psf. For the UH-1H shape with and without the TRSC, it is evident in figures 27 and 28 that c_y and c_z are sensitive to a dynamic pressure variation. Care is required in interpreting the data at dynamic pressures different from the representative full-scale value of $q = 10$ psf.

Only one spoiler configuration (S_{12}) was investigated for the UH-1H shape and results are shown in figure 29. Direct comparison of the c_z and c_y variations for the three UH-1H configurations (without the TRSC, with the TRSC, and with the TRSC and S_{12}) are given in figure 30. The general pattern of c_y and c_z increments for S_{12} holds rather well for the three levels of dynamic pressure shown. The S_{12} spoiler is effective in beneficially increasing c_y for a range of ϕ from $-8°$ to $50°$; however, there is the associated penalty in increased c_z.

The change in pressure distributions as a result of adding the S_{12} spoiler configuration shown in figure 31 illustrates the mechanism of altering the air load on the UH-1H boom section. The upper spoiler separates the flow on the left side of the shape, thus raising pressure on that side. On the right side, there is the beneficial decrease in the pressure. It is also evident that the increased down load c_z is primarily the result of lower pressures on the bottom of the UH-1H section caused by the upper spoiler. The lower spoiler becomes effective as ϕ becomes more negative. The interpretation of the effects is, of

course, somewhat affected by uncertainty introduced by the nonrepresentative level of dynamic pressure for figure 31. Figures 32 and 33 are offered to relieve, somewhat, that concern. Figure 32 indicates that for $\phi = 20°$, though the pattern changes between $q = 30$ psf and 20 psf, the negative pressure peak location is unchanged. Figure 33 suggests little change in pressure patterns as a result of the variation of dynamic pressure. Figures 31 through 33 offer a basis for relocation of spoilers to alter the effect on c_y and c_z if desired.

Summary of Results

An investigation has been conducted in the Langley 4- by 7-Meter Tunnel on three tail boom cross-sectional shapes of current helicopters. The purpose of the investigation was to determine two-dimensional aerodynamic forces and pressure distributions on these cross-sectional shapes over a flow incidence range from $-45°$ to $90°$ inclusive of hovering and sideward flight. These shapes represented, at reduced scale, the cross section of the tail booms of the AH-64, UH-60, and UH-1H helicopters, which together constitute the bulk of the U.S. Army helicopter fleet. Reynolds number was varied over a range of dynamic pressure from 1.5 to 50 psf. Also, the effects of tail rotor drive-shaft covers and spoilers were investigated. The results of this investigation are summarized as follows:

1. The departure of the shape of a helicopter tail boom from a circular cross section has a major effect on the aerodynamic loads, although the details of the noncircular shapes have a relatively minor effect. The addition of tail rotor drive-shaft covers to the tail boom cross sections also affected the variations of the side-force and vertical-force coefficients.

2. Viscosity effects were experienced by the three tail boom cross sections, and analyses of air loads on a helicopter operated at low flight speeds may need to account for them.

3. The addition of spoilers to the shapes (with tail rotor drive-shaft covers) beneficially increased the side-force coefficients of all three tail booms over a significant flow incidence range, thus indicating a potential to reduce the thrust required for directional control by a helicopter in right sideward flight. A disadvantage noted with the spoilers was increased down load.

NASA Langley Research Center
Hampton, VA 23665-5225
September 13, 1985

References

1. Amer, K. B.; Prouty, R. W.; Walton, R. P.; and Engle, J. E.: Handling Qualities of Army/Hughes YAH-64 Advanced Attack Helicopters. Preprint No. 78-31, *34th Annual National Forum*, American Helicopter Soc., May 1978.
2. Delany, Noel K.; and Sorensen, Norman E.: *Low-Speed Drag of Cylinders of Various Shapes.* NACA TN 3038, 1953.
3. Polhamus, Edward C.: *Effect of Flow Incidence and Reynolds Number on Low-Speed Aerodynamic Characteristics of Several Noncircular Cylinders With Applications to Directional Stability and Spinning.* NASA TR R-29, 1959. (Supersedes NACA TN 4176.)
4. Polhamus, Edward C.; Geller, Edward W.; and Grunwald, Kalman J.: *Pressure and Force Characteristics of Noncircular Cylinders as Affected by Reynolds Number With a Method Included for Determining the Potential Flow About Arbitrary Shapes.* NASA TR R-46, 1959.
5. Lockwood, Vernard E.: *Effects of Reynolds Number and Flow Incidence on the Force Characteristics of a Family of Flat-Front Cylinders.* NASA TN D-3932, 1967.
6. Fage, A.; and Warsap, J. H.: *The Effects of Turbulence and Surface Roughness on the Drag of a Circular Cylinder.* R & M No. 1283, British A.R.C., 1930.
7. Achenbach, E.; and Heinecke, E.: On Vortex Shedding From Smooth and Rough Cylinders in the Range of Reynolds Numbers 6×10^3 to 5×10^6. *J. Fluid Mech.*, vol. 109, Aug. 1981, pp. 239-251.
8. Taylor, P.: A Method of Predicting Fuselage Loads in Hover. Paper No. 49, *Seventh European Rotorcraft and Powered Lift Aircraft Forum*, Deutsche Gesellschaft fur Luft- und Raumfahrt e.v., Sept. 1981.

TABLE I. SPOILER CONFIGURATIONS

Spoiler configuration	Height of aluminum spoiler, in.	Position
AH-64 shape		
S_1	1	53° from top centerline
S_2	2	53° from top centerline
UH-60 shape		
S_1	1	35° from top centerline
S_2	2	35° from top centerline
S_{12}	1	35° from top centerline
	2	25° from bottom centerline
S_{21}	2	35° from top centerline
	1	25° from bottom centerline
UH-1H shape		
S_{12}	1	35° from top centerline
	2	25° from bottom centerline

TABLE II. COORDINATES OF UH-1H AND UH-60 MODELS

[Note the convention of positive z downward]

(a) UH-1H shape

y, in.	z, in.
0	−8.70
1	−8.70
2	−8.70
3	−8.65
4	−8.55
5	−8.10
6	−7.00
6.5	−5.60
6.9	−3.00
7.0	0
6.9	3.00
6.5	5.20
6.0	6.25
5.0	7.40
4	8.05
3	8.45
2	8.65
1	8.70
0	8.70

(b) UH-60 shape

y, in.	z, in.
0	−8.7
1	−8.65
2	−8.50
3	−8.15
4	−7.50
5	−6.70
5.5	−5.30
5.8	−3.00
5.9	0
5.8	3.0
5.5	5.05
5	6.65
4	8.40
3	9.20
2	9.70
1	9.95
0	10.00

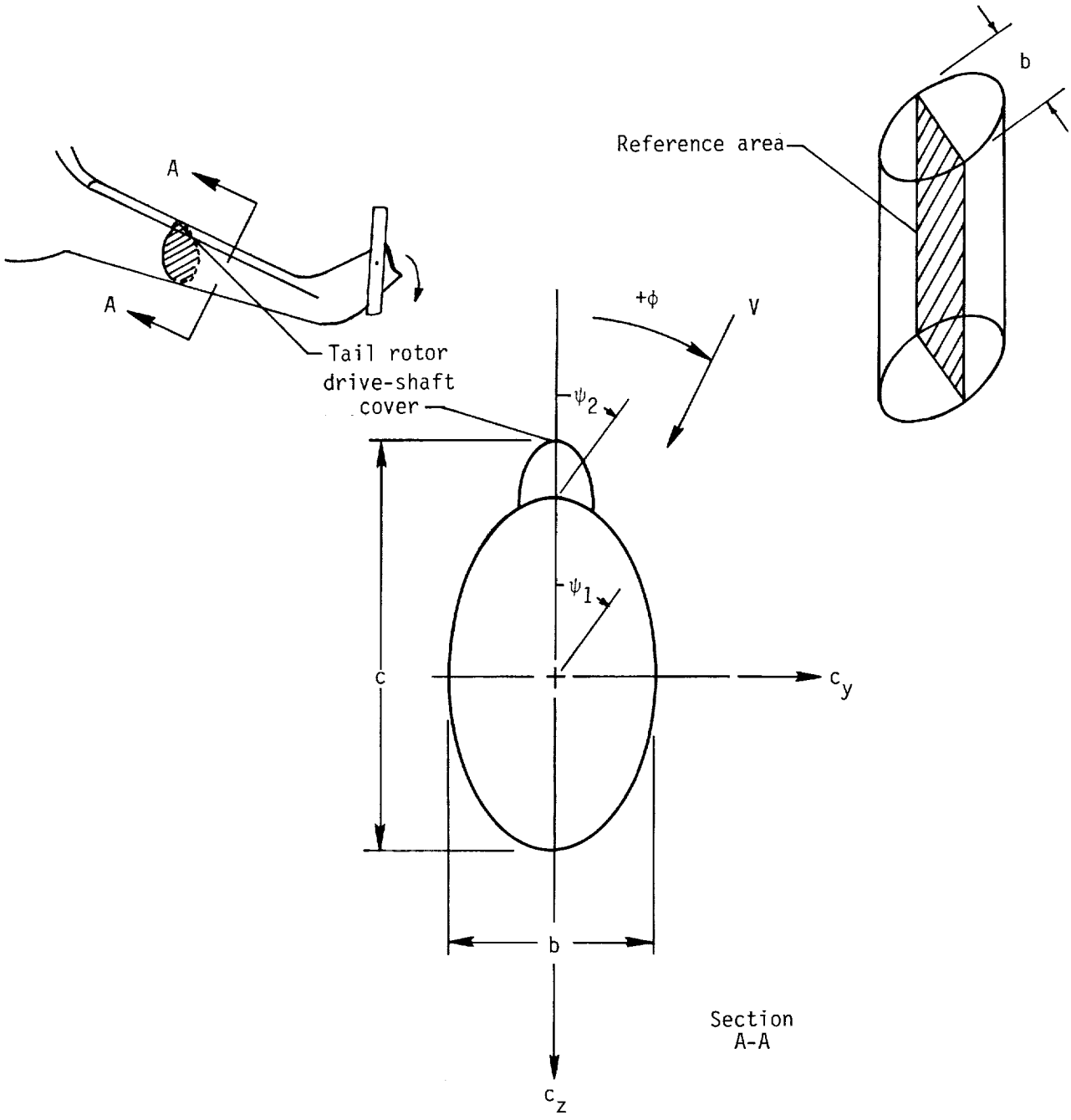

Figure 1. Convention for positive sense of flow inclination, cylinder reference dimensions, and aerodynamic coefficients.

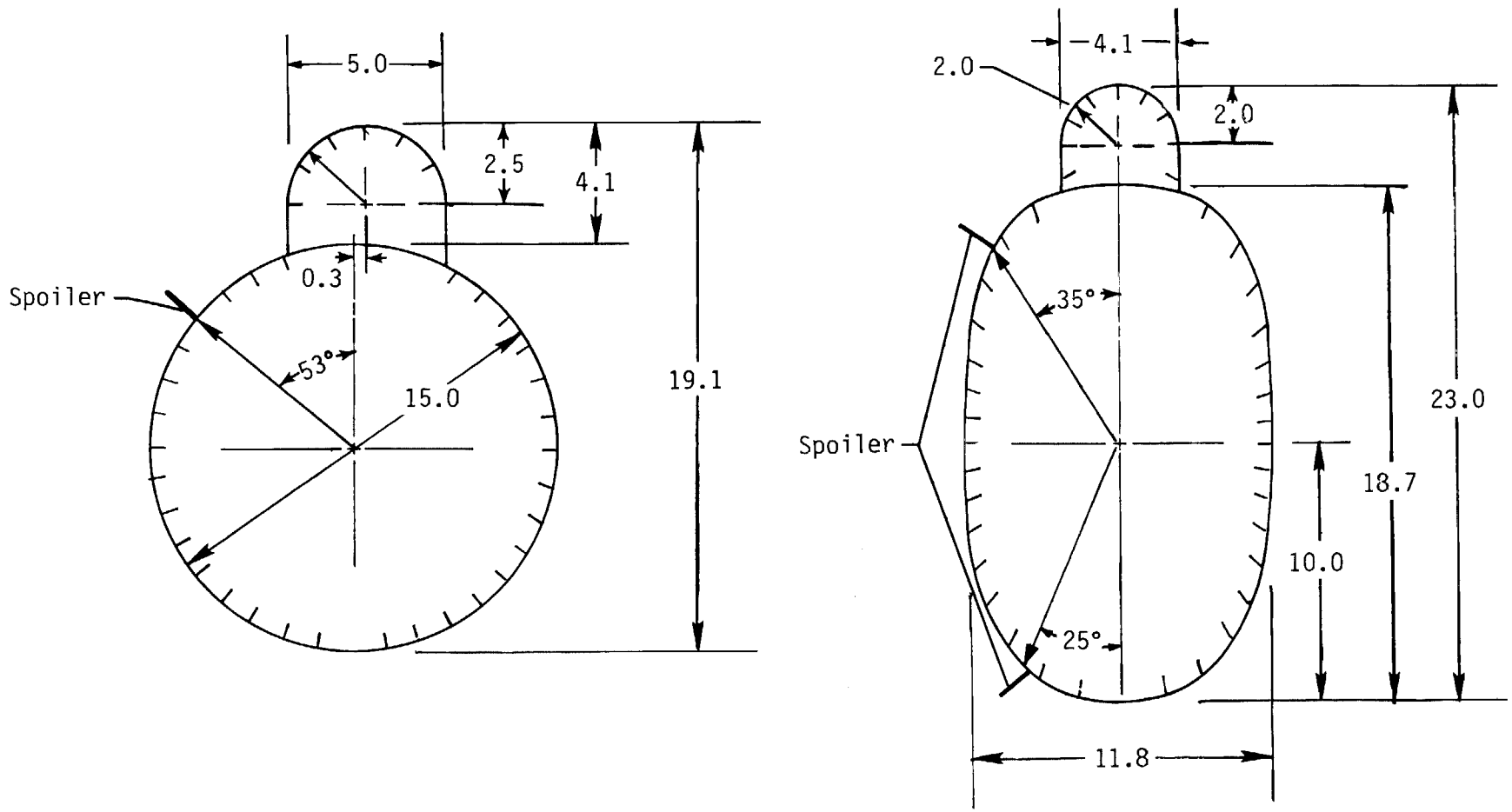

(a) AH-64 shape.

(b) UH-60 shape.

Figure 2. Model cross sections of AH-64, UH-60, and UH-1H shapes. Tick marks indicate location of ports. Dimensions are given in inches unless otherwise indicated.

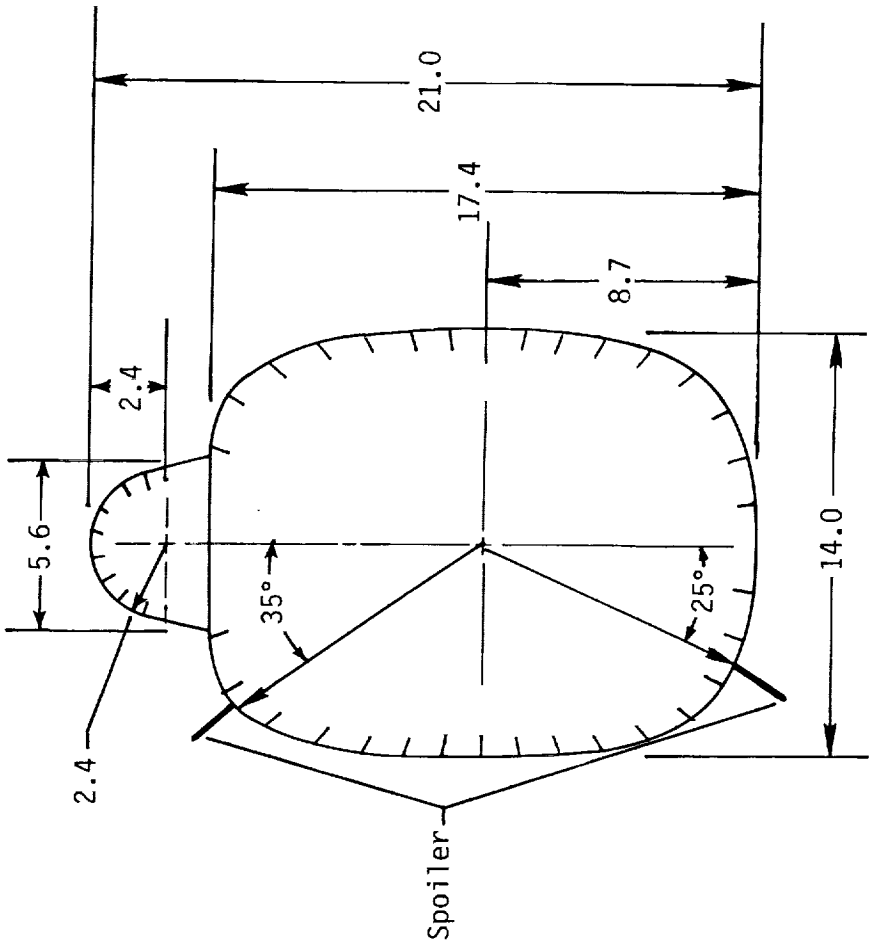

(c) UH-1H shape.

Figure 2. Concluded.

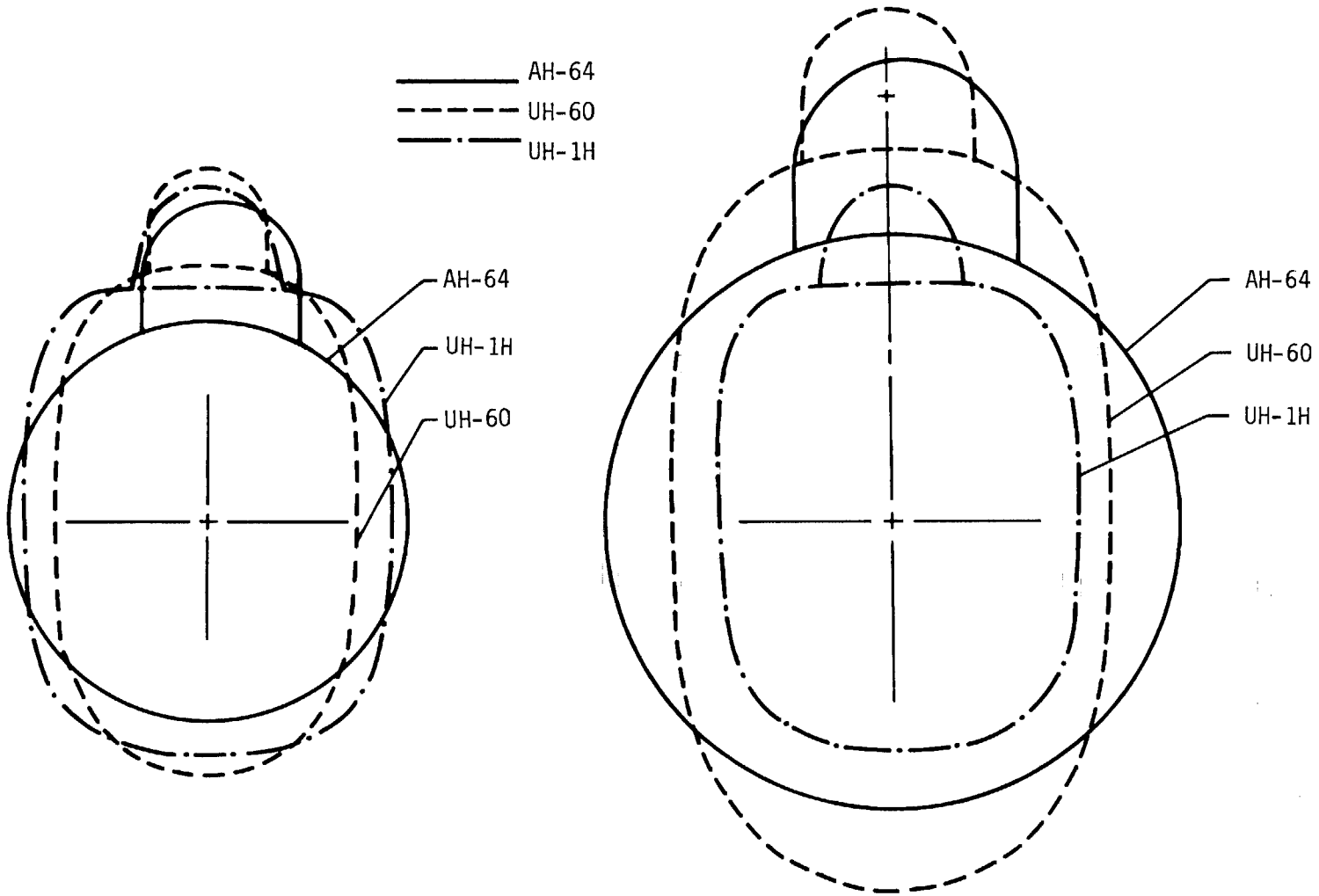

(a) Model scale, as tested.

(b) At full scale.

Figure 3. Relative size comparison of model and full-scale helicopter of AH-64, UH-60, and UH-1H shapes.

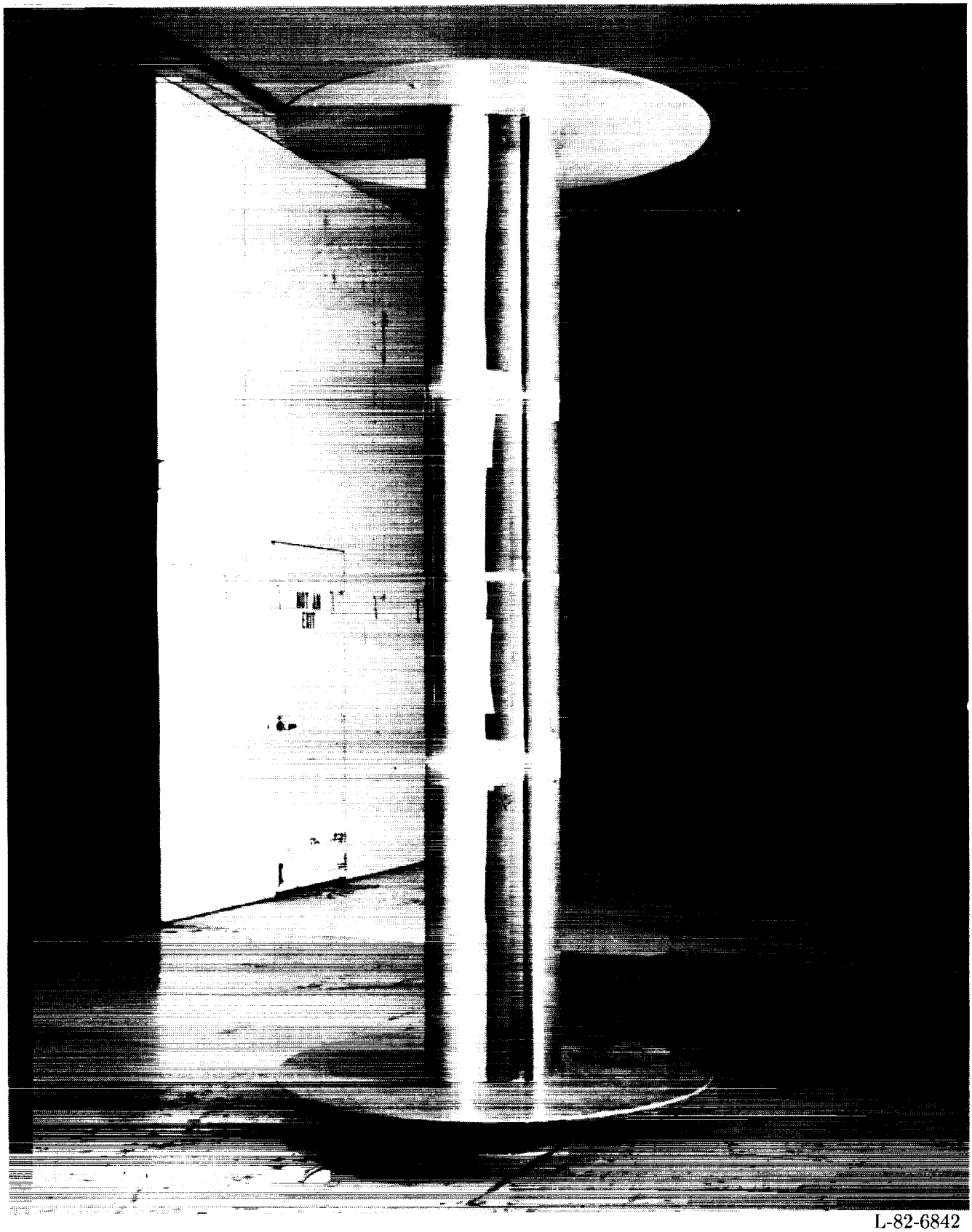

L-82-6842

Figure 4. Two-dimensional test apparatus in the Langley 4- by 7-Meter Tunnel. AH-64 cross section shown.

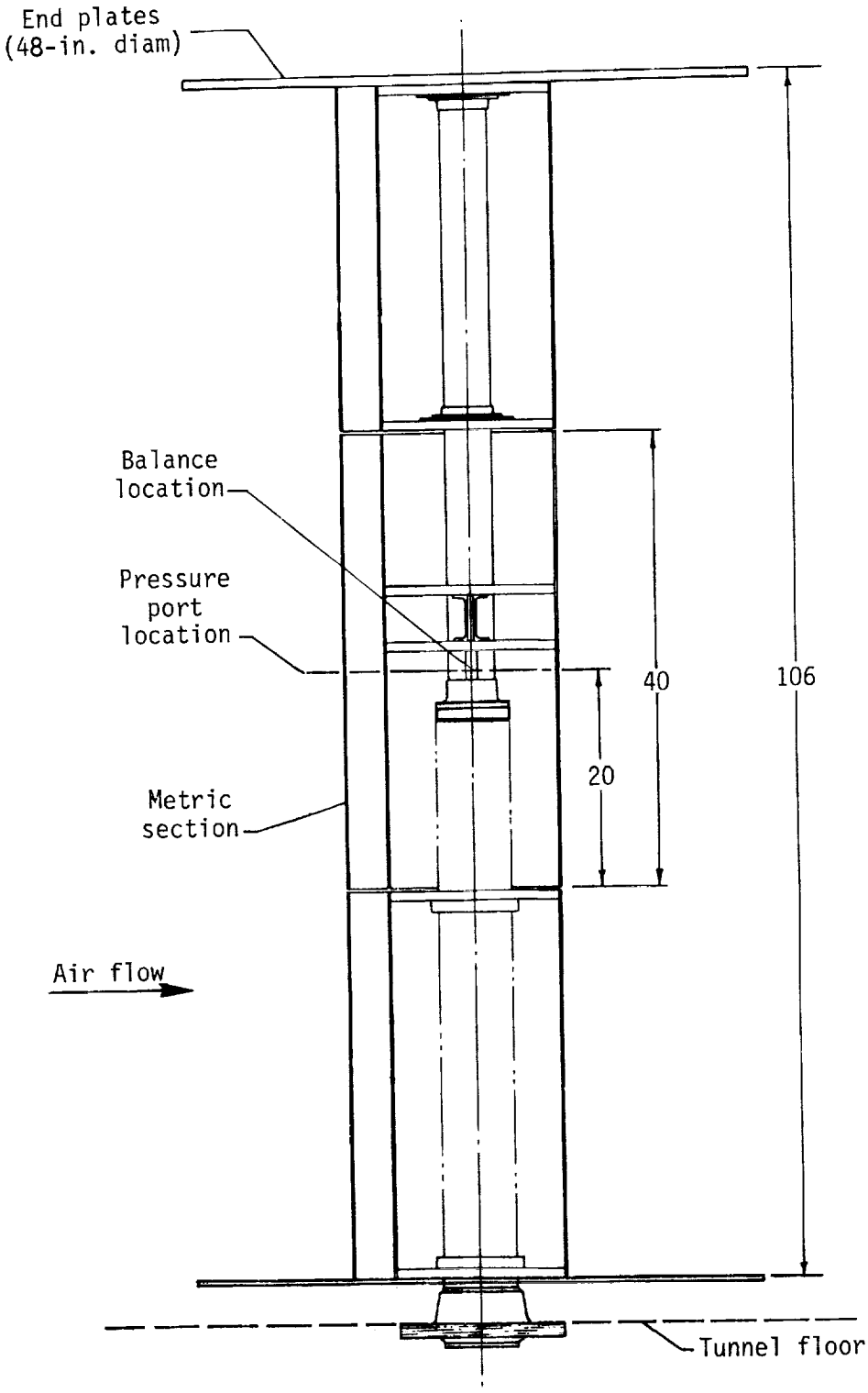

Figure 5. Schematic drawing of helicopter cross-sectional test apparatus. Dimensions are given in inches.

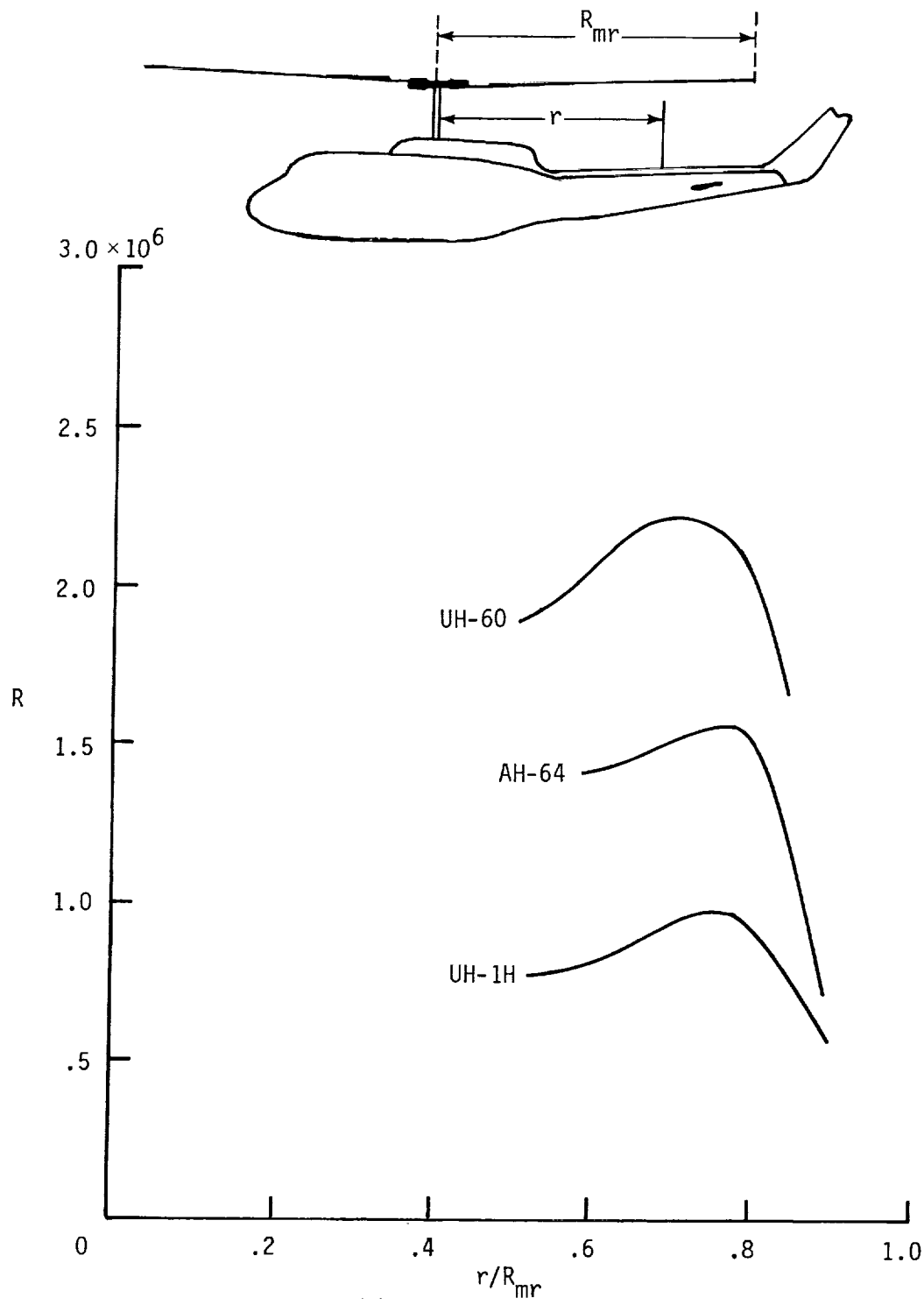

(a) Full-scale Reynolds number distribution.

Figure 6. Nominal Reynolds number distribution on full-scale tail boom and range of Reynolds number of present investigation.

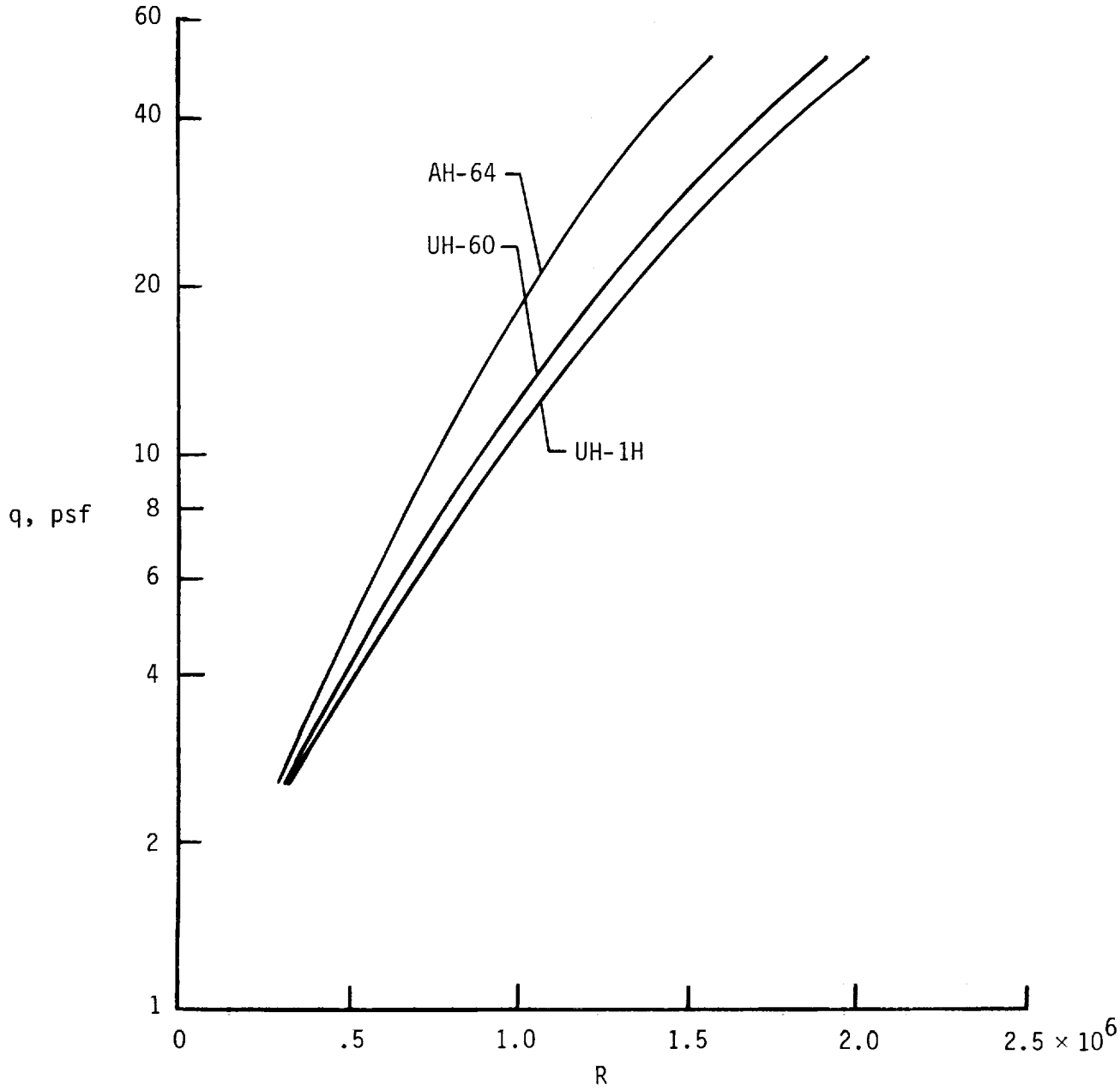

(b) Test dynamic pressure and corresponding Reynolds number.

Figure 6. Concluded.

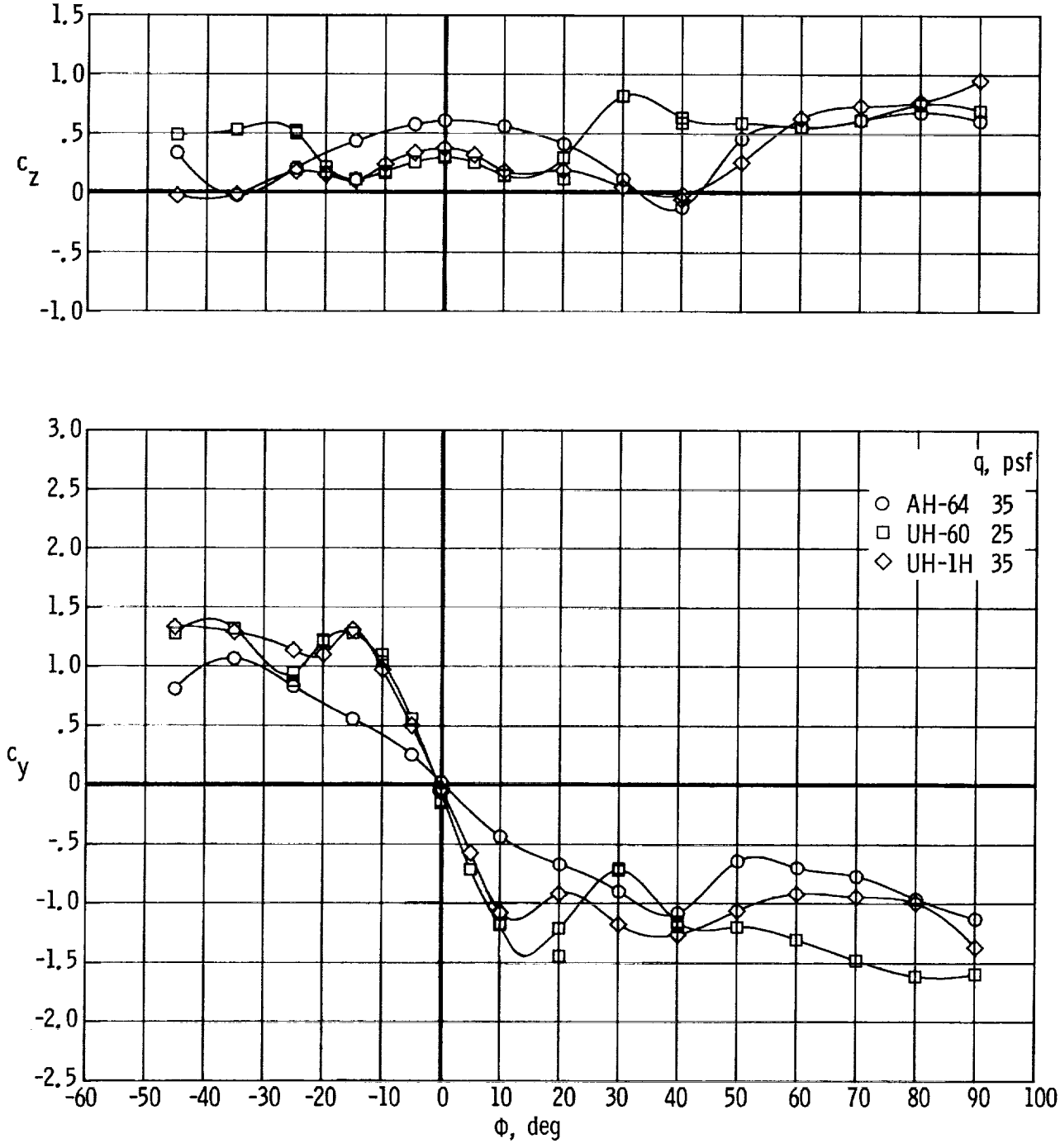

Figure 7. Comparison of effects of flow incidence on drag and side force of AH-64, UH-60, and UH-1H shapes with TRSC on.

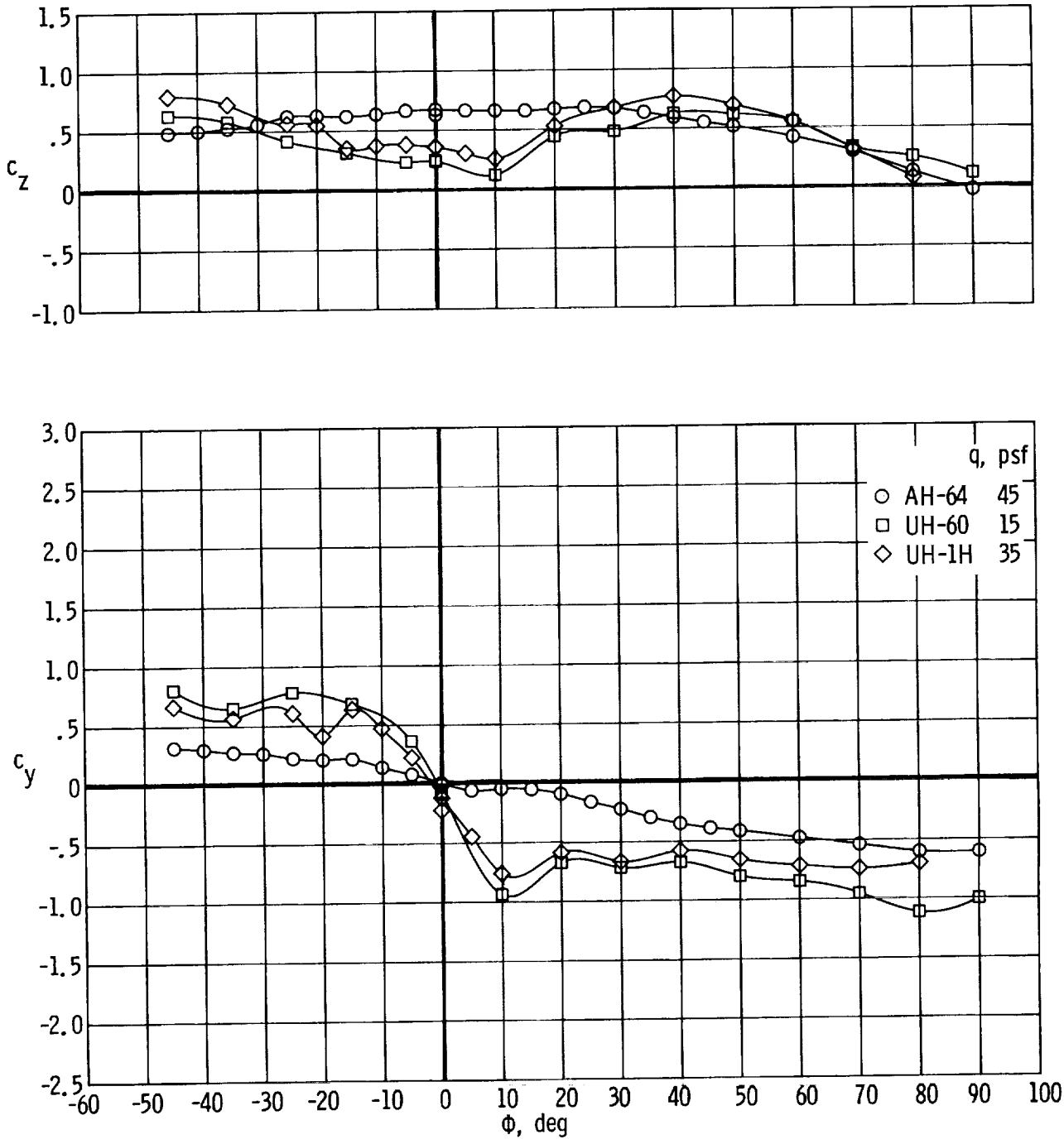

Figure 8. Comparison of effects of flow incidence on drag and side force of AH-64, UH-60, and UH-1H shapes without TRSC.

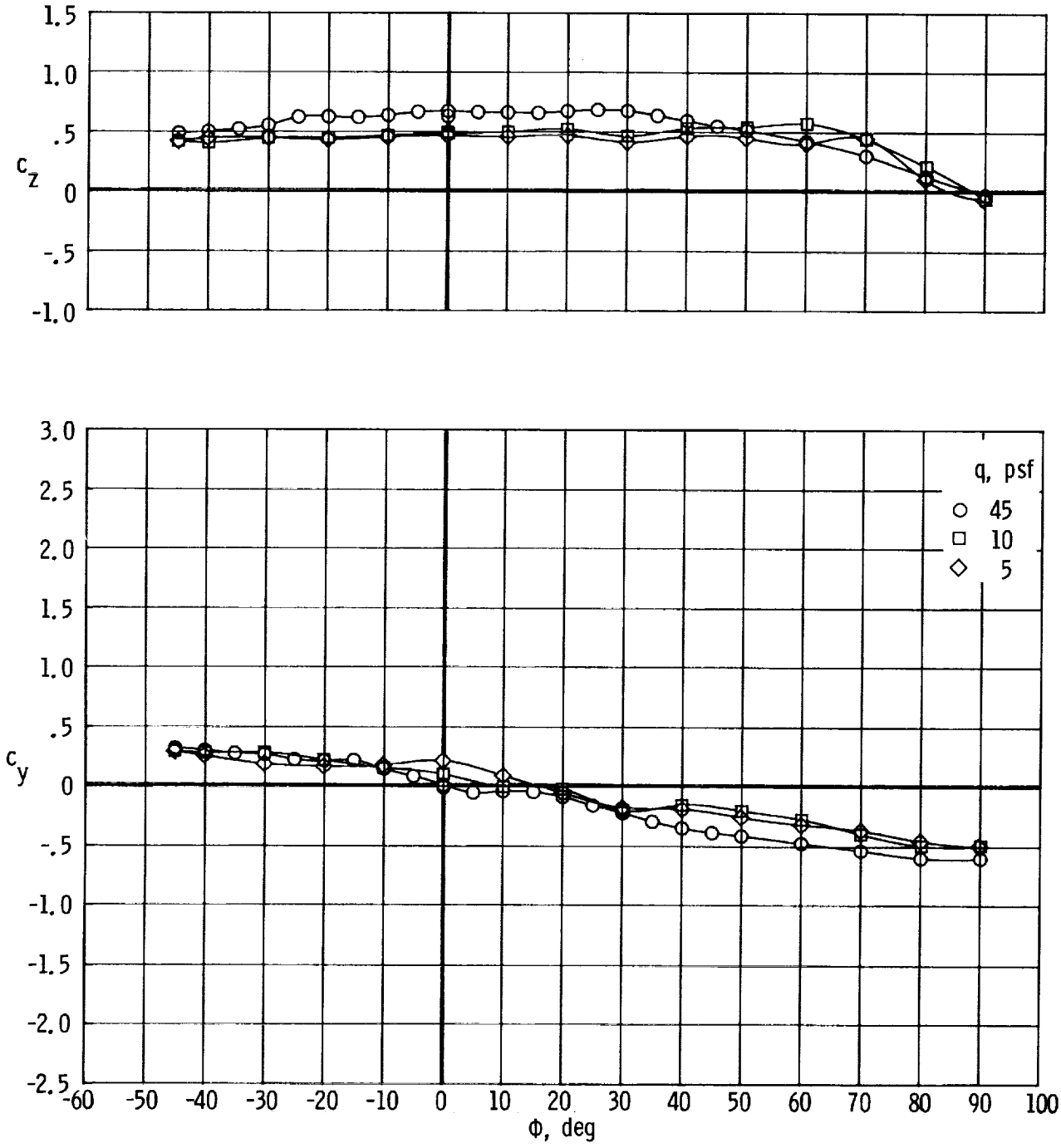

(a) c_z and c_y plotted against ϕ.

Figure 9. Effects of dynamic pressure on drag and side force of AH-64 shape without TRSC.

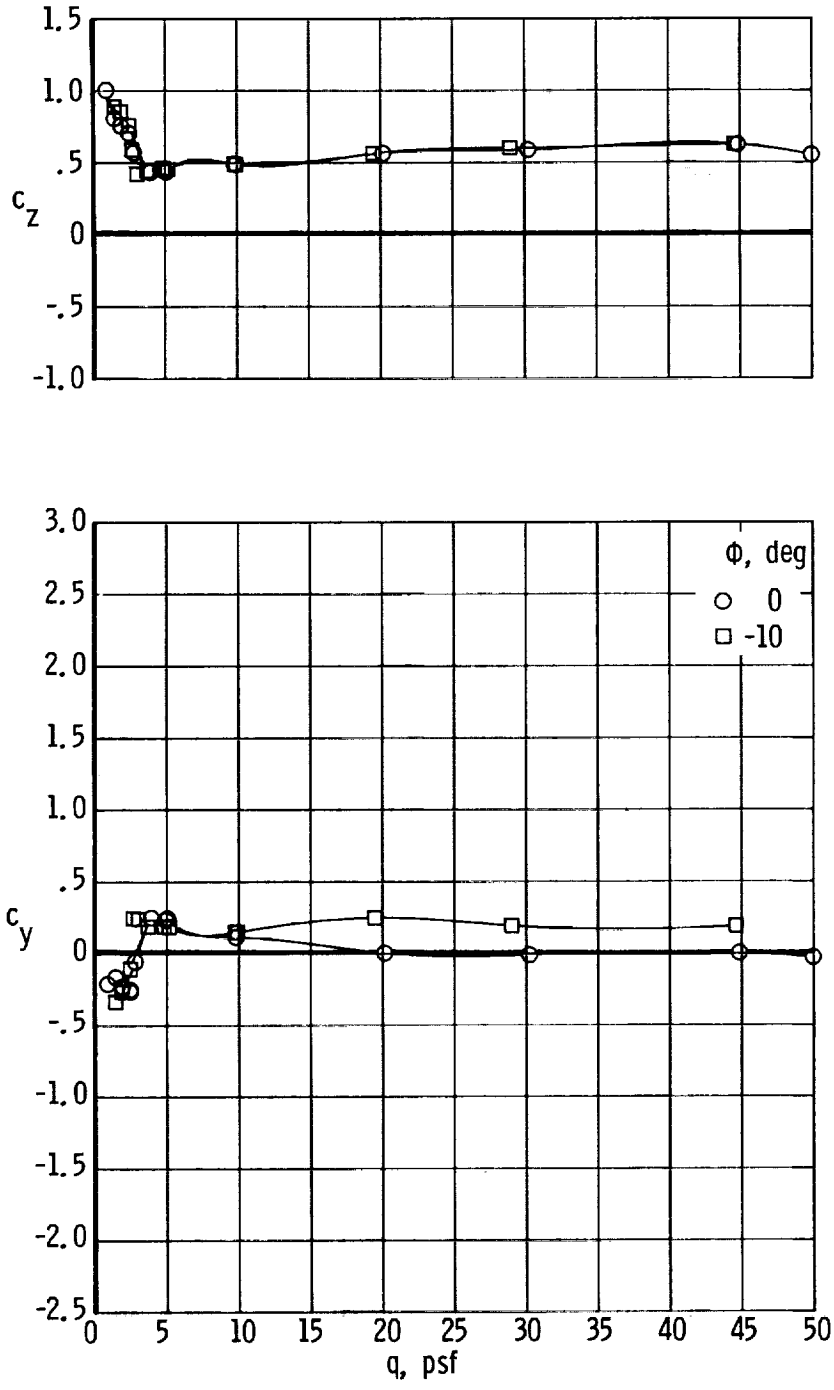

(b) c_z and c_y plotted against q.

Figure 9. Concluded.

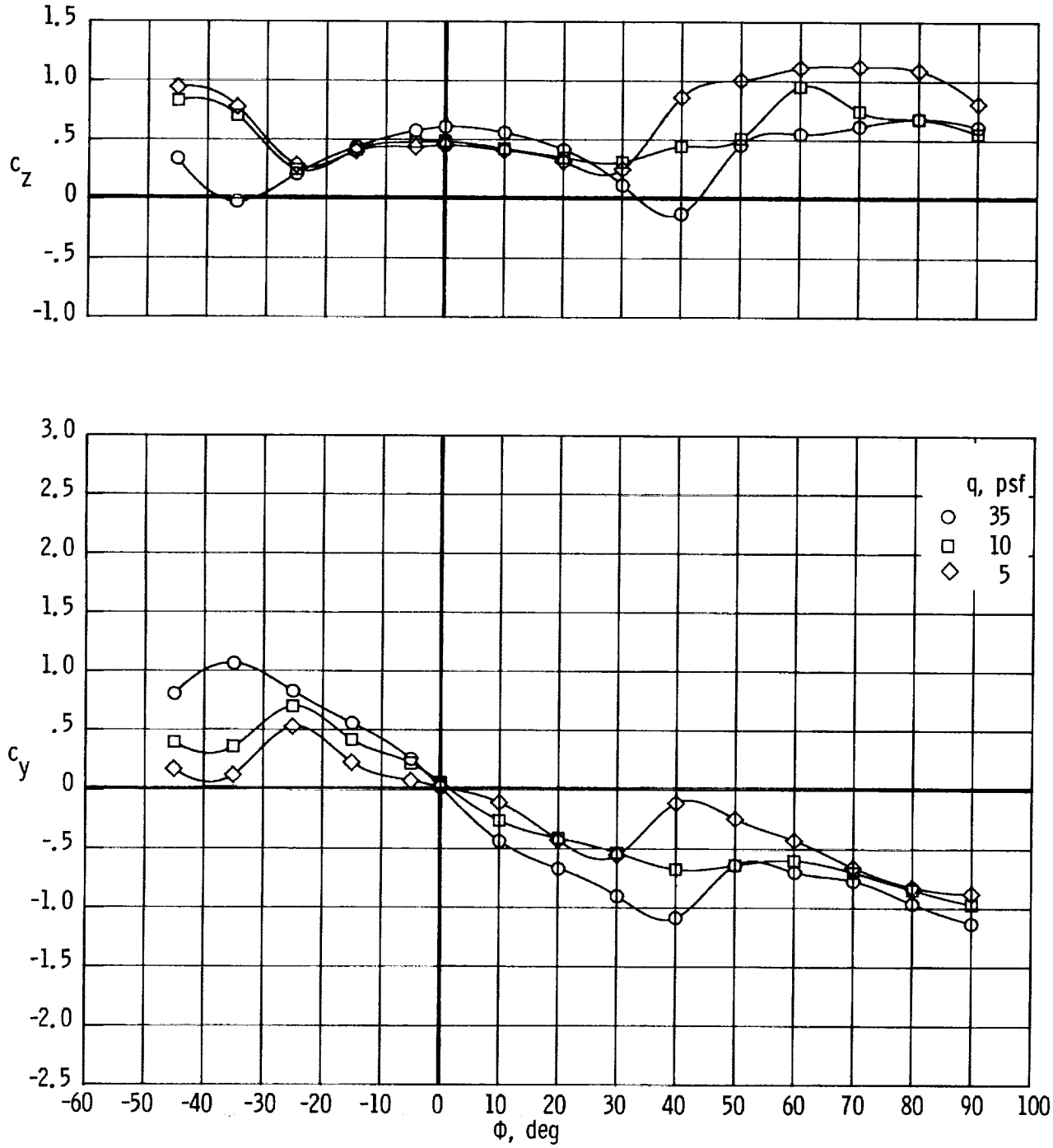

(a) c_z and c_y plotted against ϕ.

Figure 10. Effects of dynamic pressure on drag and side force of AH-64 shape with TRSC.

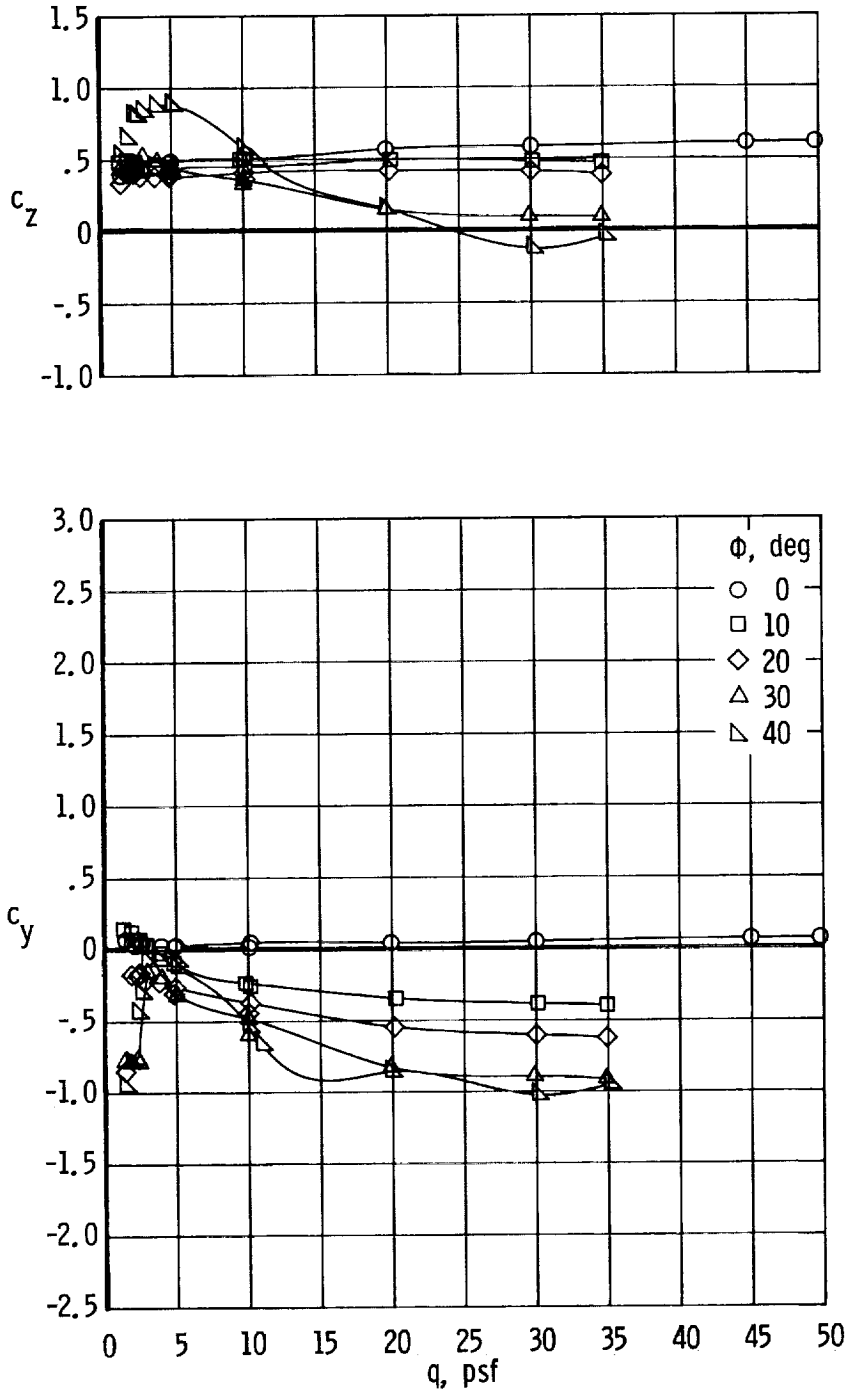

(b) c_z and c_y plotted against q.

Figure 10. Concluded.

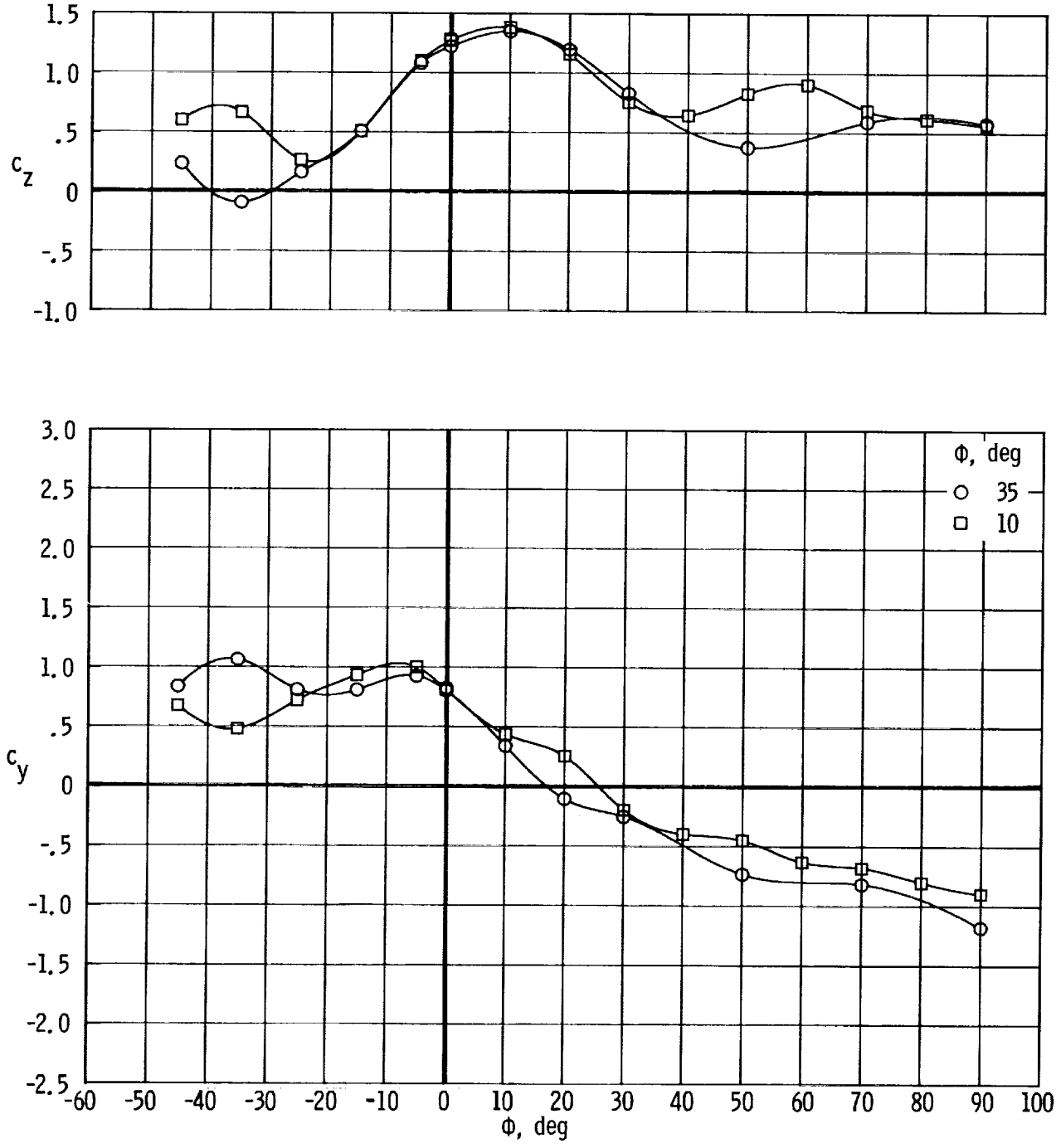

(a) c_z and c_y plotted against ϕ.

Figure 11. Effects of dynamic pressure on drag and side force of AH-64 shape with TRSC and S_1 spoiler.

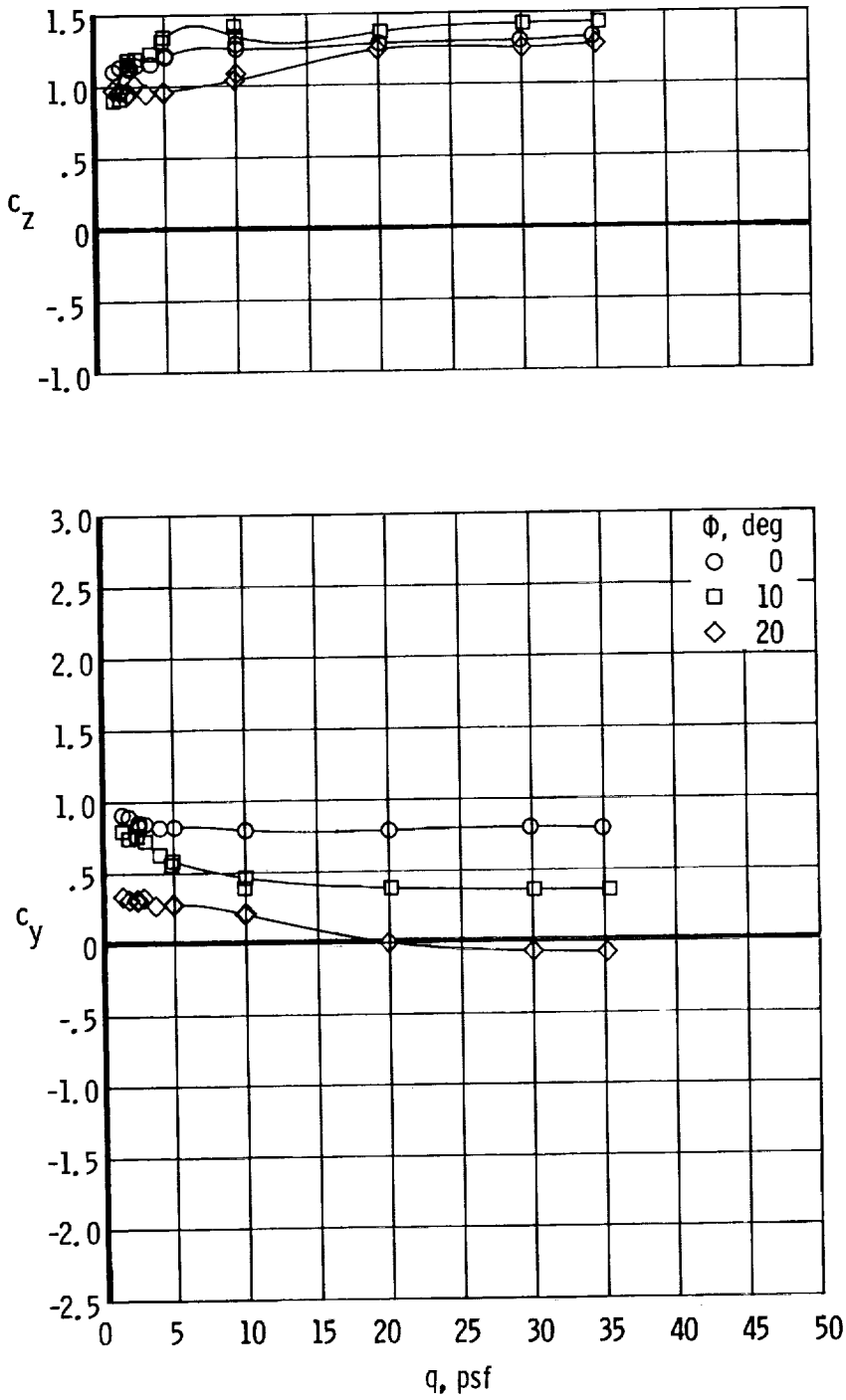

(b) c_z and c_y plotted against q.

Figure 11. Concluded.

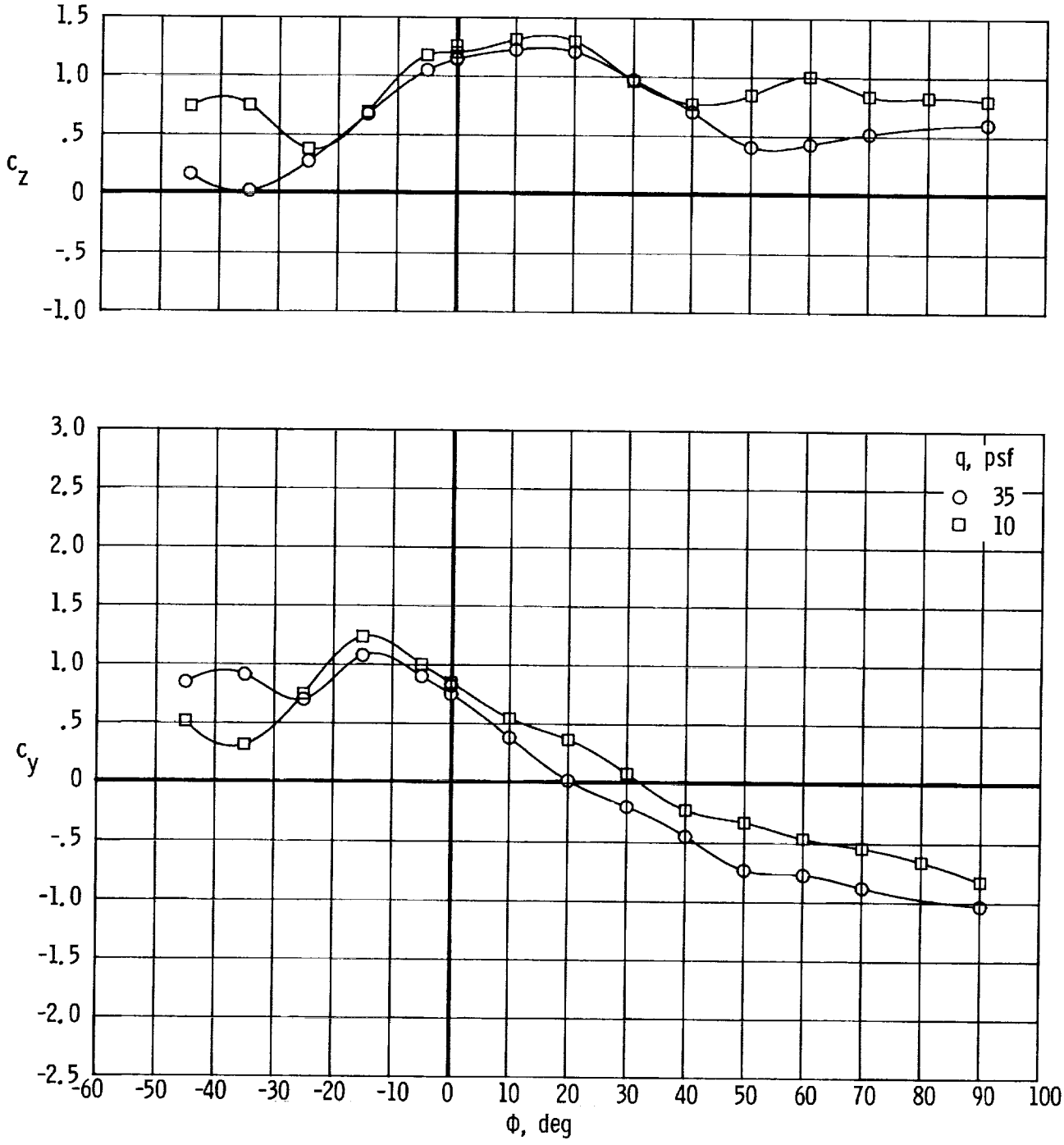

(a) c_z and c_y plotted against ϕ.

Figure 12. Effects of dynamic pressure on drag and side force of AH-64 with TRSC and S_2 spoiler.

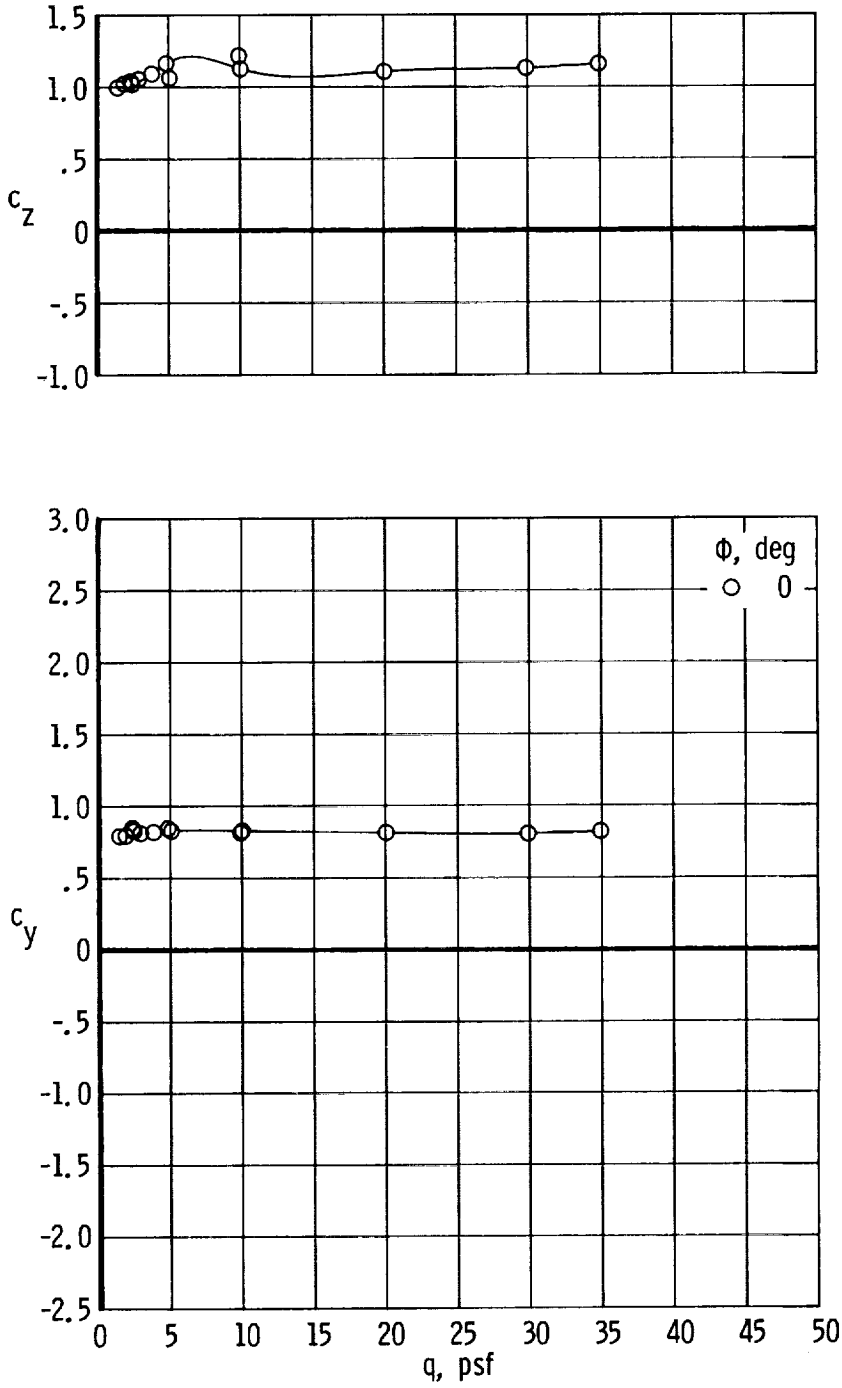

(b) c_z and c_y plotted against q.

Figure 12. Concluded.

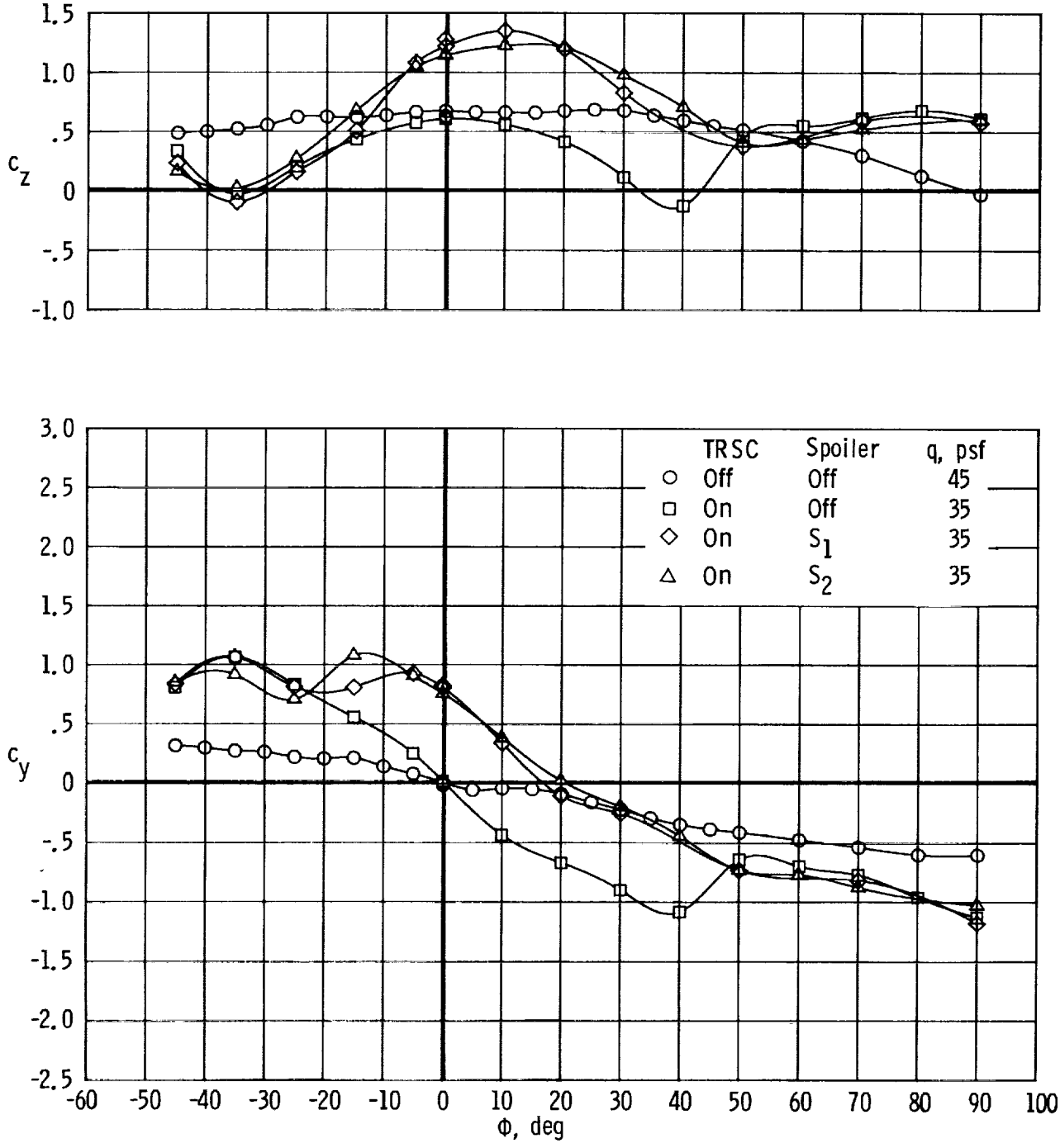

Figure 13. Comparison of effects of flow incidence on drag and side force of AH-64 shape with and without TRSC with S_1 and S_2 spoilers.

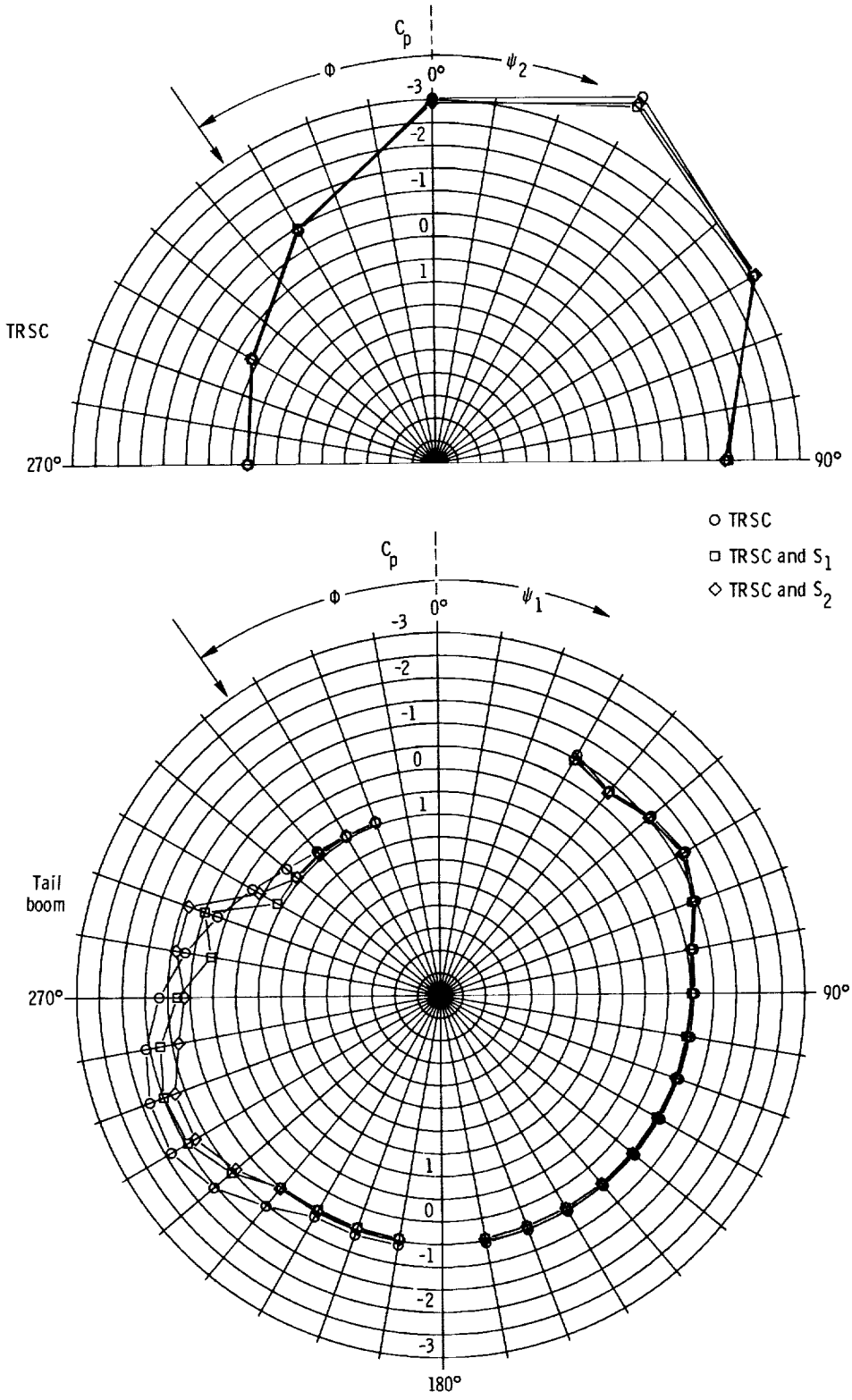

(a) $\phi = -35°$.

Figure 14. Comparison of pressure distributions for AH-64 shape with TRSC and S_1 and S_2 spoilers at various flow incidence angles at $q = 35$ psf.

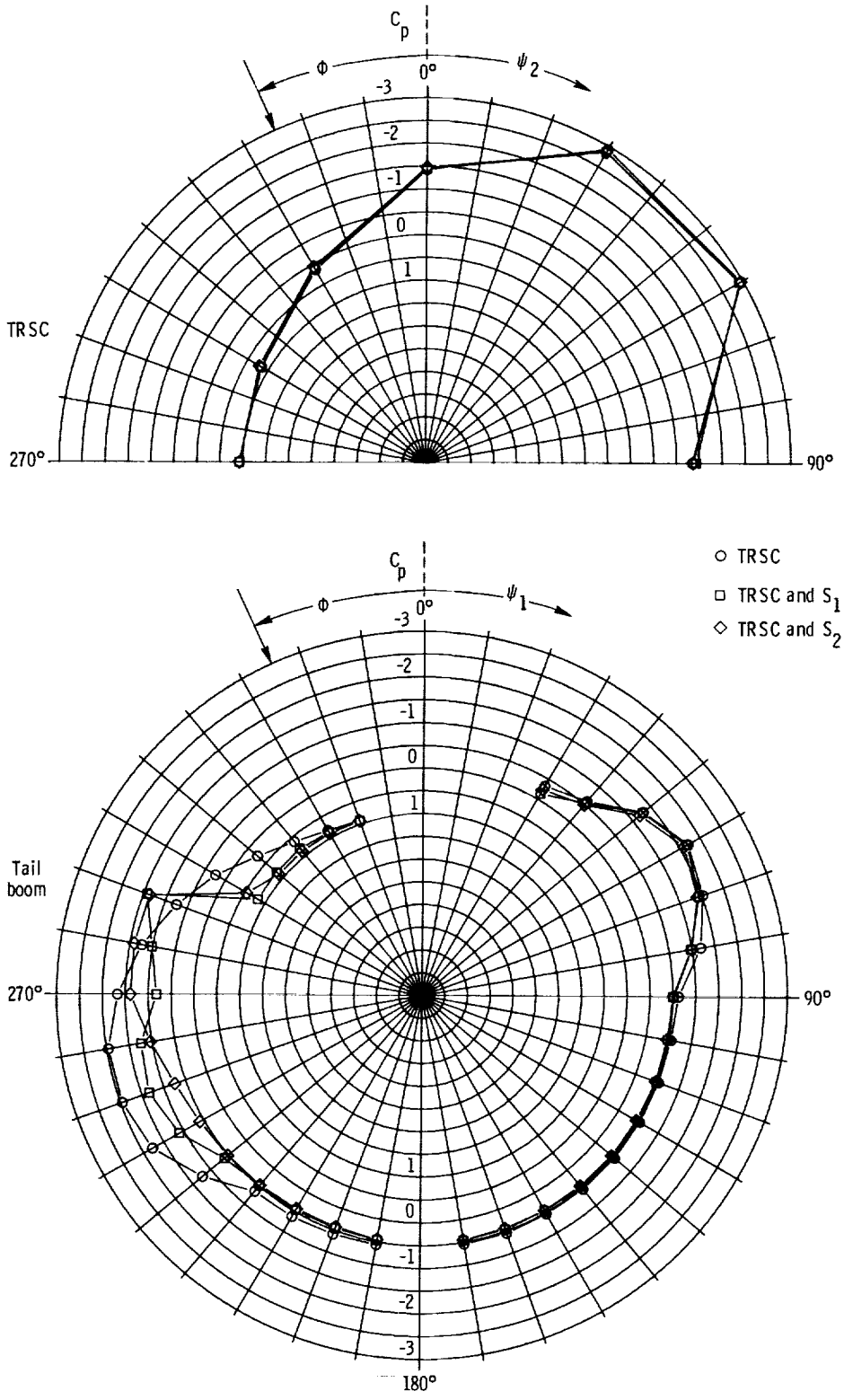

(b) $\phi = -25°$.

Figure 14. Continued.

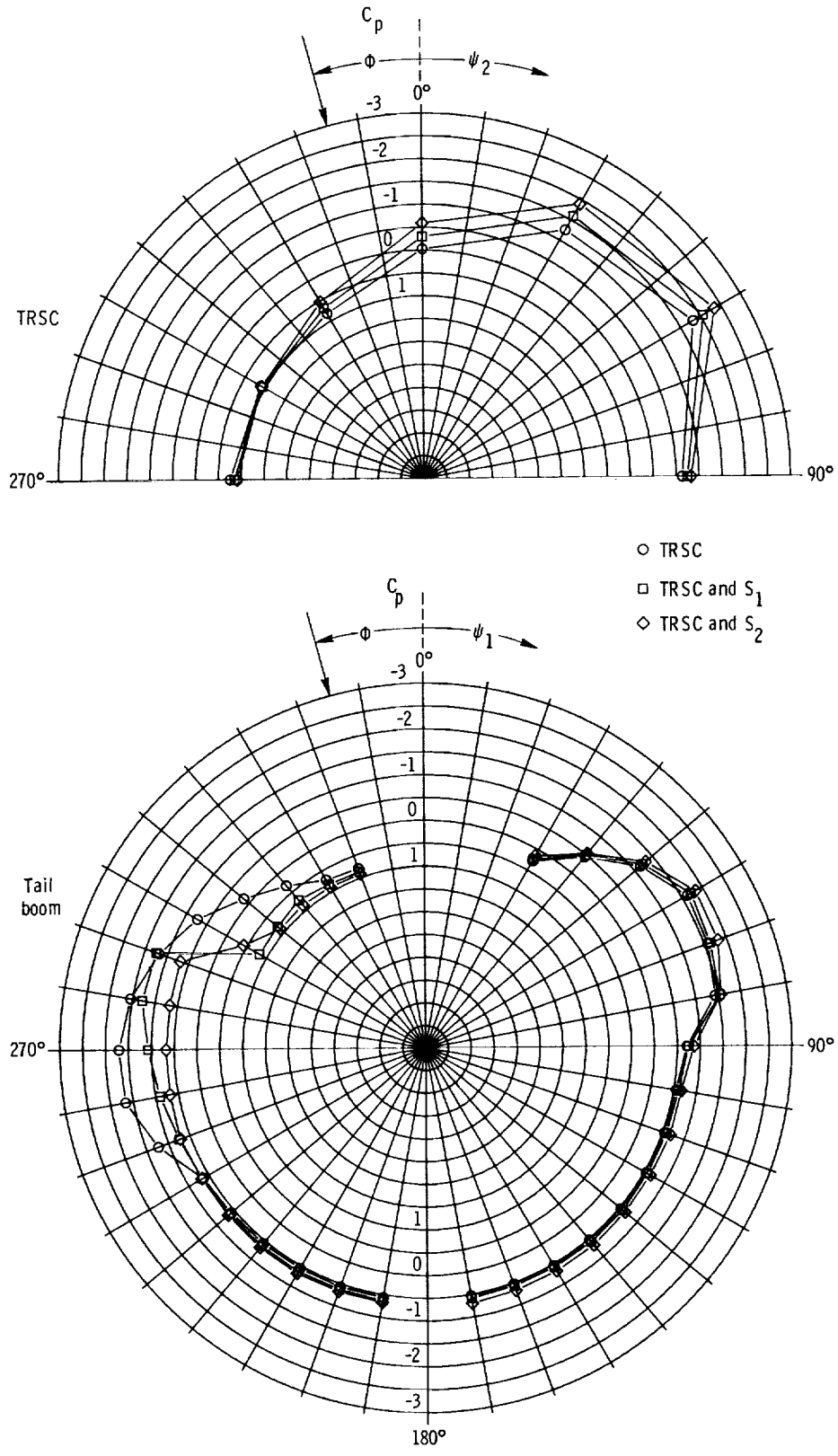

(c) $\phi = -15°$.

Figure 14. Continued.

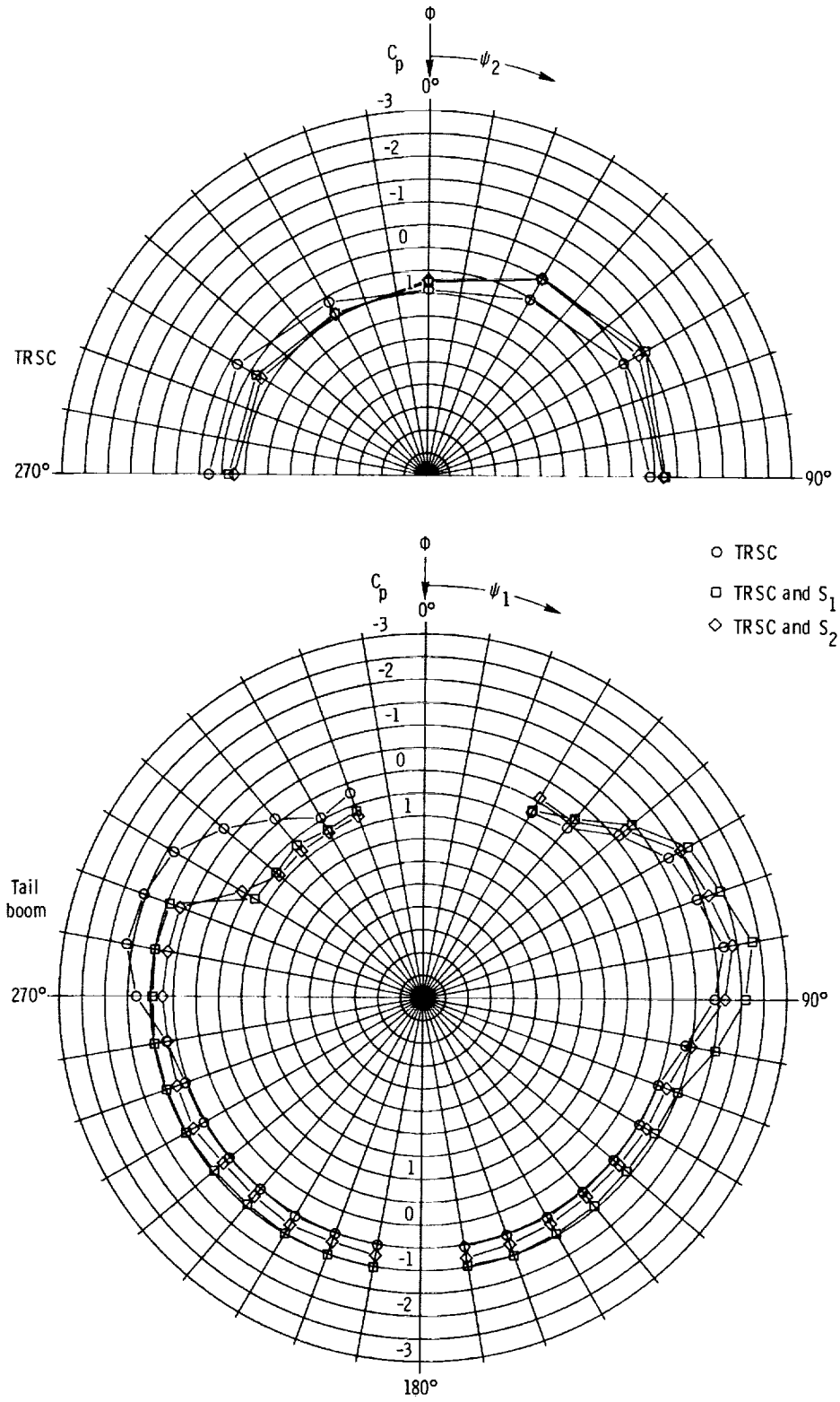

(d) $\phi = 0°$.

Figure 14. Continued.

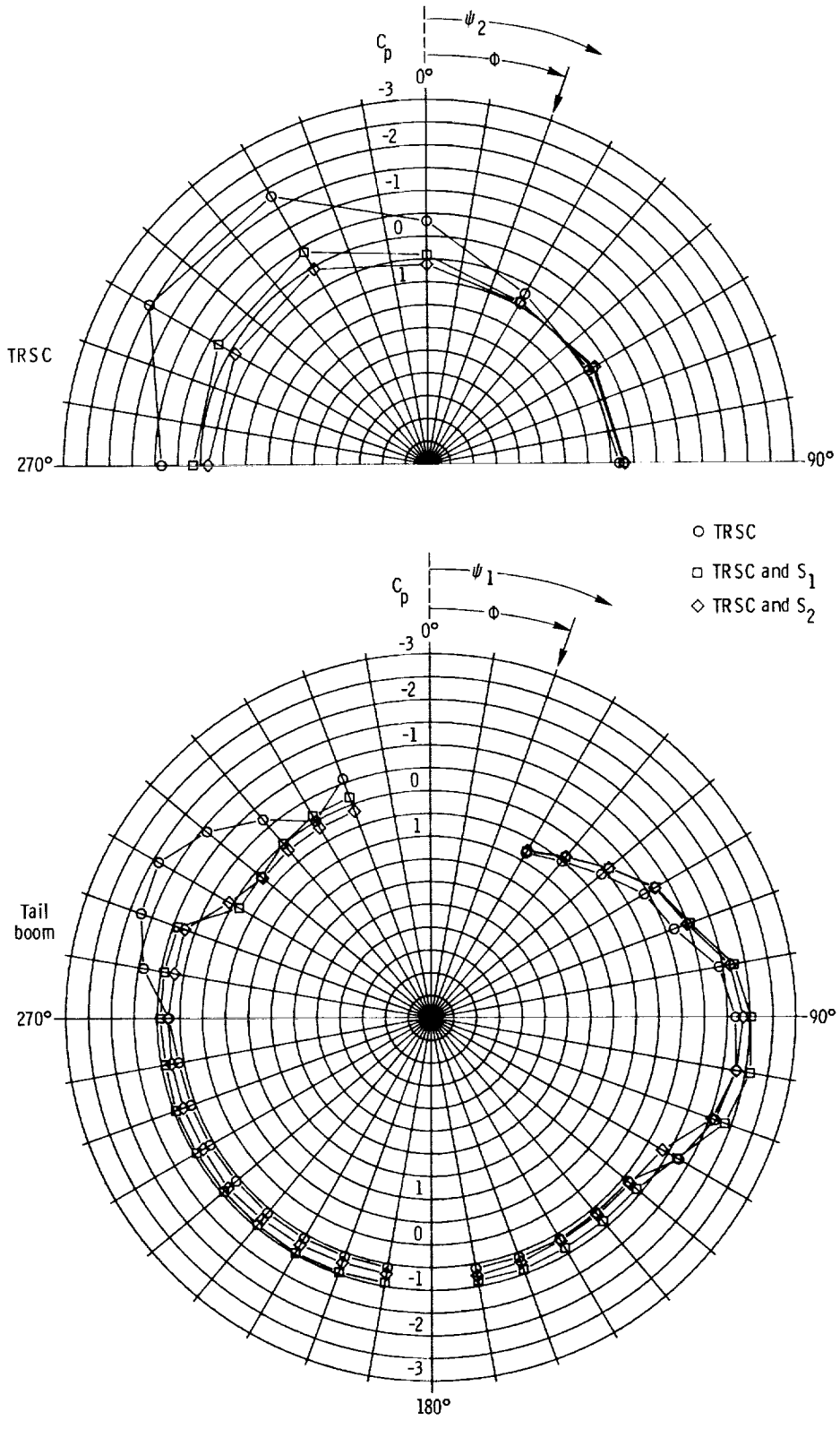

(e) $\phi = 20°$.

Figure 14. Continued.

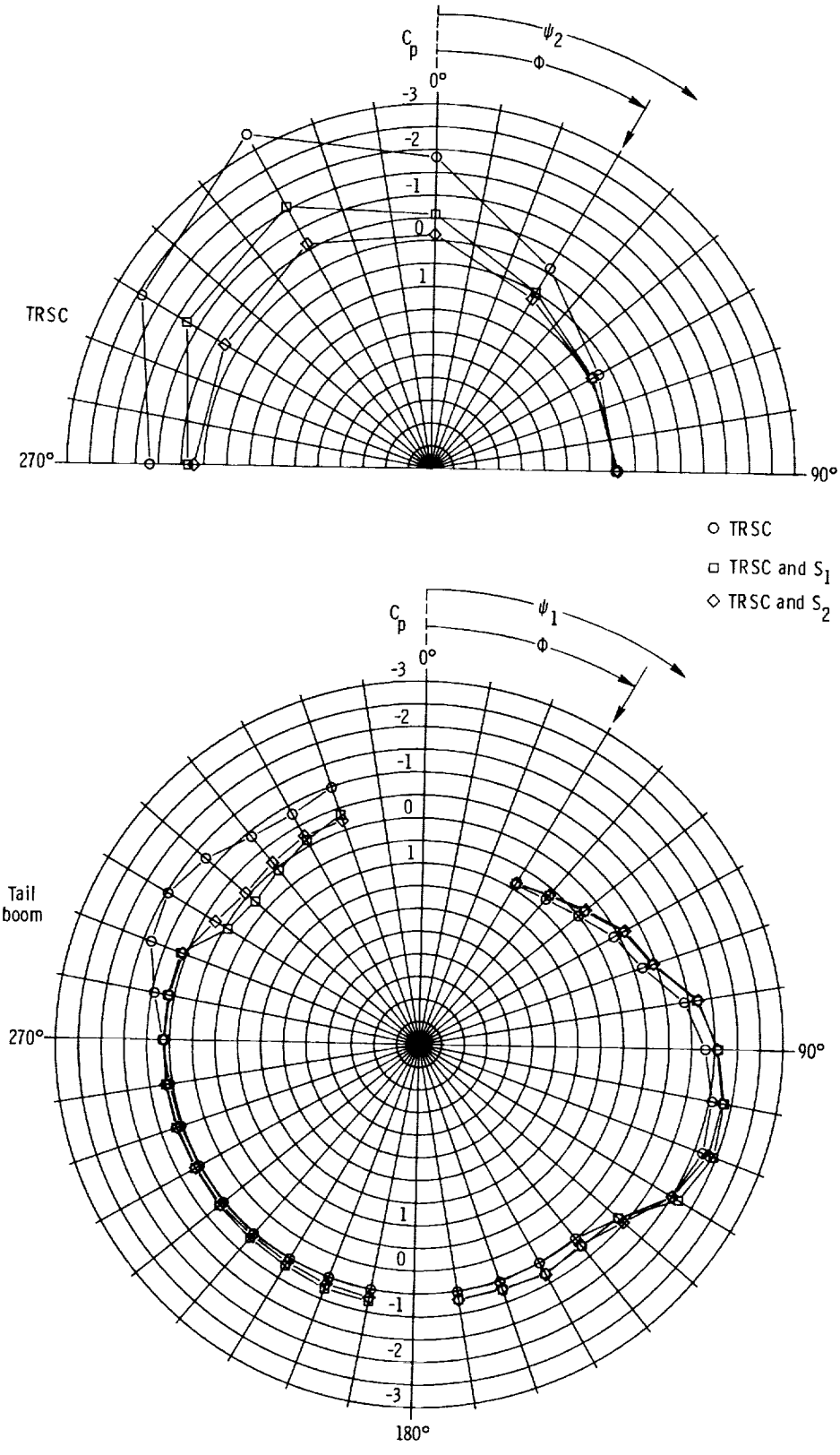

(f) $\phi = 30°$.

Figure 14. Continued.

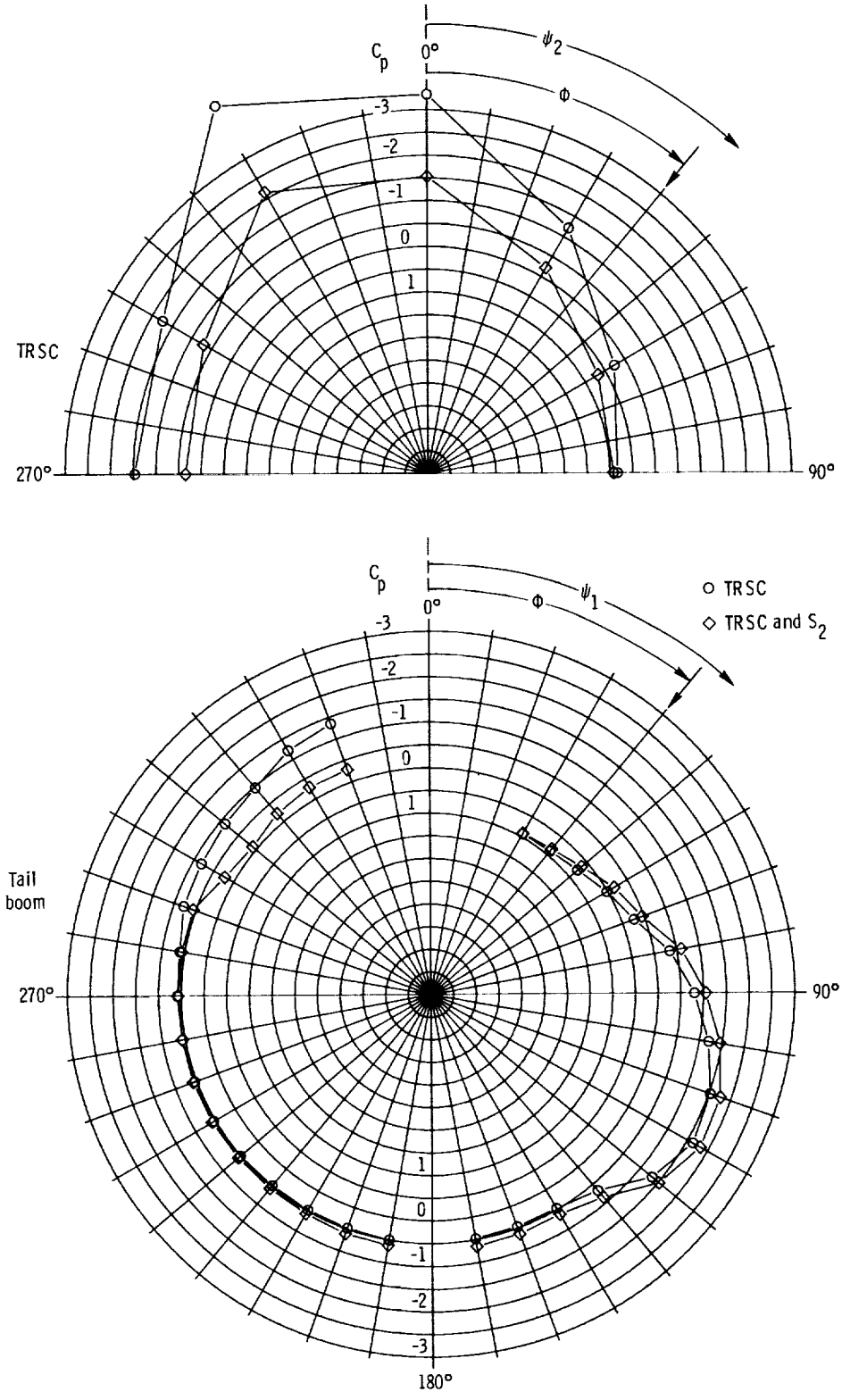

(g) $\phi = 40°$.

Figure 14. Continued.

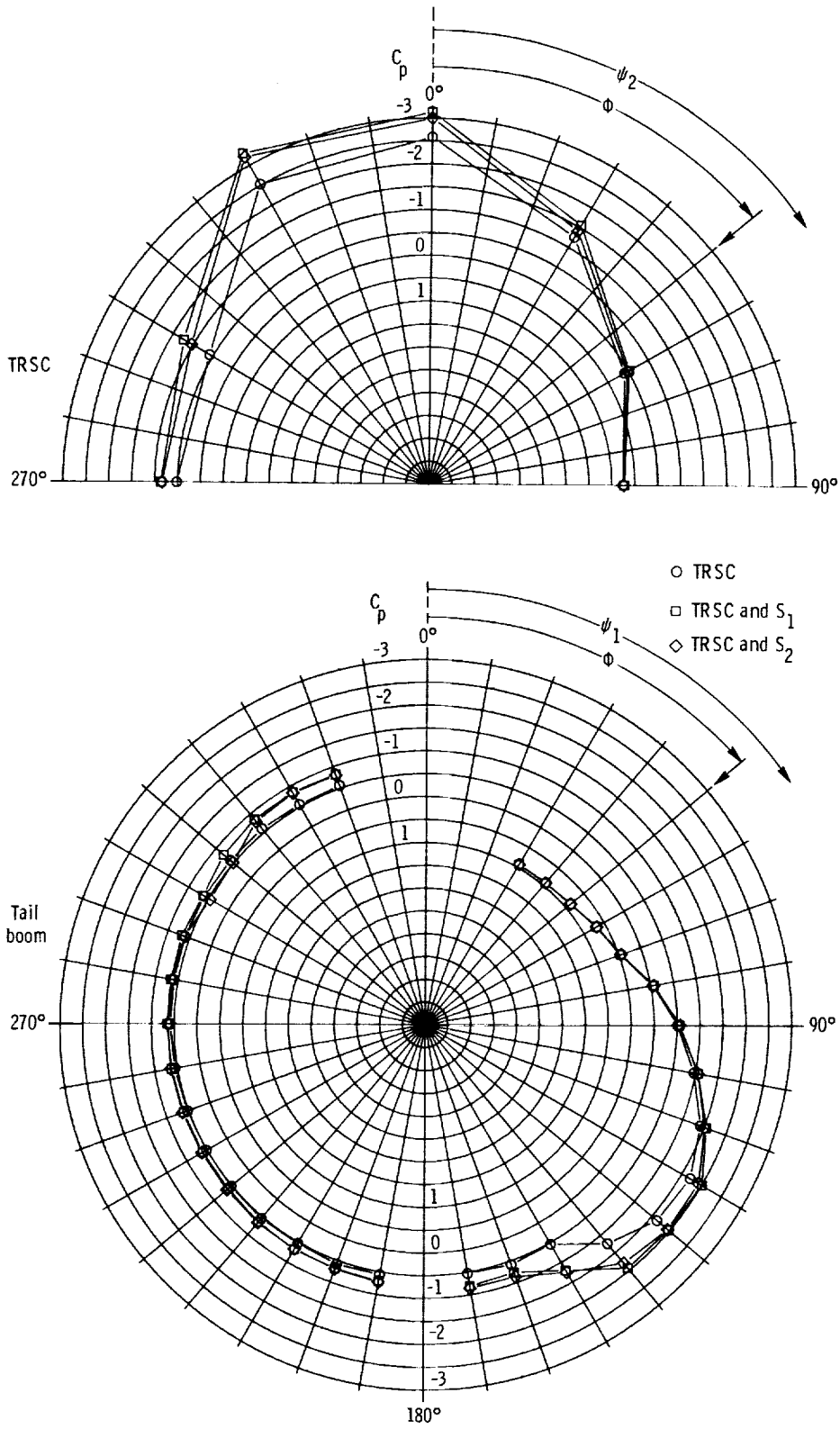

(h) $\phi = 50°$.

Figure 14. Continued.

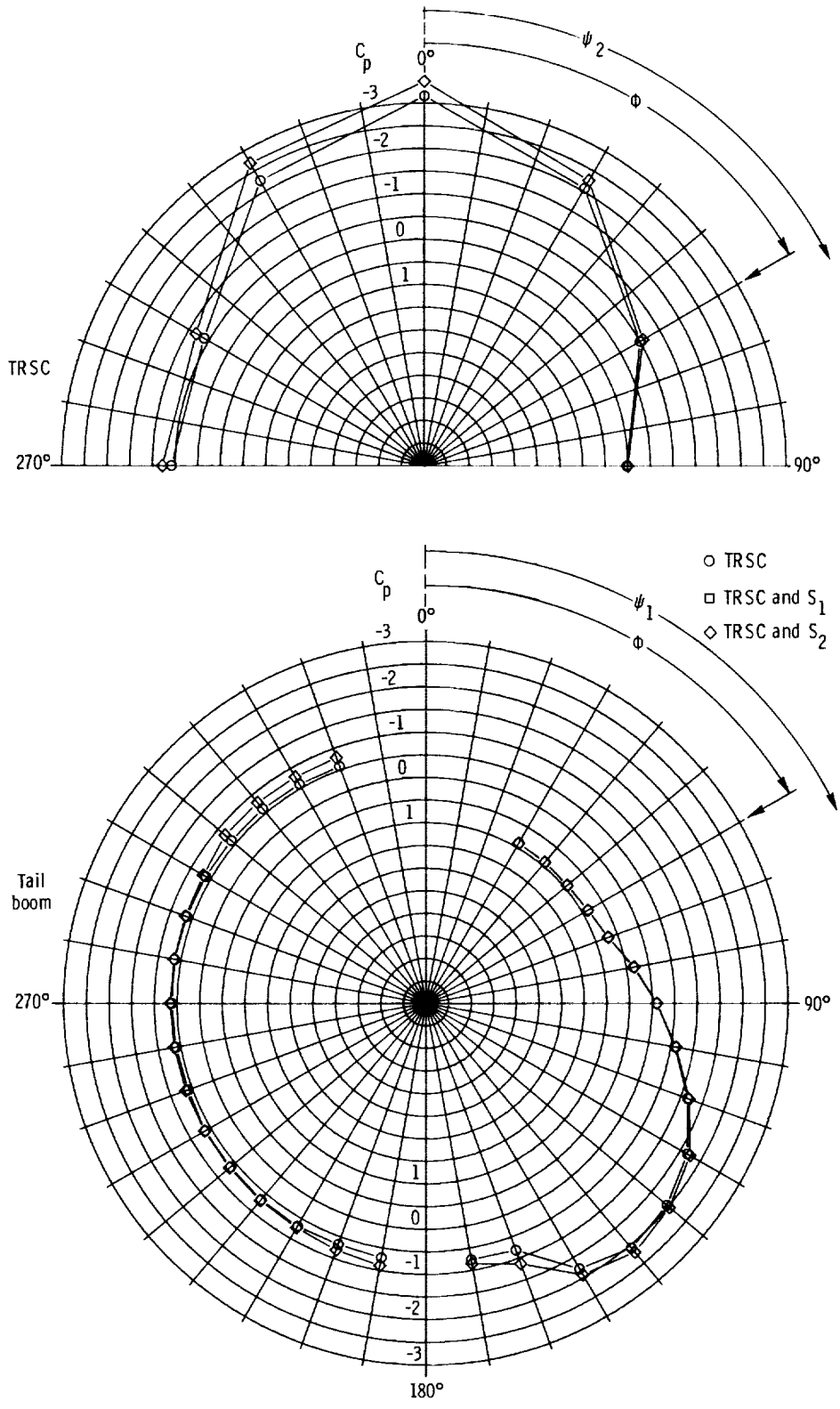

(i) $\phi = 60°$.

Figure 14. Concluded.

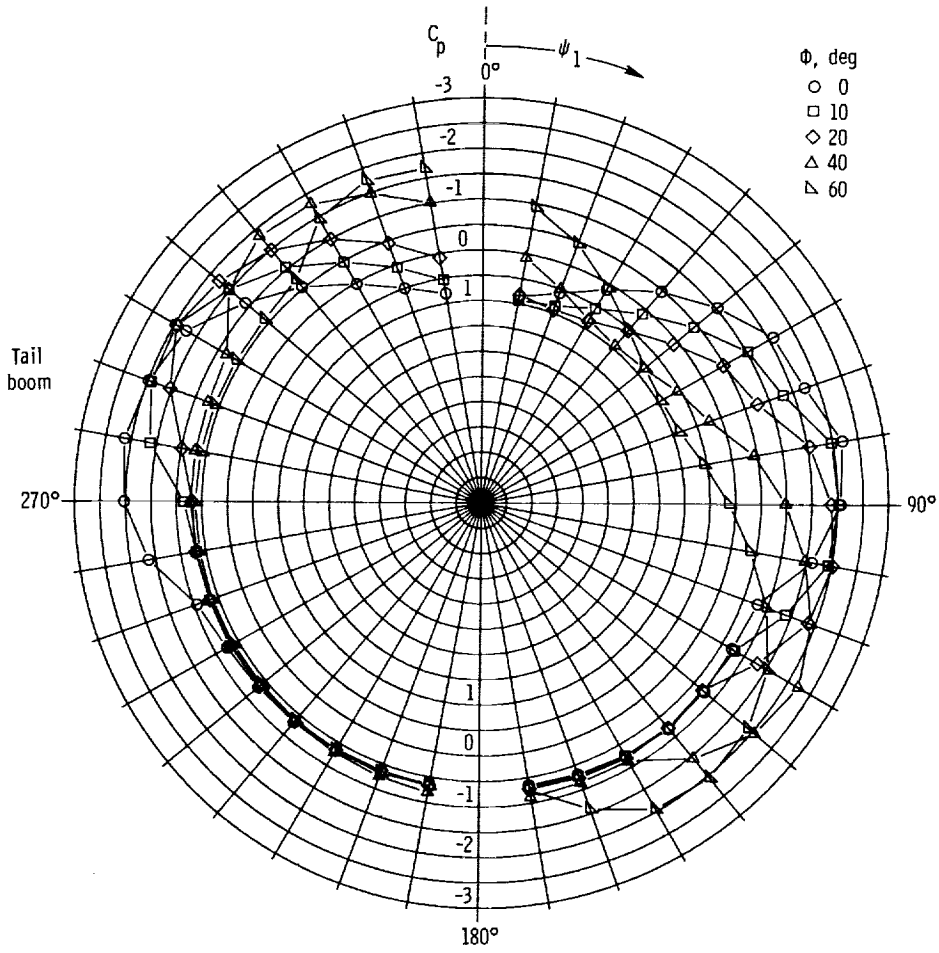

Figure 15. Effects of flow incidence on pressure distributions for AH-64 shape without TRSC at $q = 45$ psf.

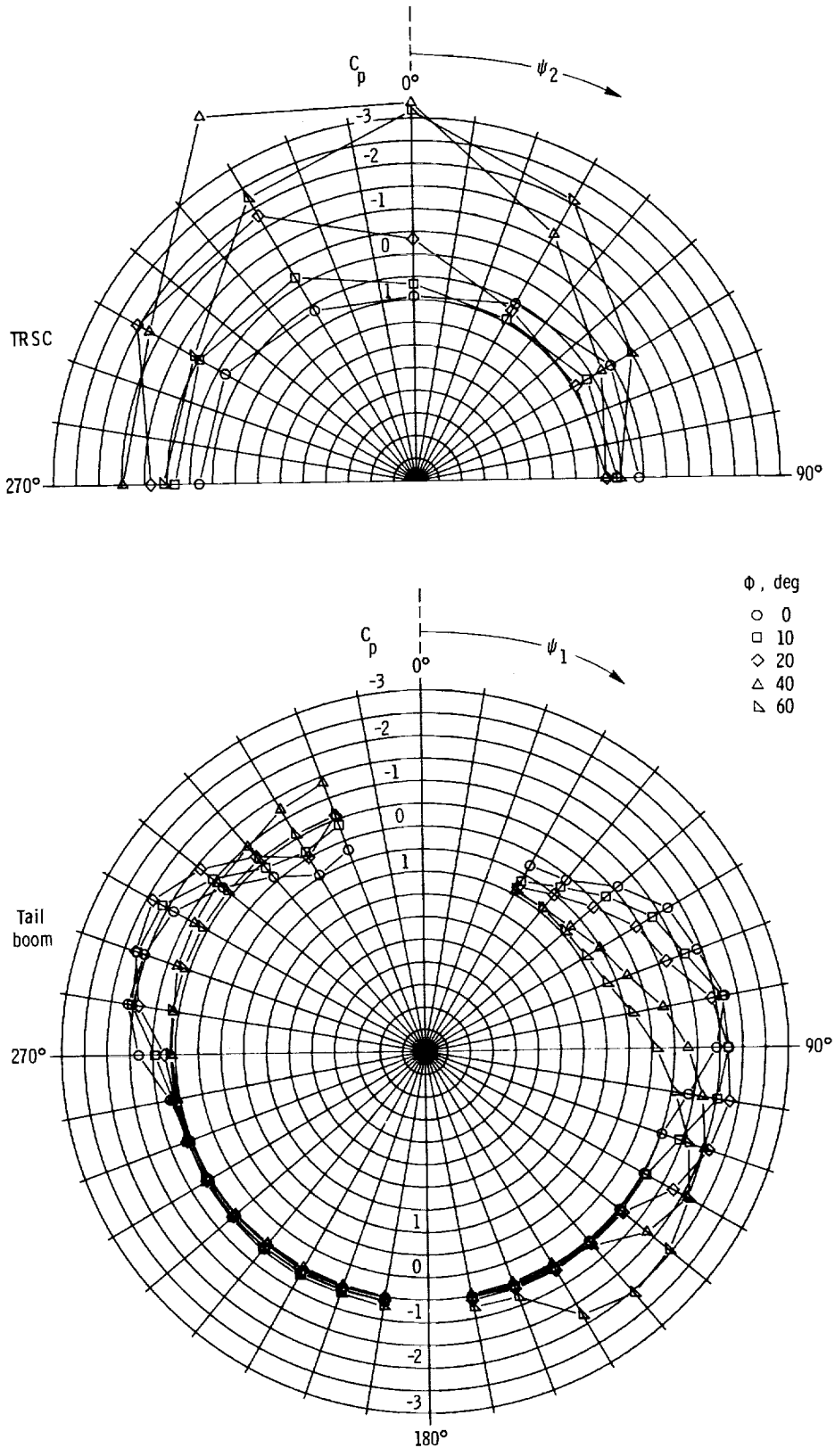

Figure 16. Effects of flow incidence on pressure distributions for the AH-64 shape with TRSC at $q = 35$ psf.

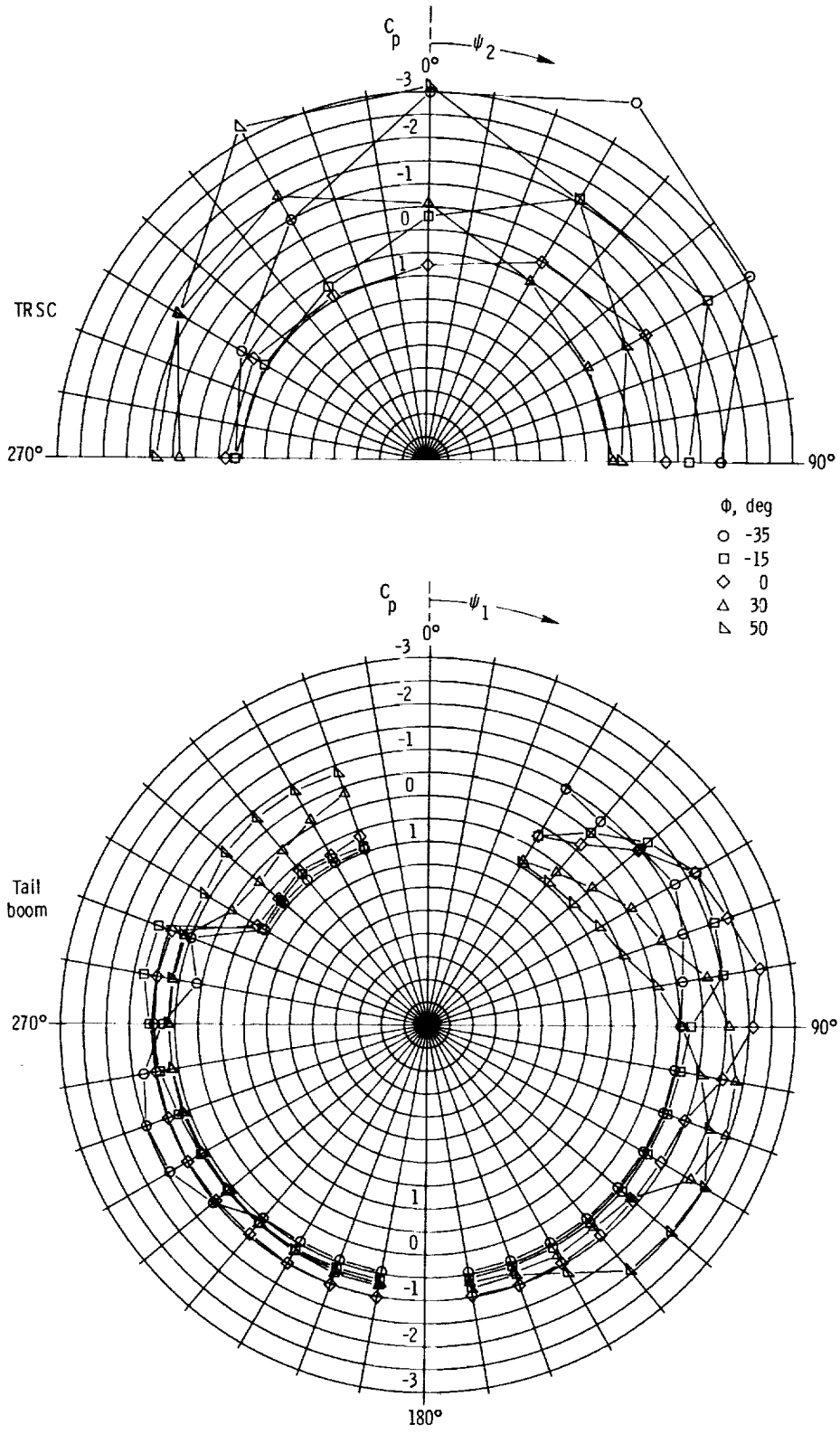

Figure 17. Effects of flow incidence on pressure distributions for AH-64 shape with TRSC and S_1 spoiler at $q = 35$ psf.

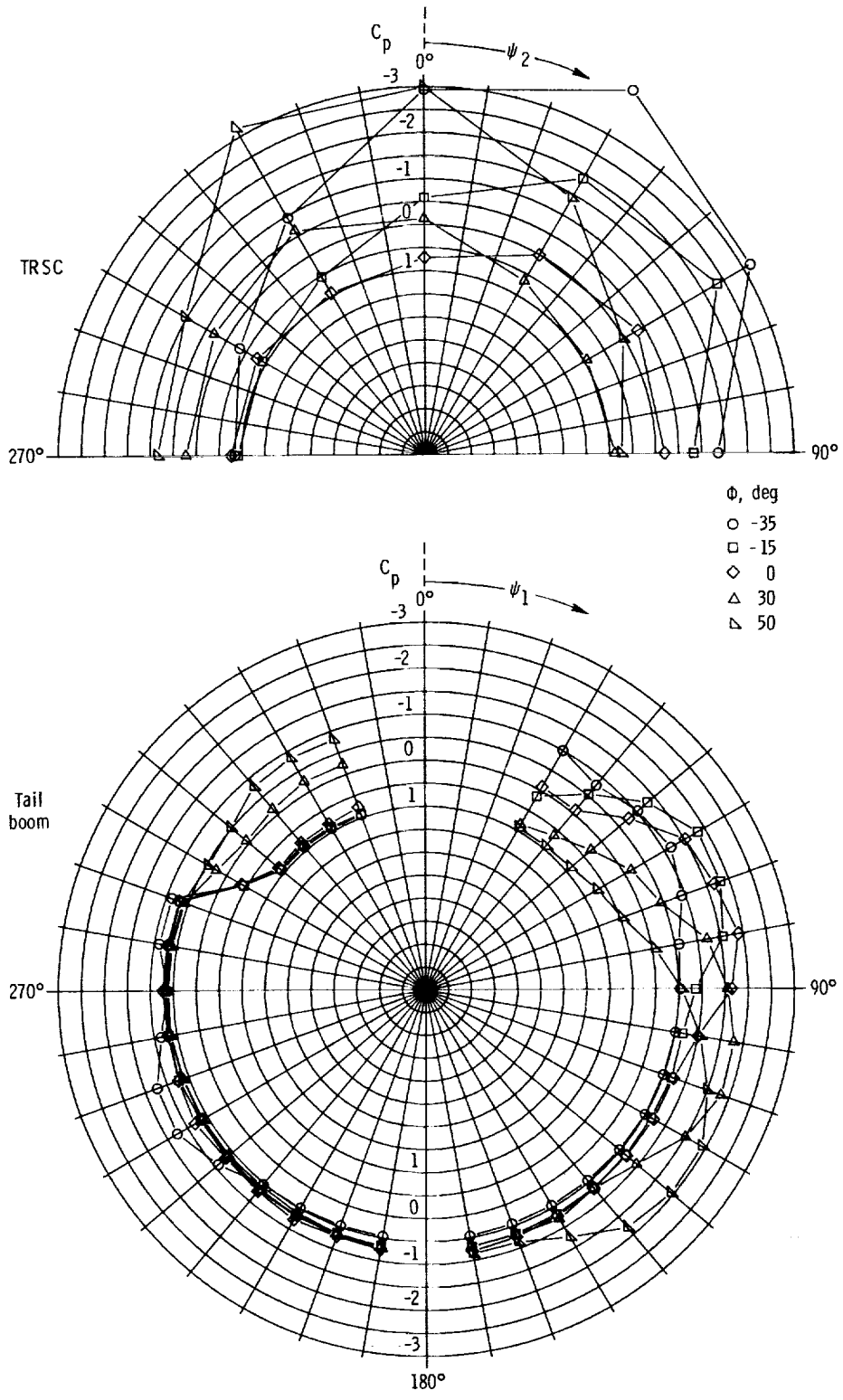

Figure 18. Effects of flow incidence on pressure distributions on AH-64 shape with TRSC and S_2 spoiler at $q = 35$ psf.

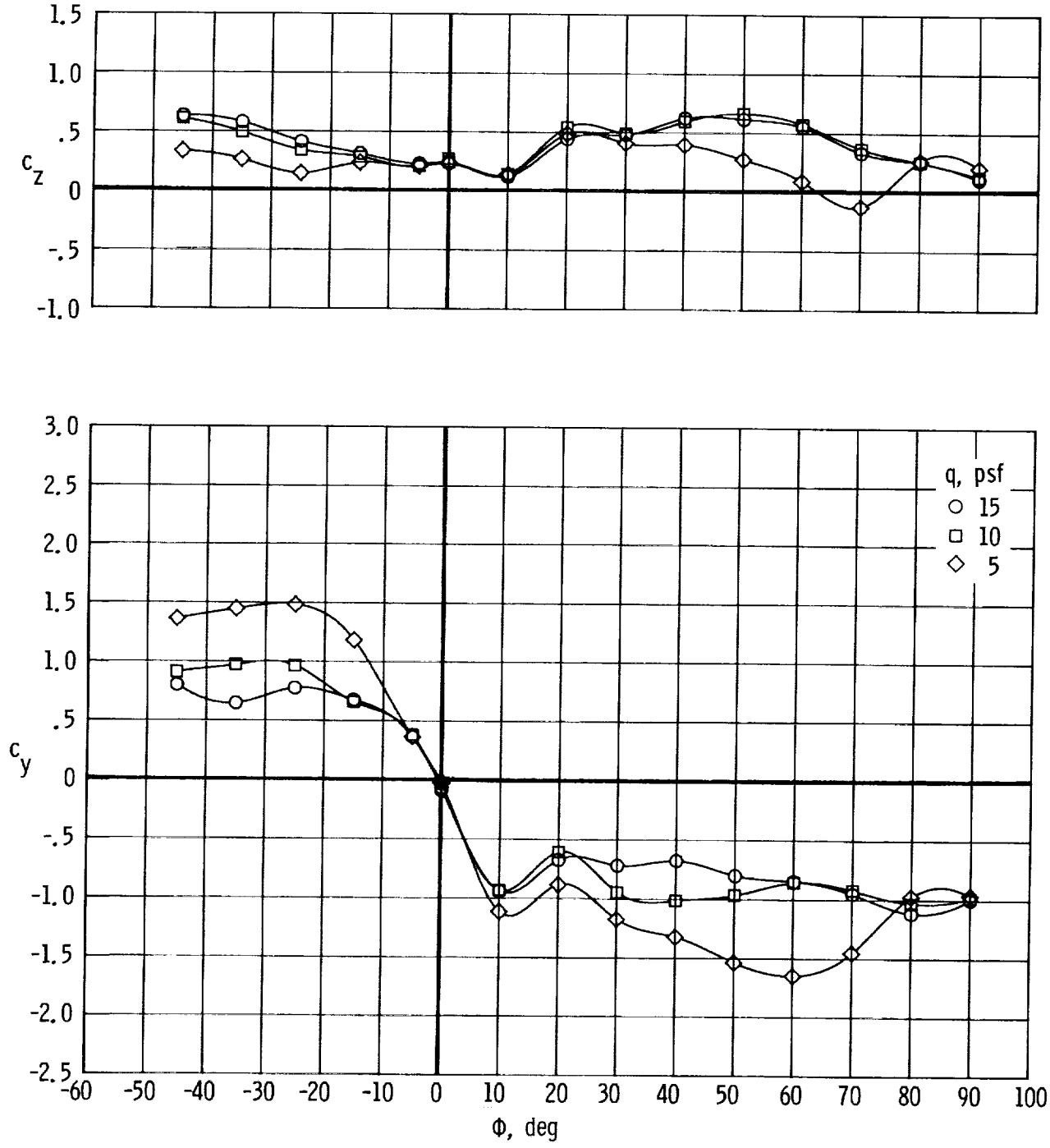

(a) c_z and c_y plotted against ϕ.

Figure 19. Effects of dynamic pressure on drag and side force of UH-60 shape without TRSC.

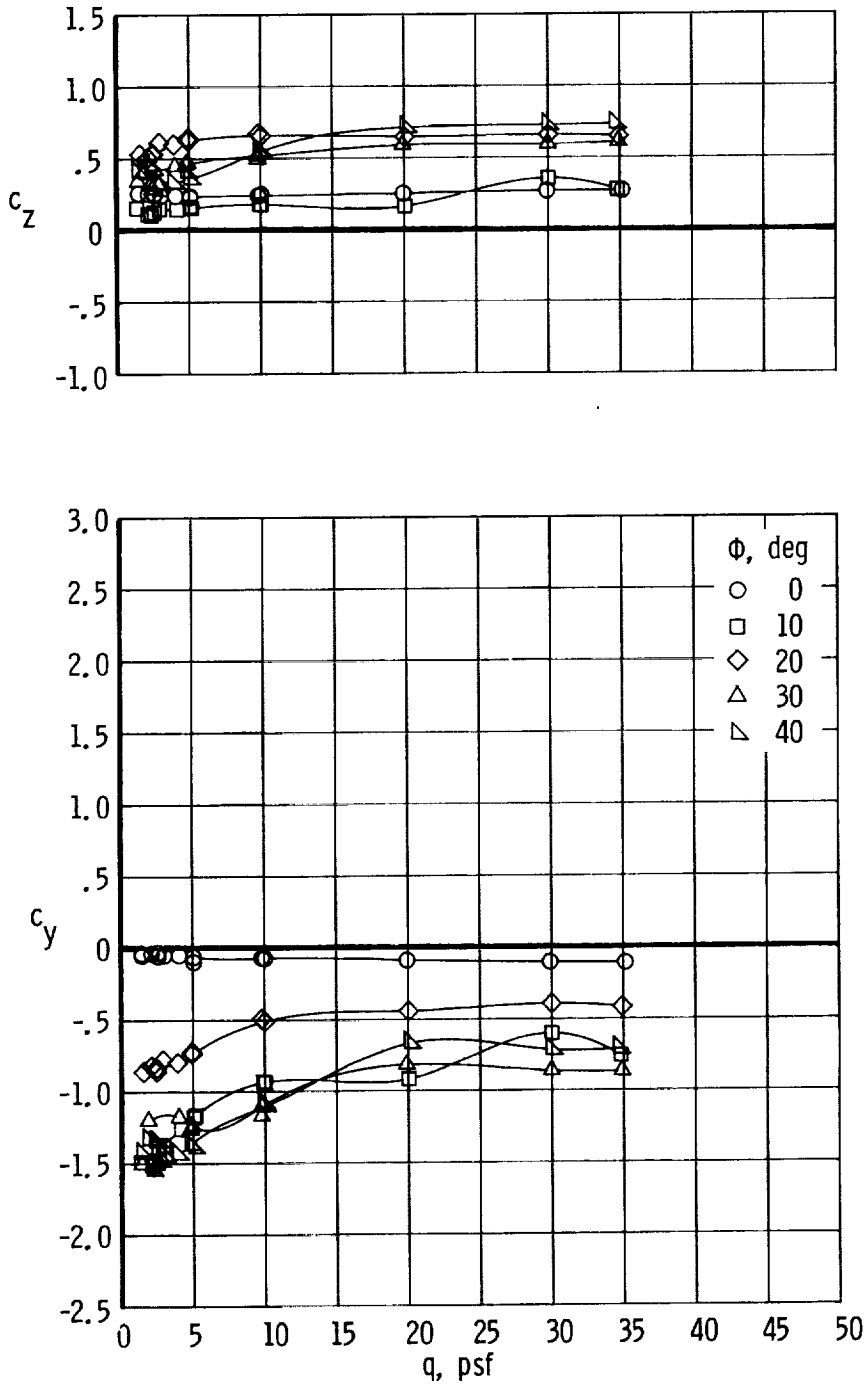

(b) c_z and c_y plotted against q.

Figure 19. Concluded.

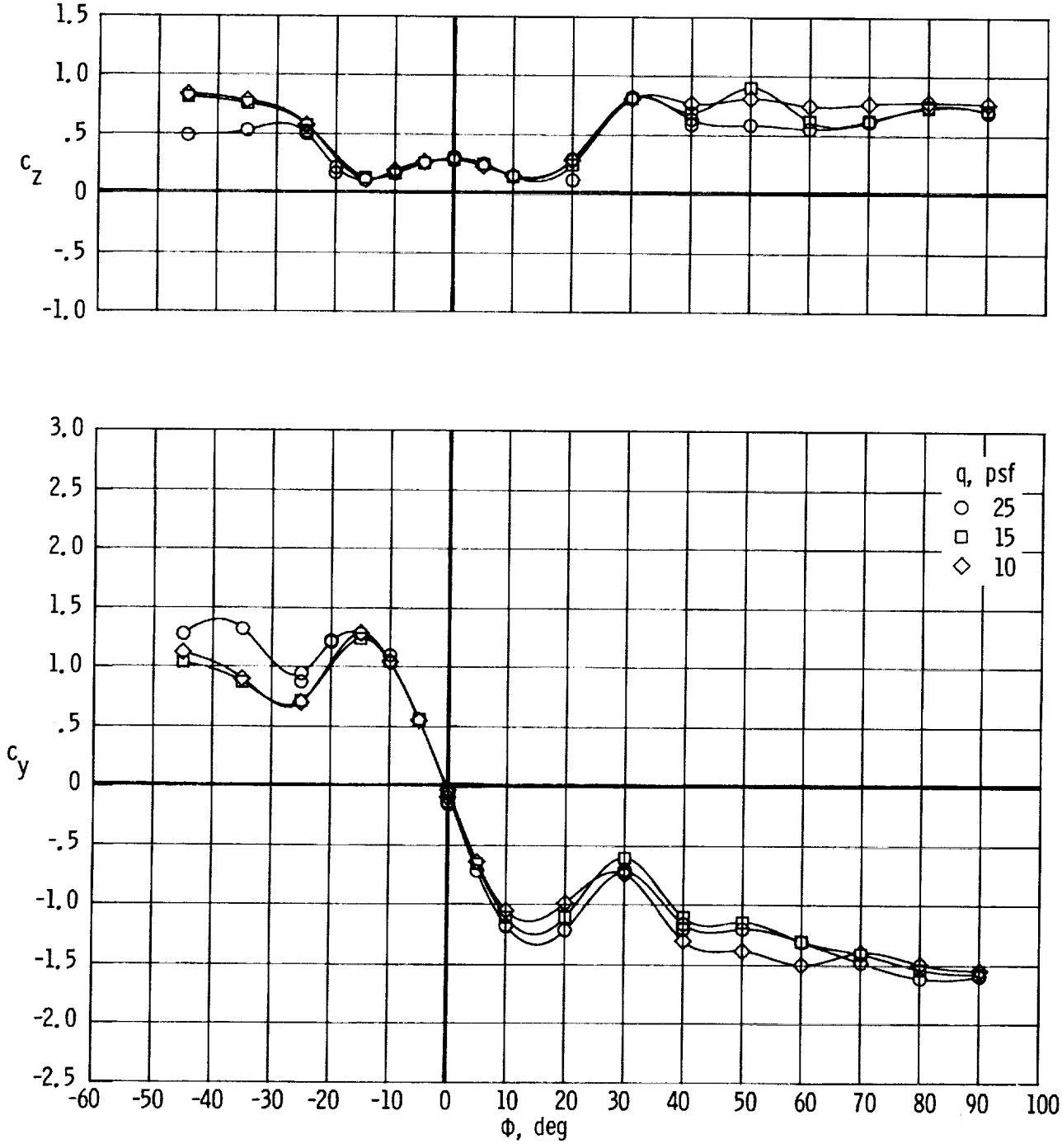

(a) c_z and c_y plotted against ϕ.

Figure 20. Effects of dynamic pressure on drag and side force of UH-60 shape with TRSC.

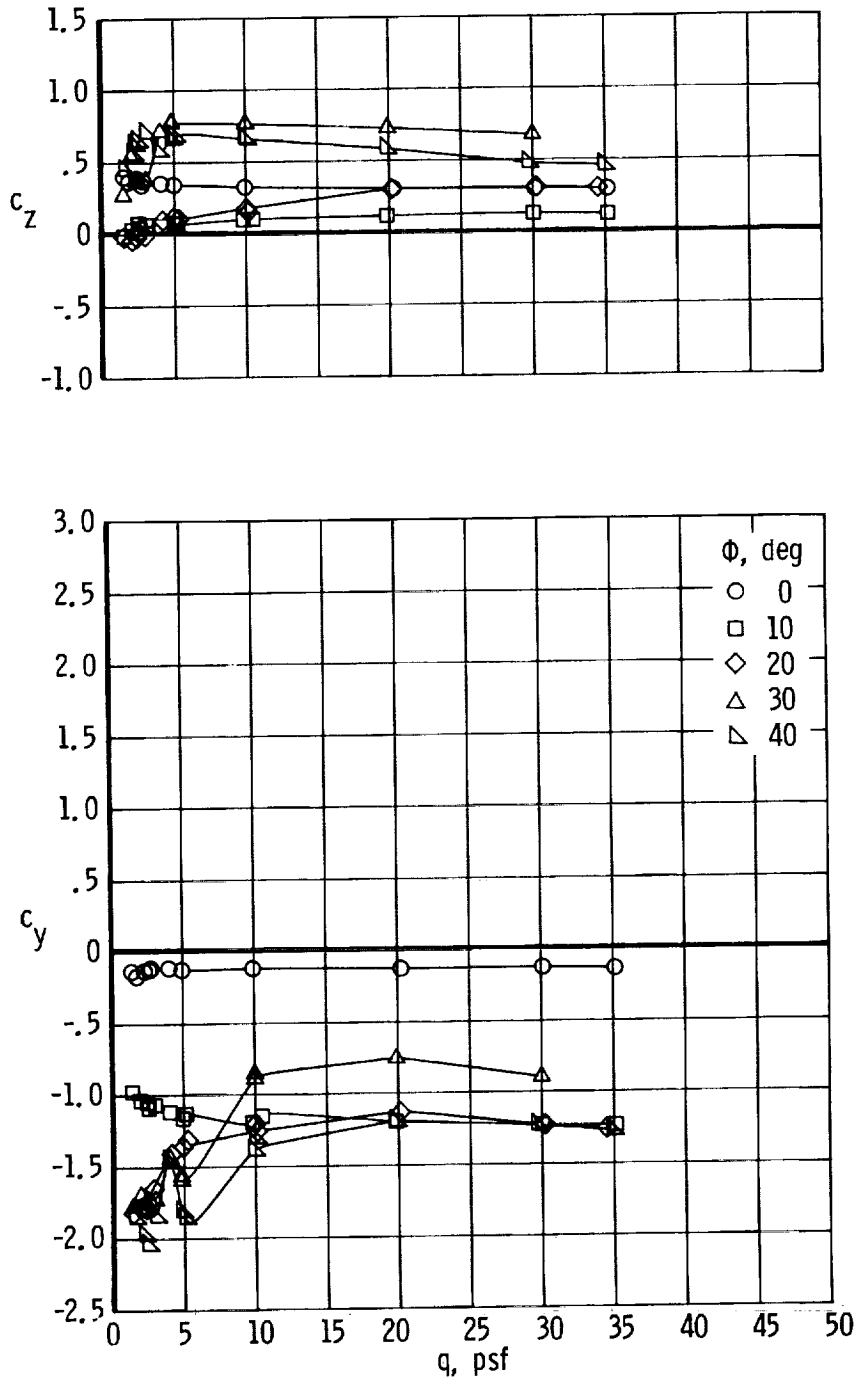

(b) c_z and c_y plotted against q.

Figure 20. Concluded.

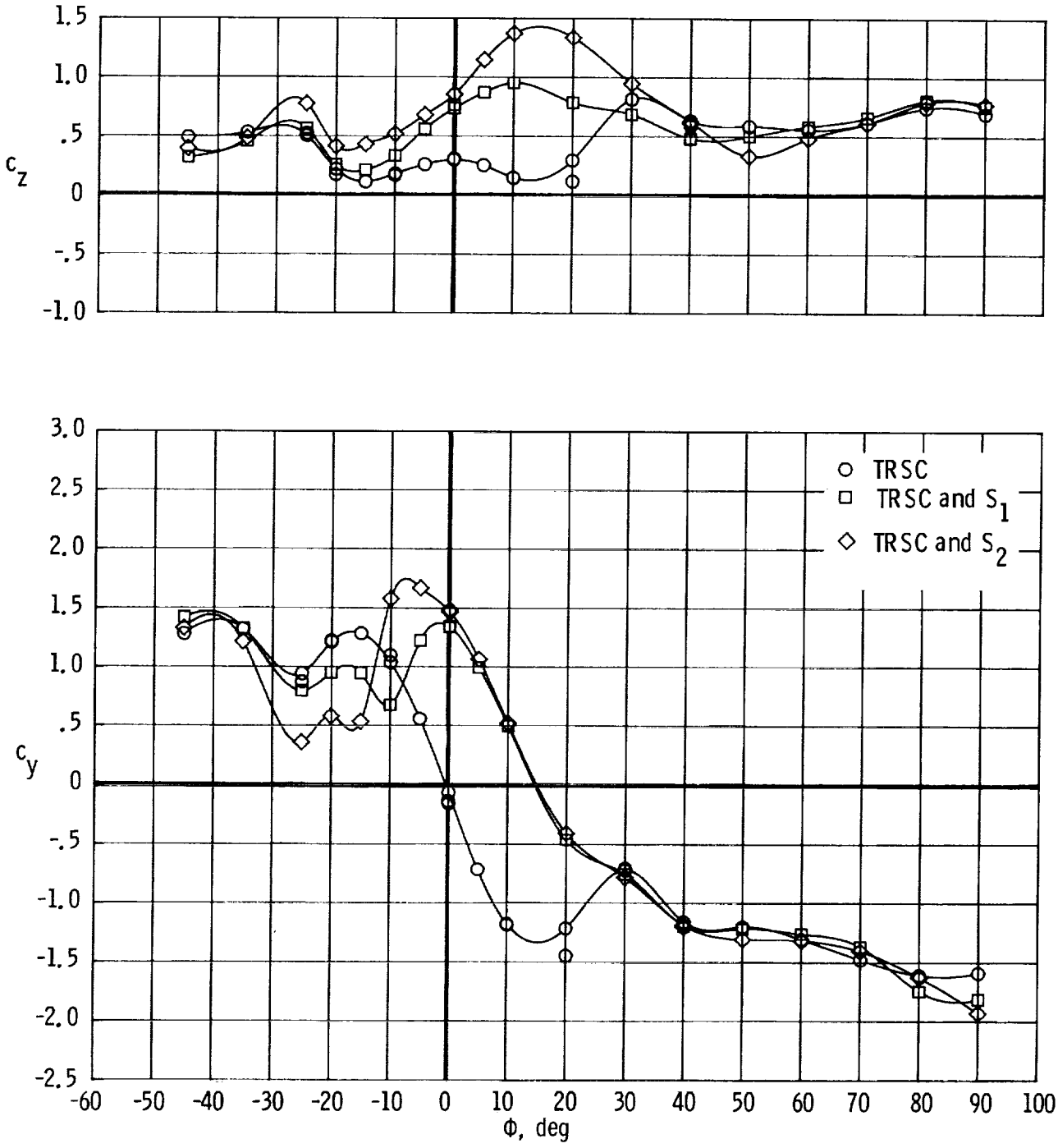

Figure 21. Comparison of drag and side-force variation with flow incidence of UH-60 shape with TRSC and S_1 and S_2 spoilers at $q = 25$ psf.

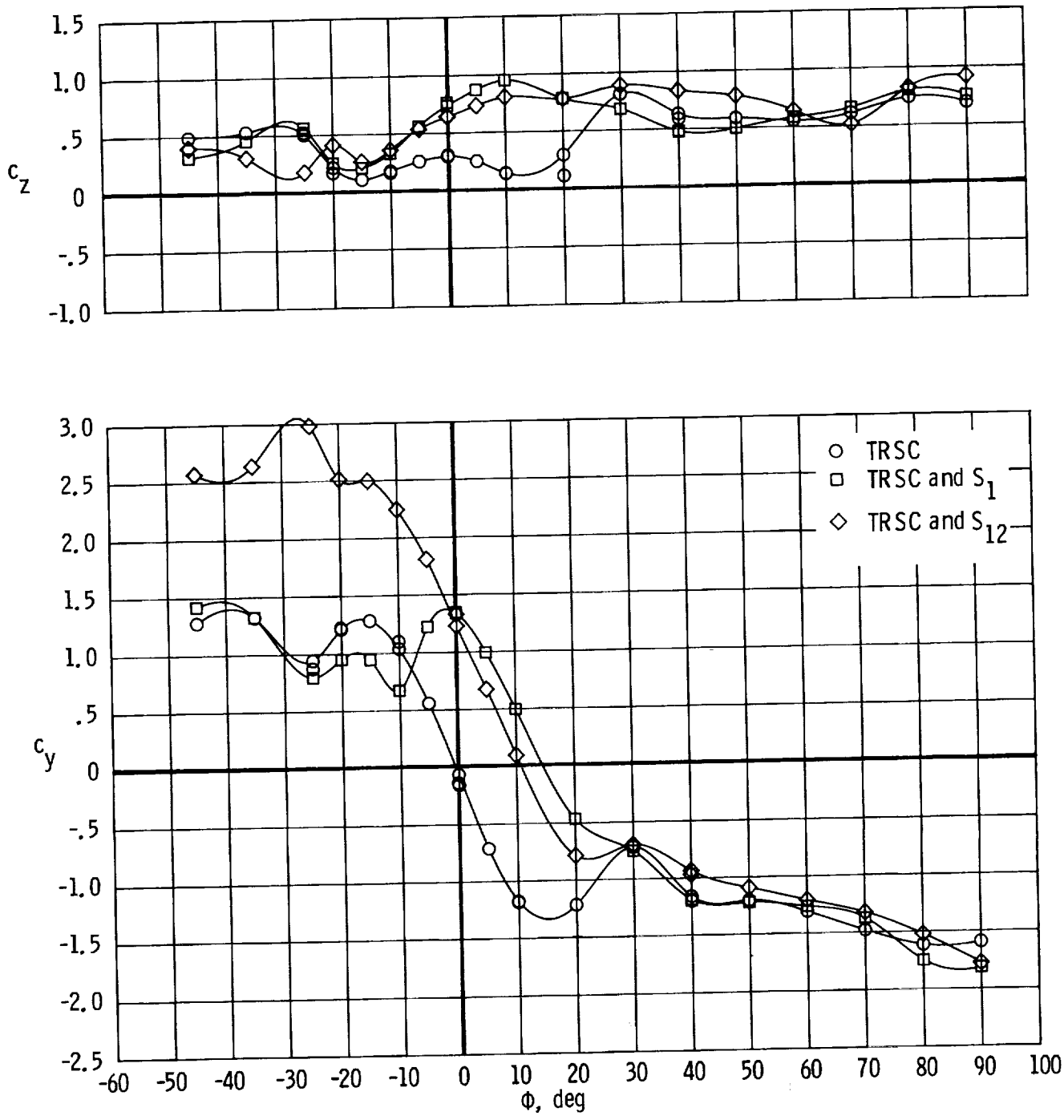

Figure 22. Comparison of drag and side-force variation with flow incidence of UH-60 shape with TRSC and spoilers S_1 and S_{12}.

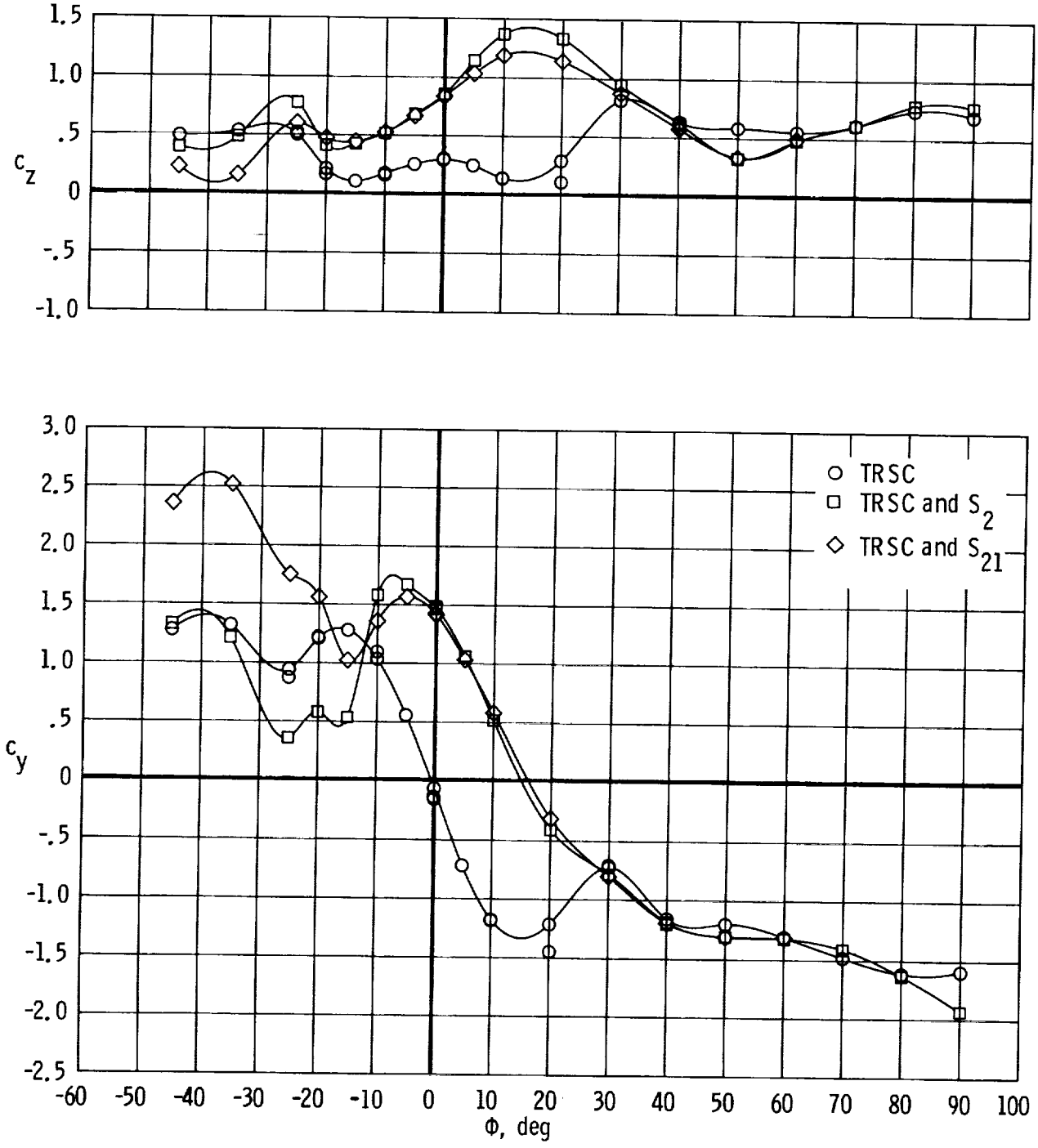

Figure 23. Comparison of drag and side-force variation with flow incidence of UH-60 shape with TRSC and spoilers S_2 and S_{21} at $q = 25$ psf.

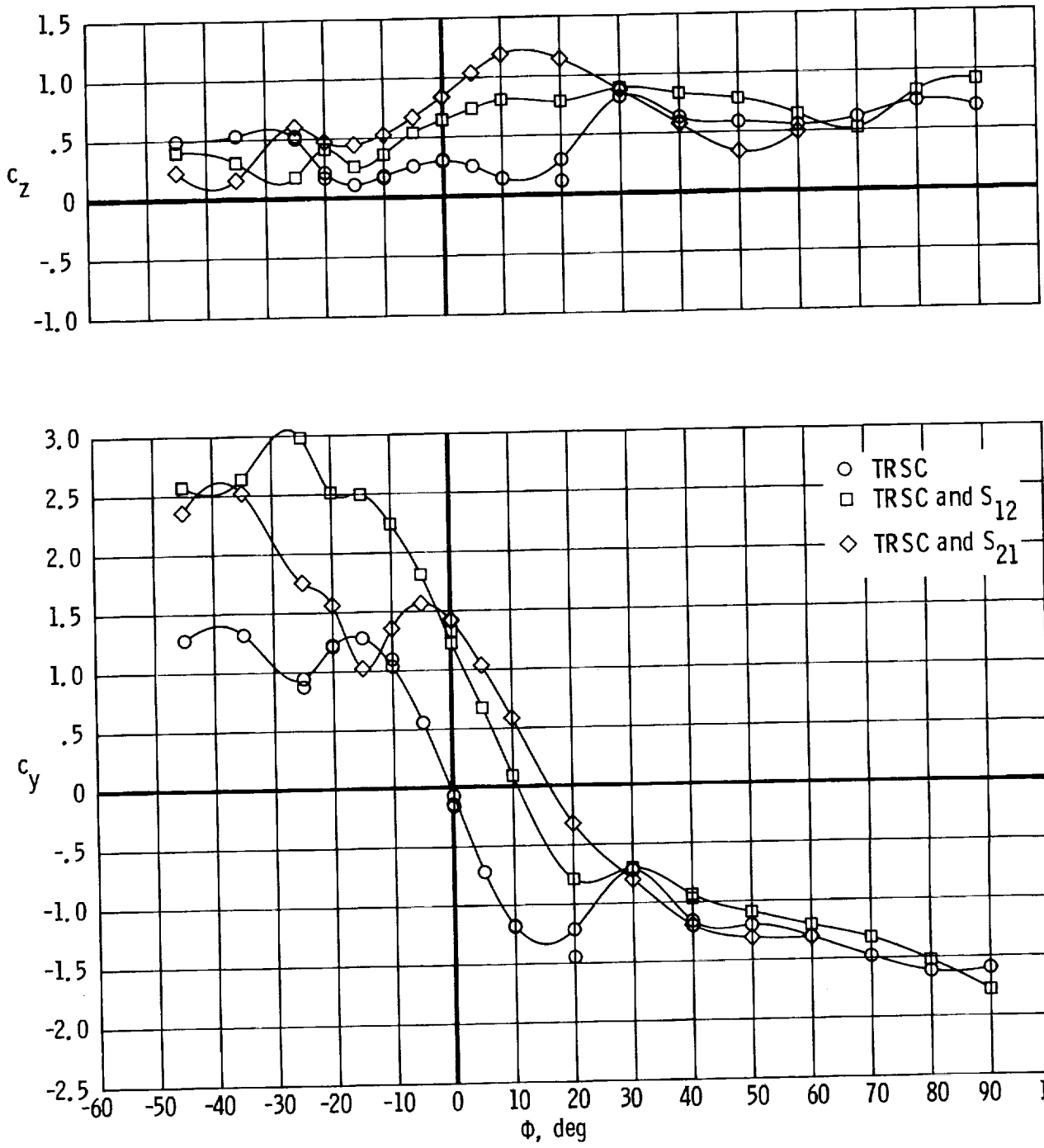

Figure 24. Comparison of drag and side-force variation with flow incidence of UH-60 shape with TRSC and spoilers S_{12} and S_{21} at $q = 25$ psf.

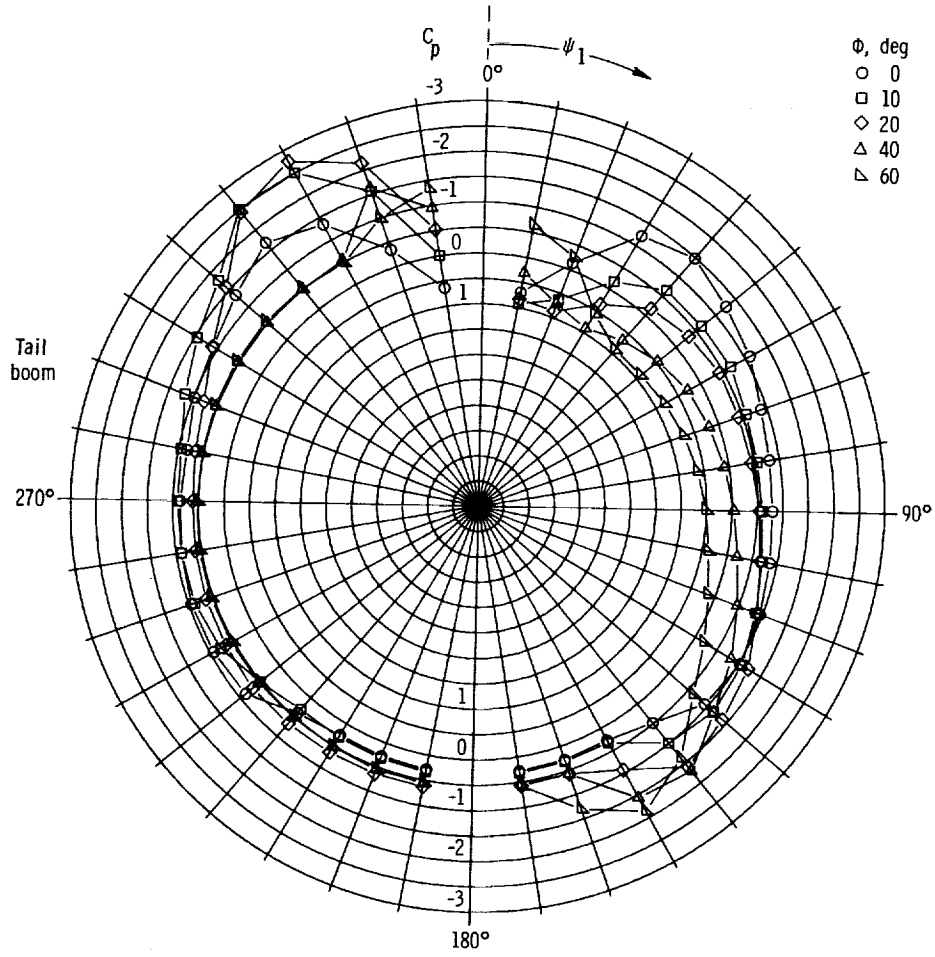

Figure 25. Effects of flow incidence on pressure distributions on UH-60 shape without TRSC at $q = 15$ psf.

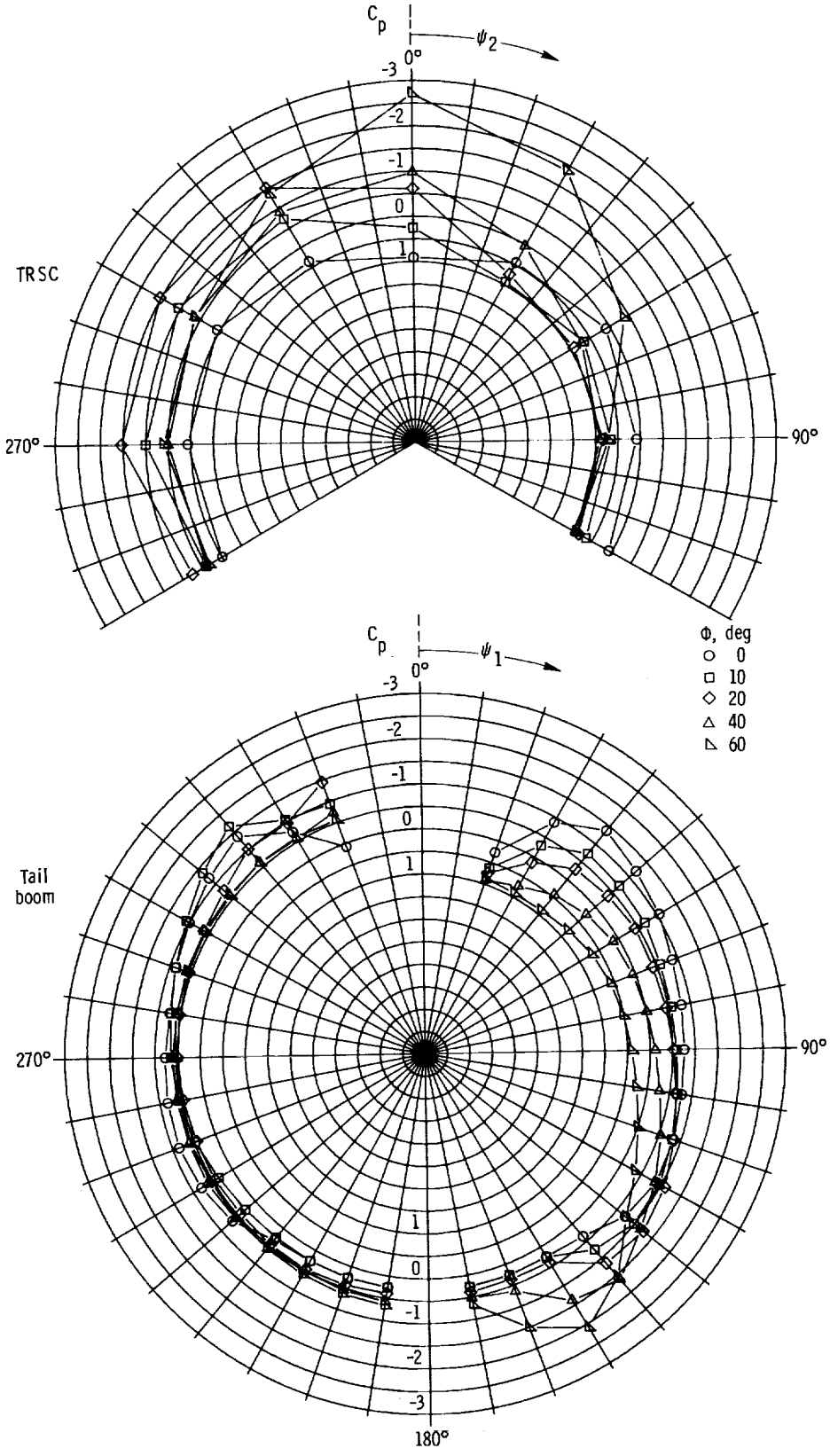

Figure 26. Effects of flow incidence on pressure distributions on UH-60 shape with TRSC at $q = 15$ psf.

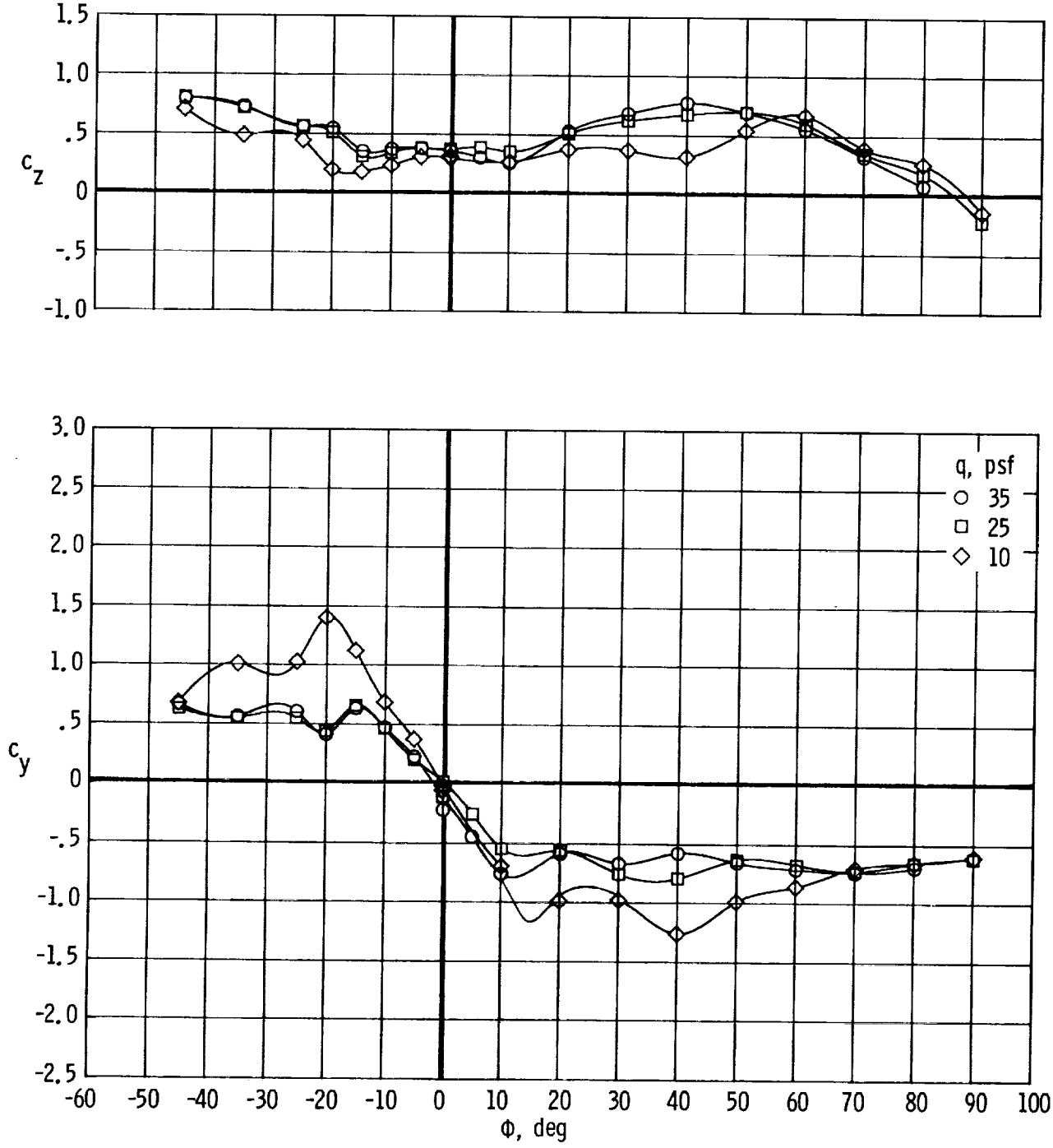

(a) c_z and c_y plotted against ϕ.

Figure 27. Effects of dynamic pressure on drag and side force of UH-1H shape without TRSC.

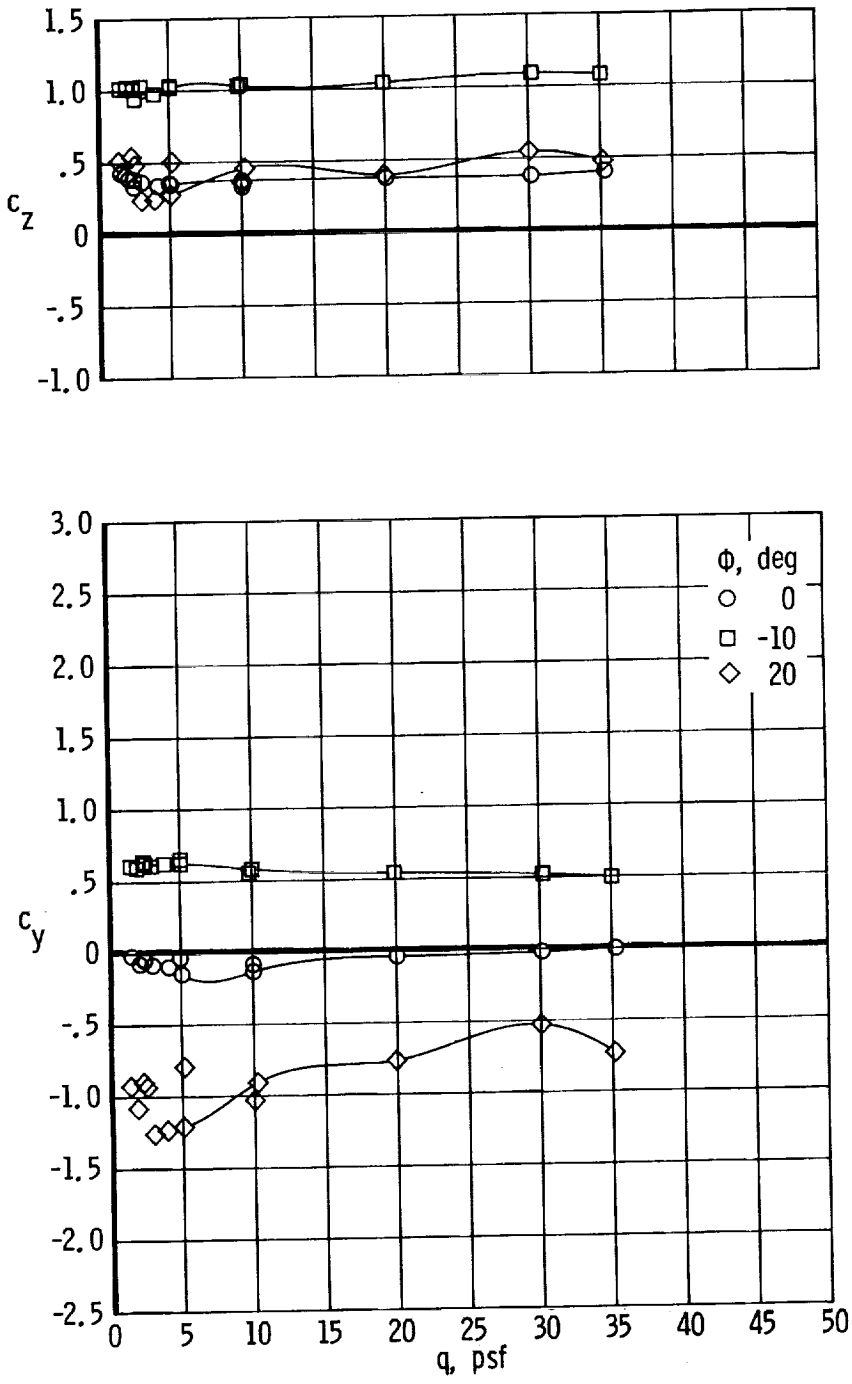

(b) c_z and c_y plotted against q.

Figure 27. Concluded.

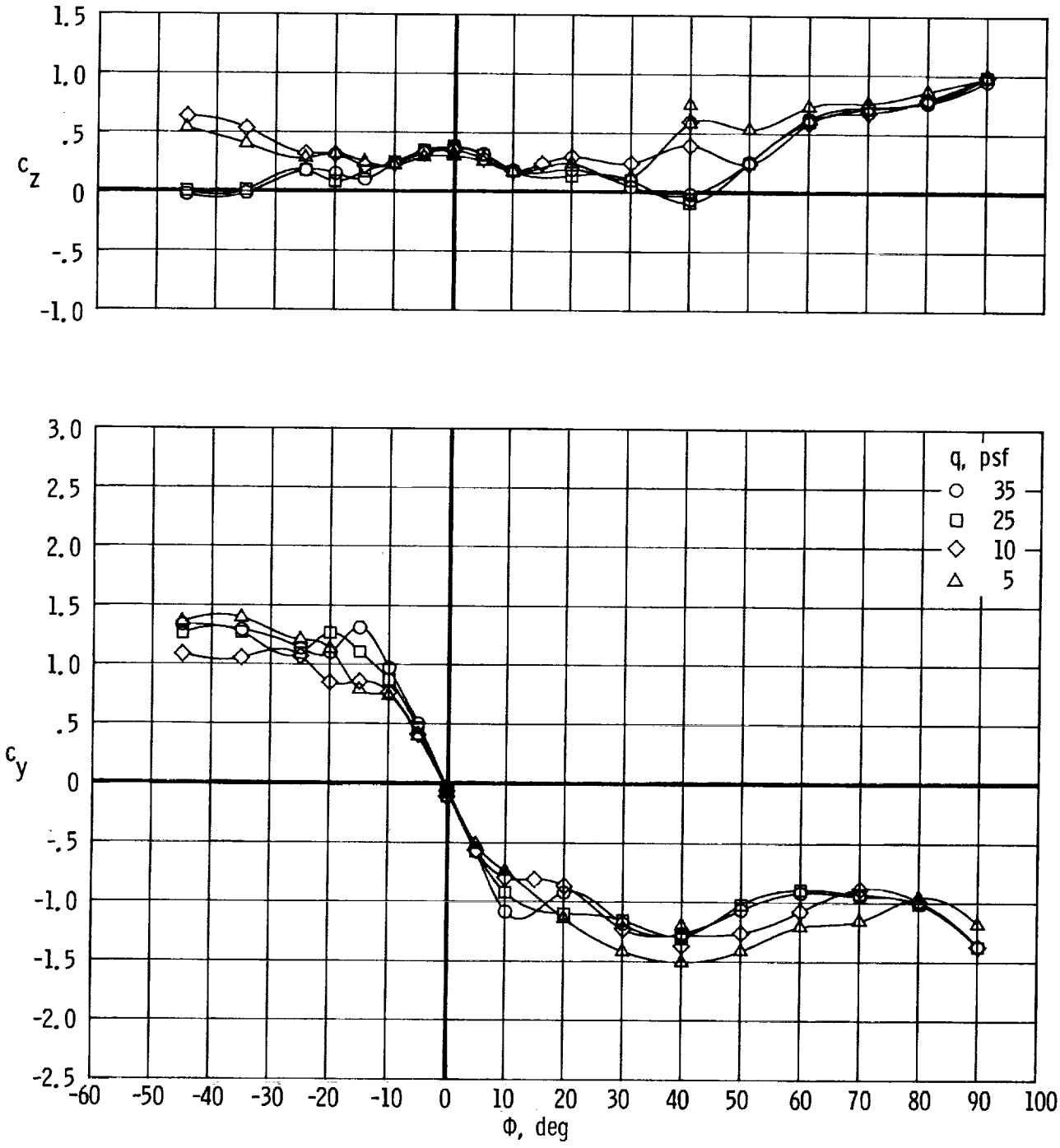

(a) c_z and c_y plotted against ϕ.

Figure 28. Effects of dynamic pressure on drag and side force of UH-1H shape with TRSC.

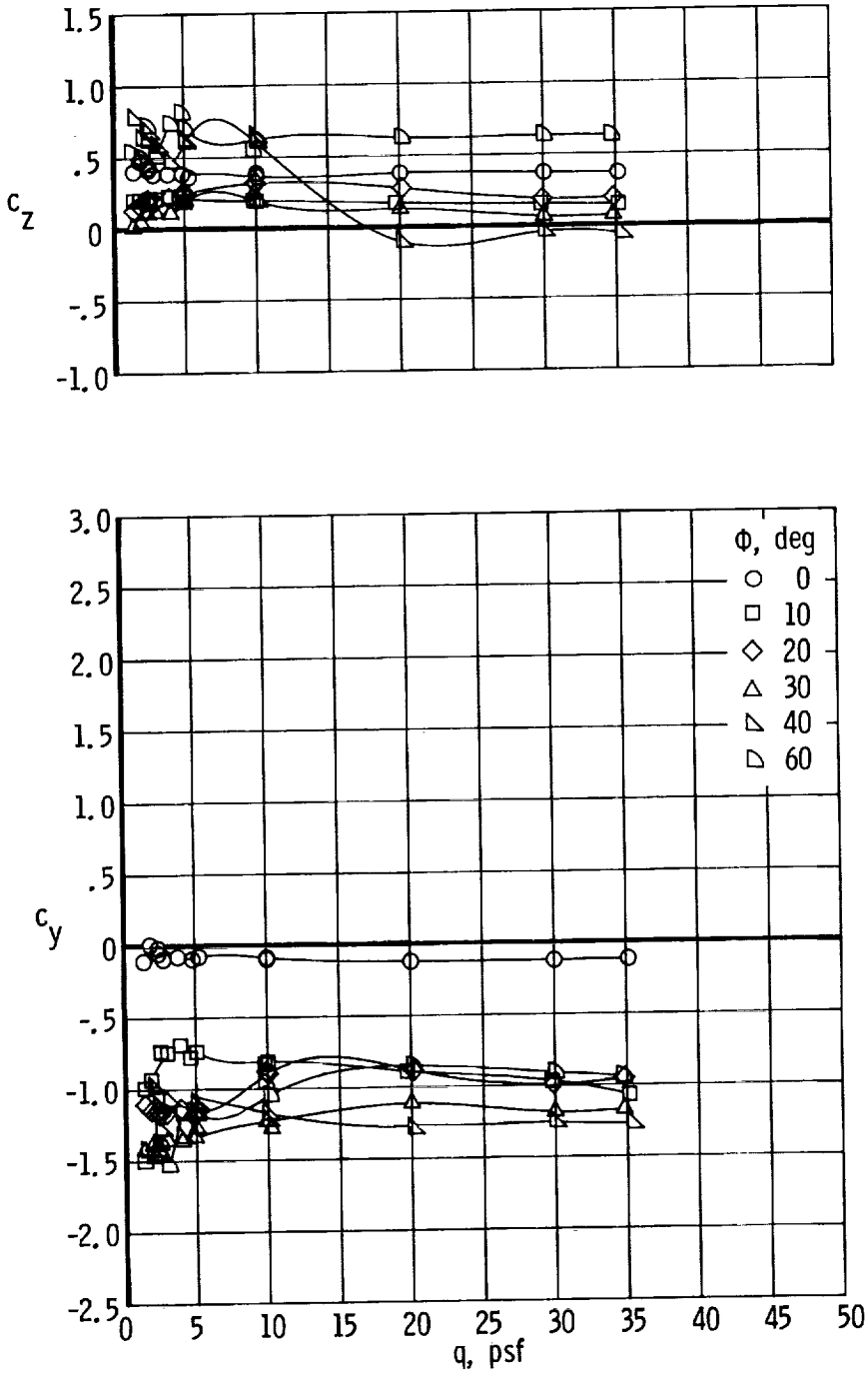

(b) c_z and c_y plotted against q.

Figure 28. Concluded.

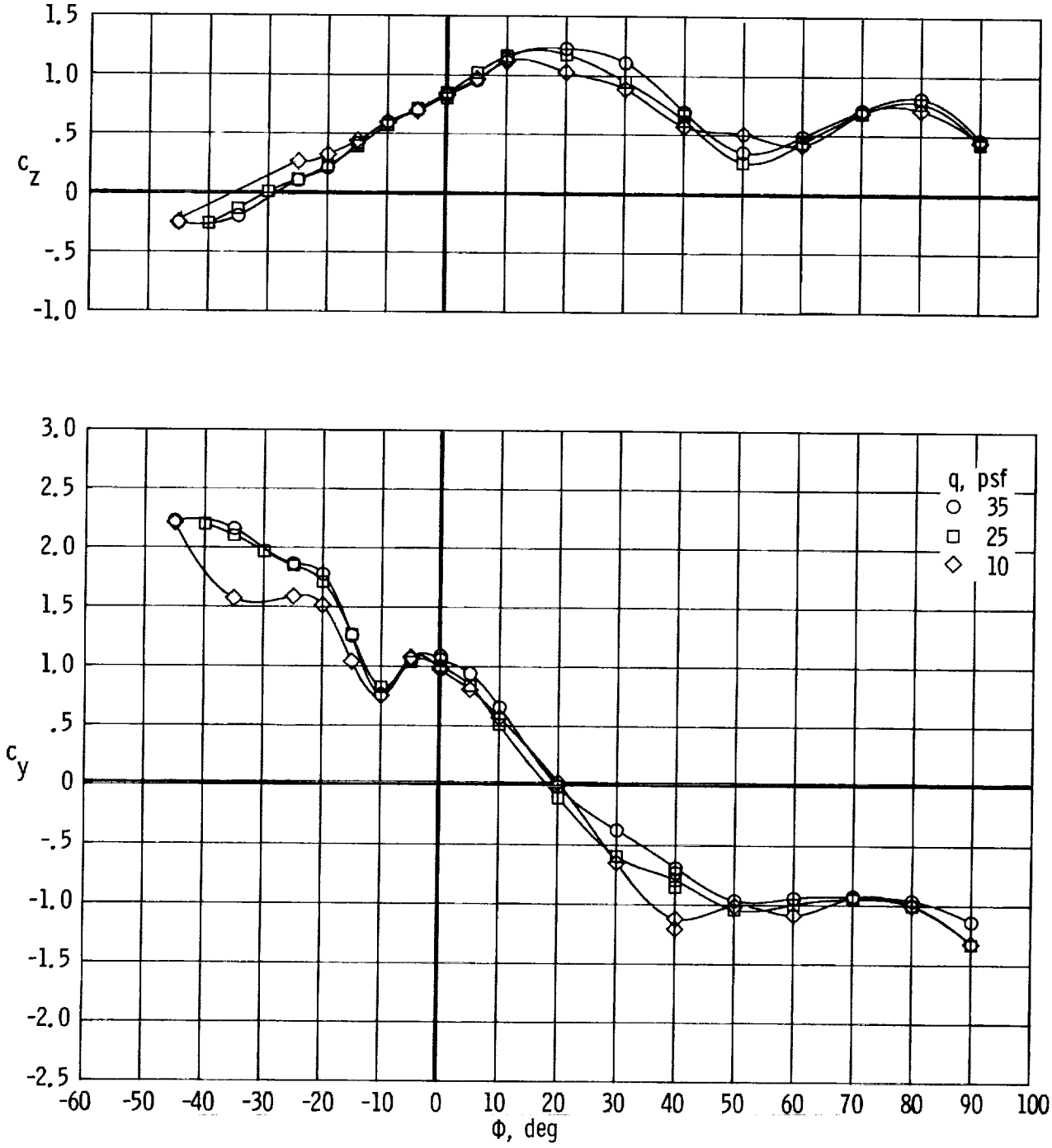

(a) c_z and c_y plotted against ϕ.

Figure 29. Effects of dynamic pressure on drag and side-force variation with flow incidence for UH-1H shape with TRSC and spoiler S_{12}.

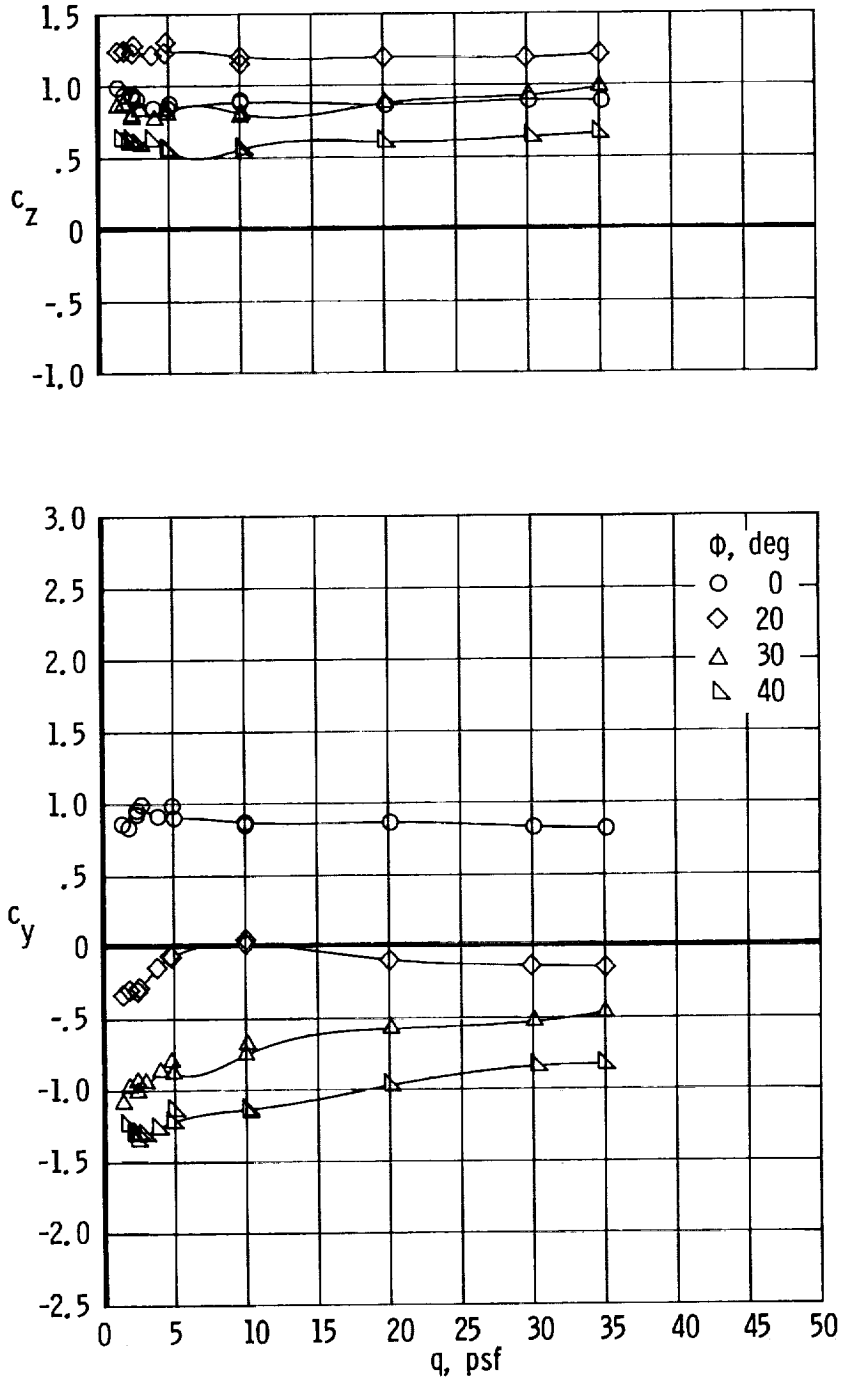

(b) c_z and c_y plotted against q.

Figure 29. Concluded.

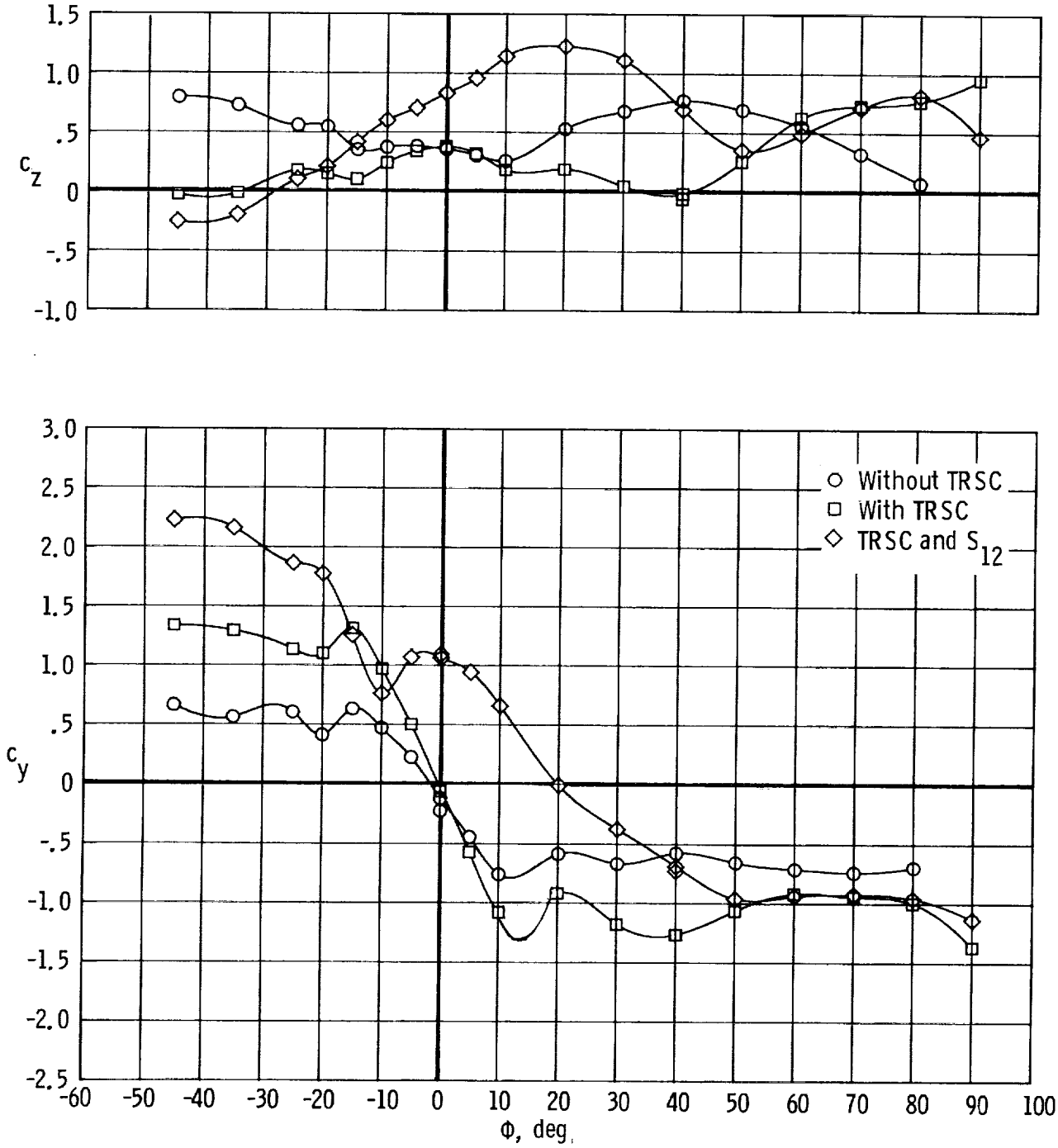

(a) $q = 35$ psf.

Figure 30. Comparison of drag and side-force variation with flow incidence for UH-1H shape with and without TRSC and with spoiler S_{12} at $q = 35$, 25, and 10 psf.

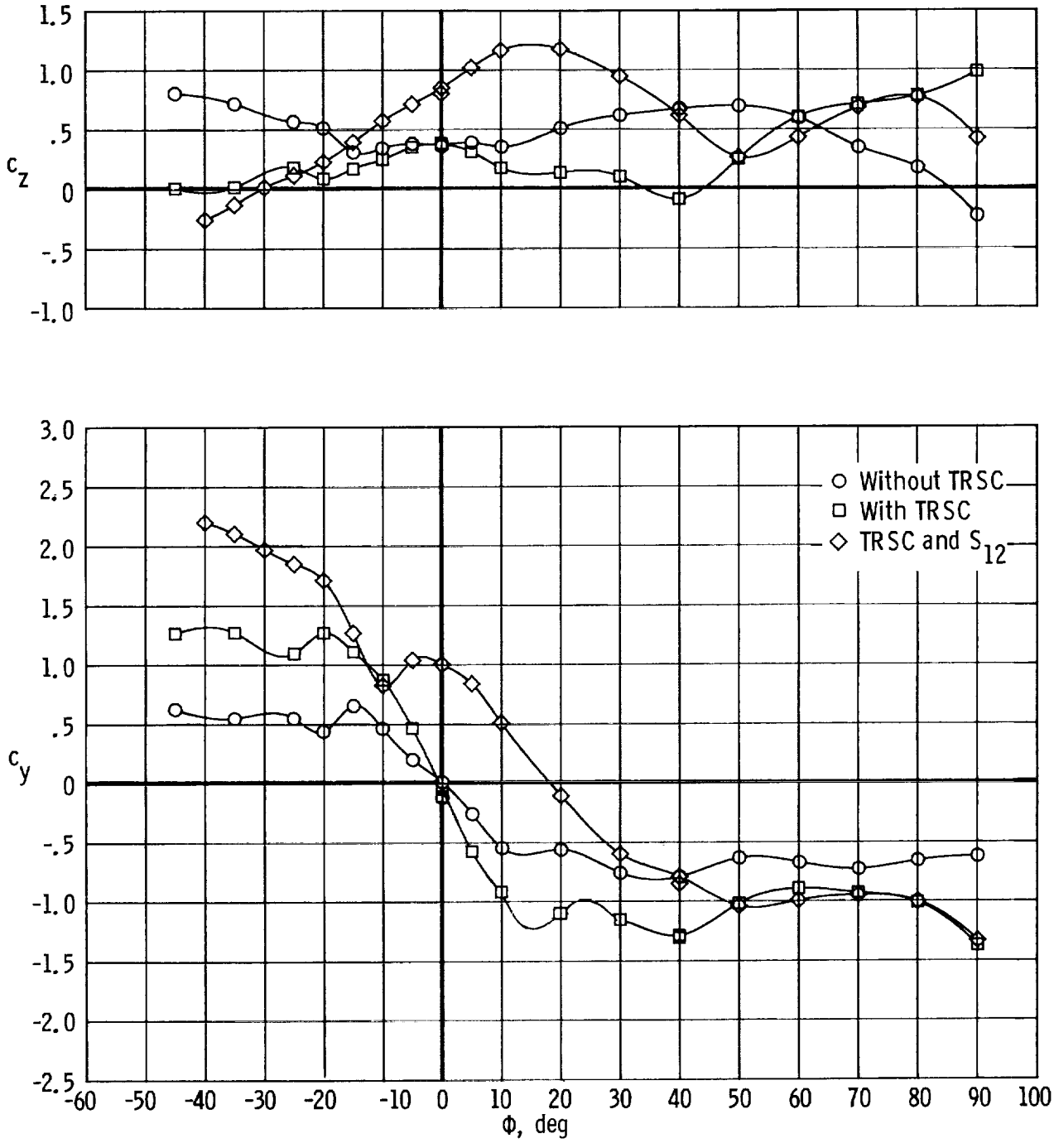

(b) $q = 25$ psf.

Figure 30. Continued.

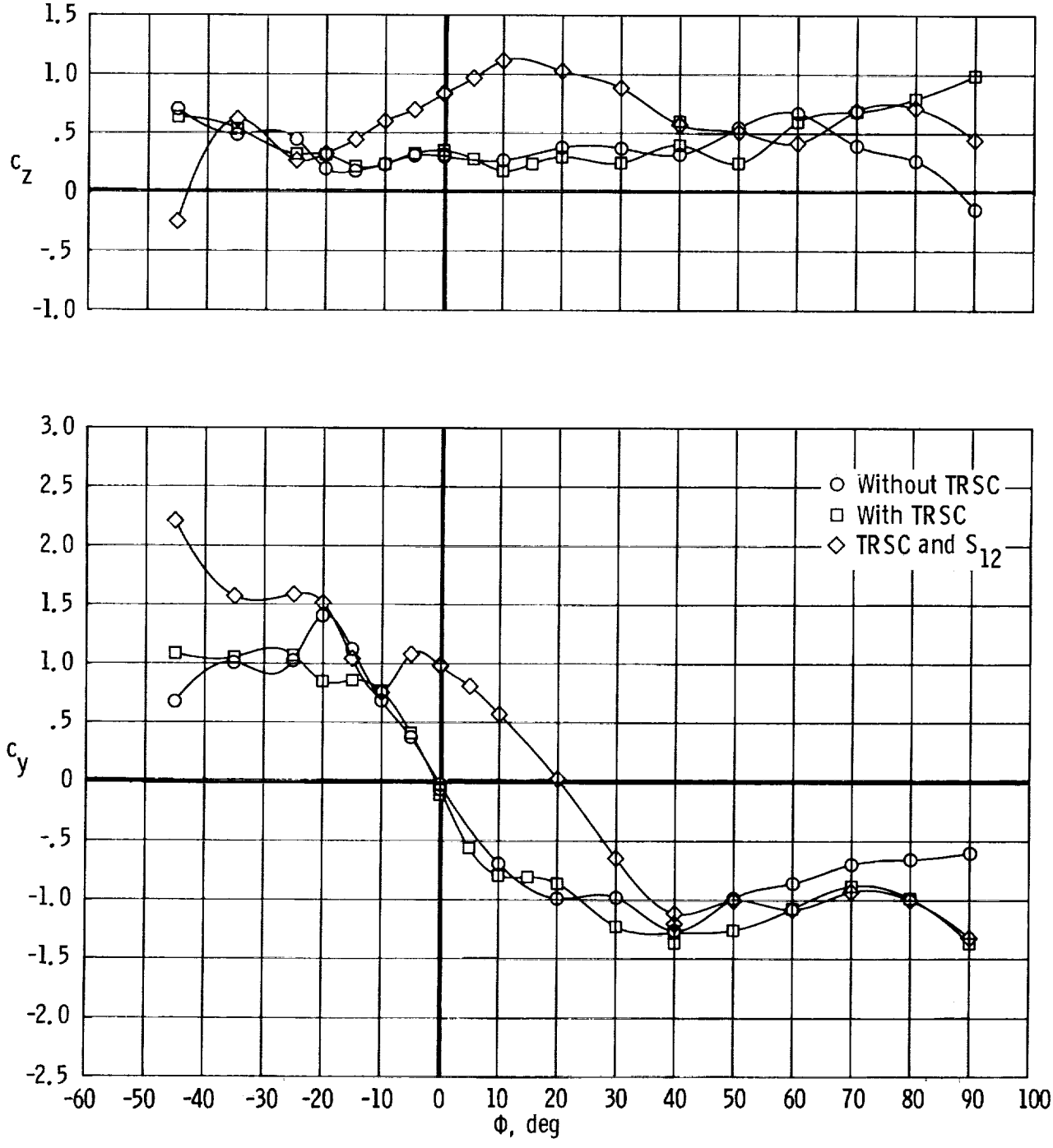

(c) $q = 10$ psf.

Figure 30. Concluded.

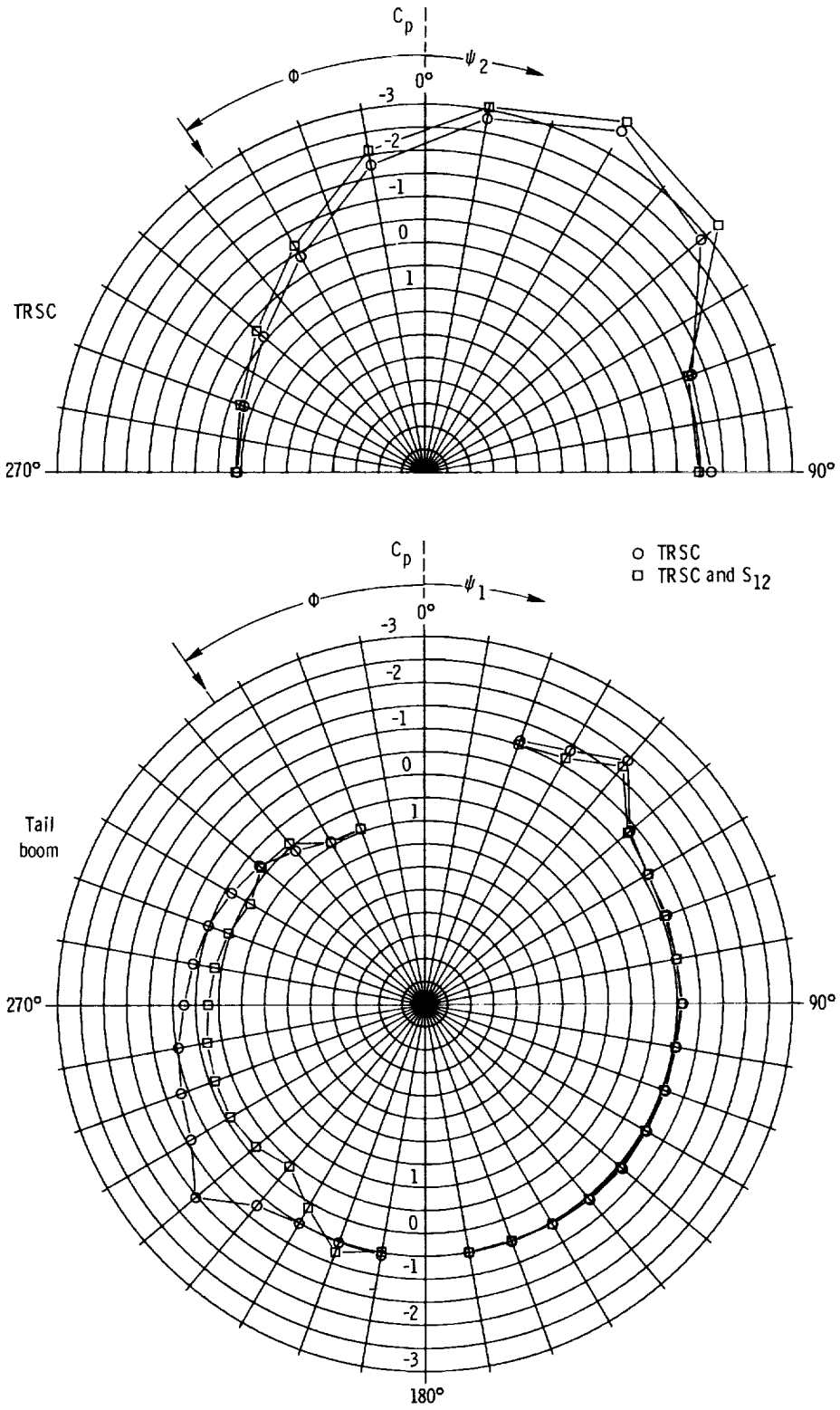

(a) $\phi = -35°$.

Figure 31. Effects of flow incidence on pressure distributions for UH-1H shape with TRSC and S_{12} spoiler at $q = 25$ psf.

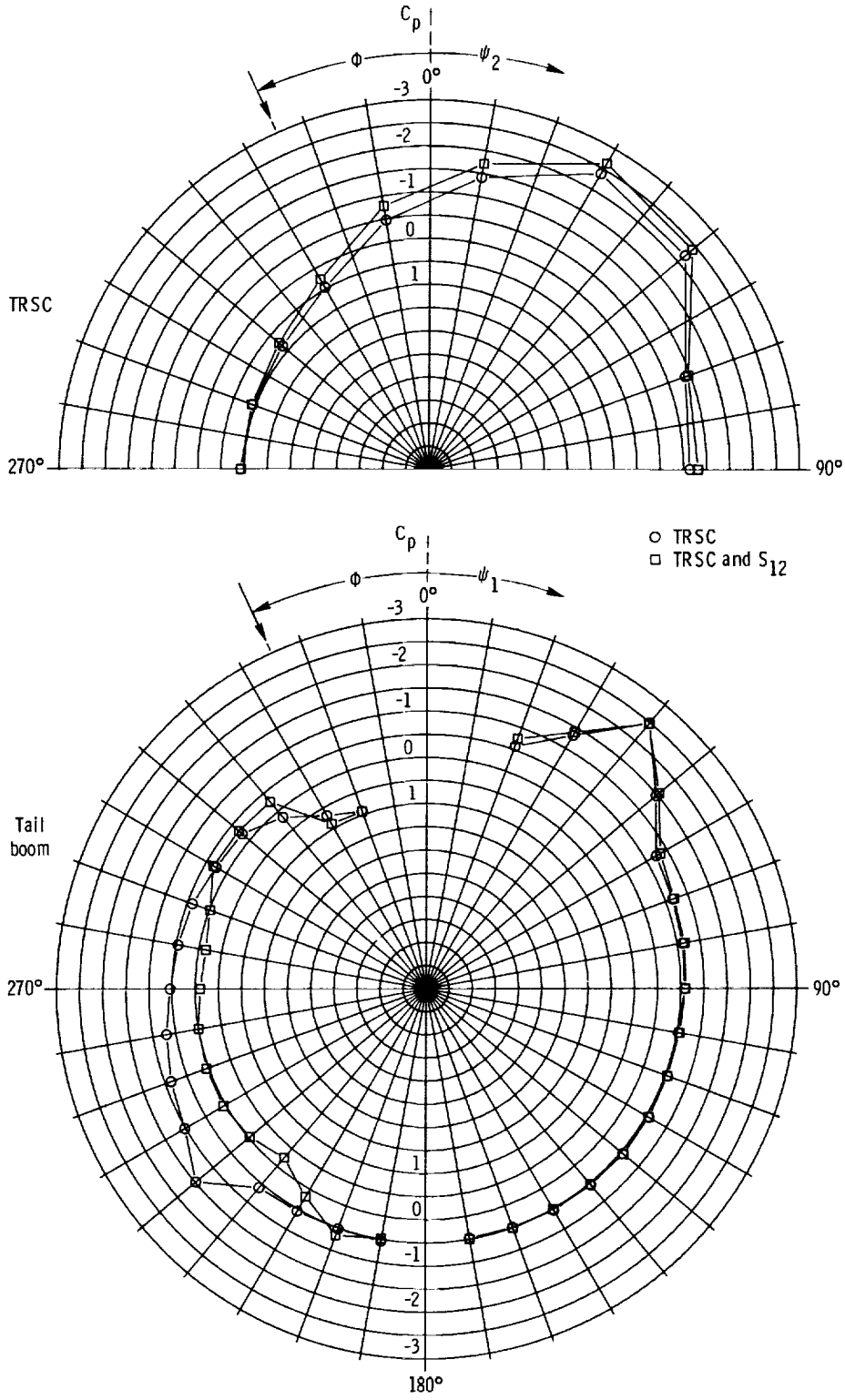

(b) $\phi = -25°$.

Figure 31. Continued.

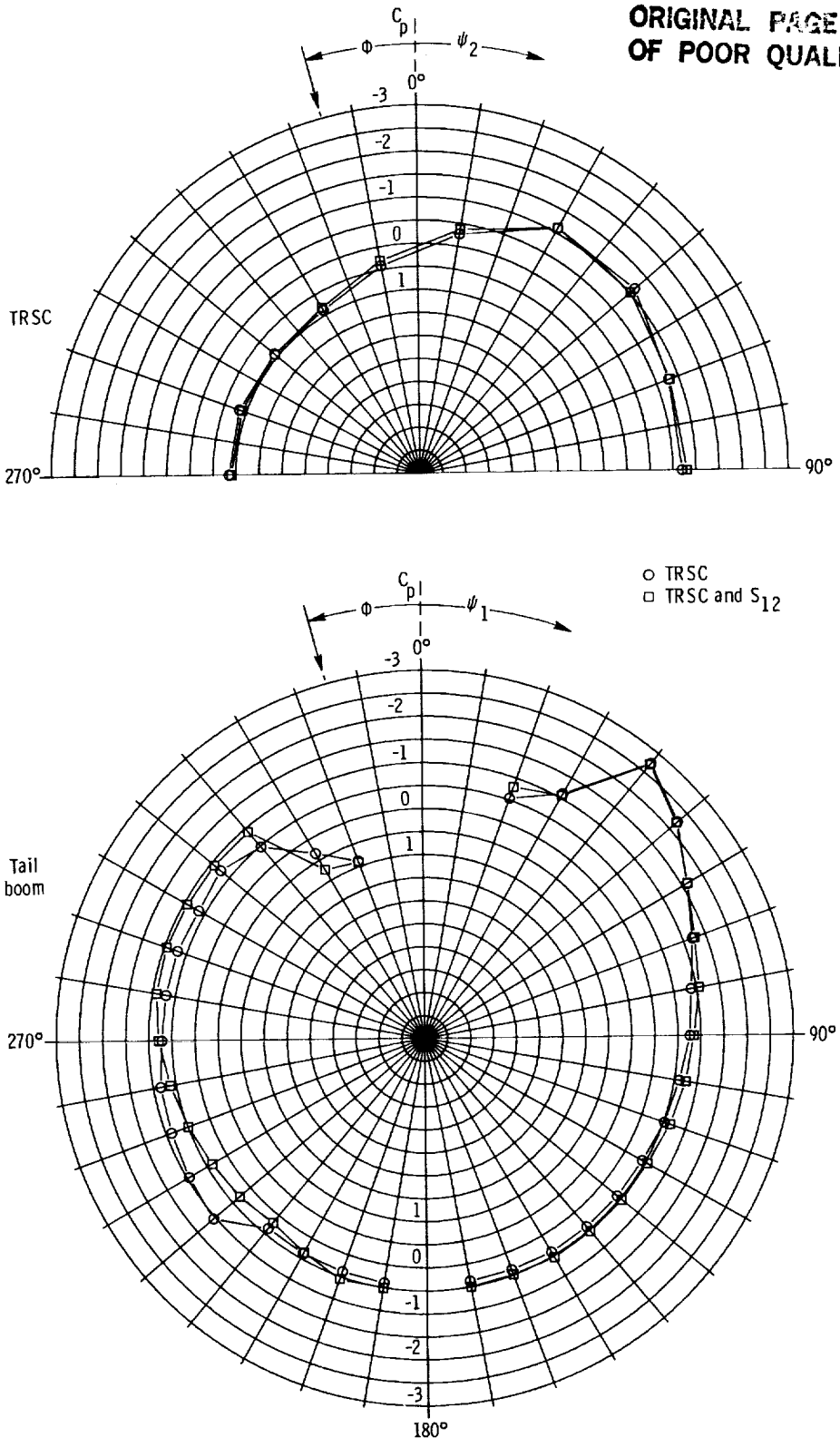

(c) $\phi = -15°$.

Figure 31. Continued.

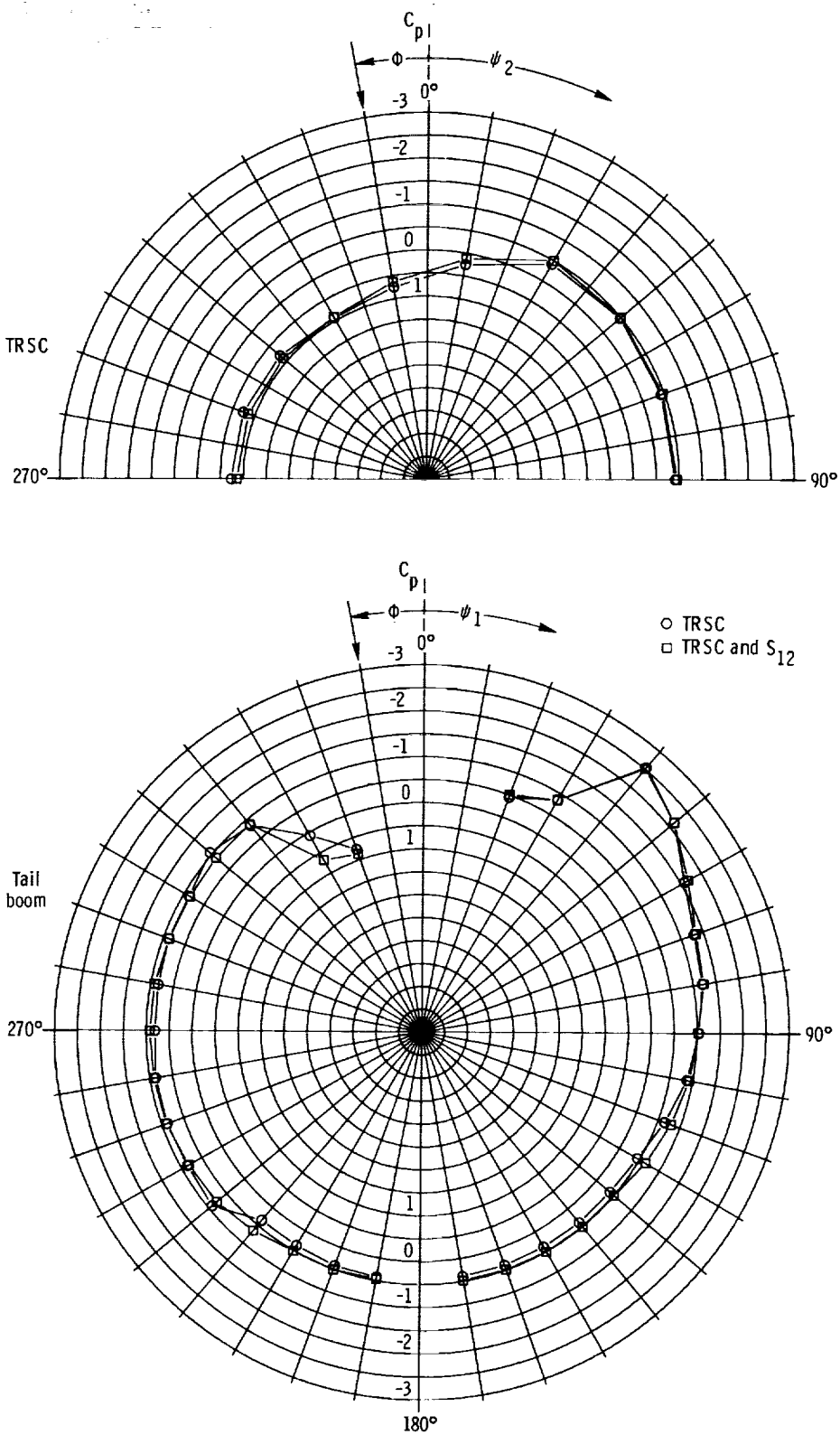

(d) $\phi = -10°$.

Figure 31. Continued.

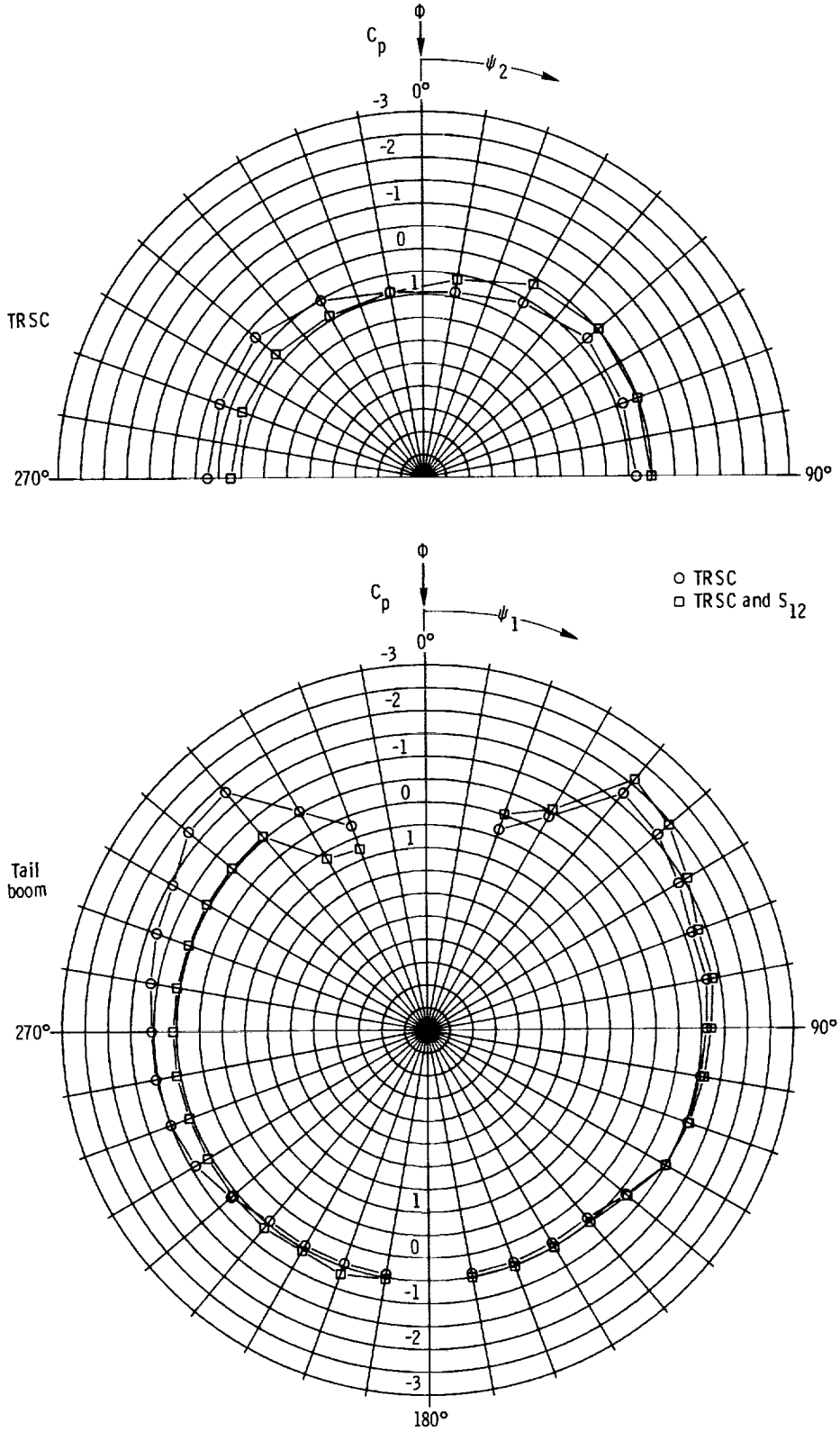

(e) $\phi = 0°$.

Figure 31. Continued.

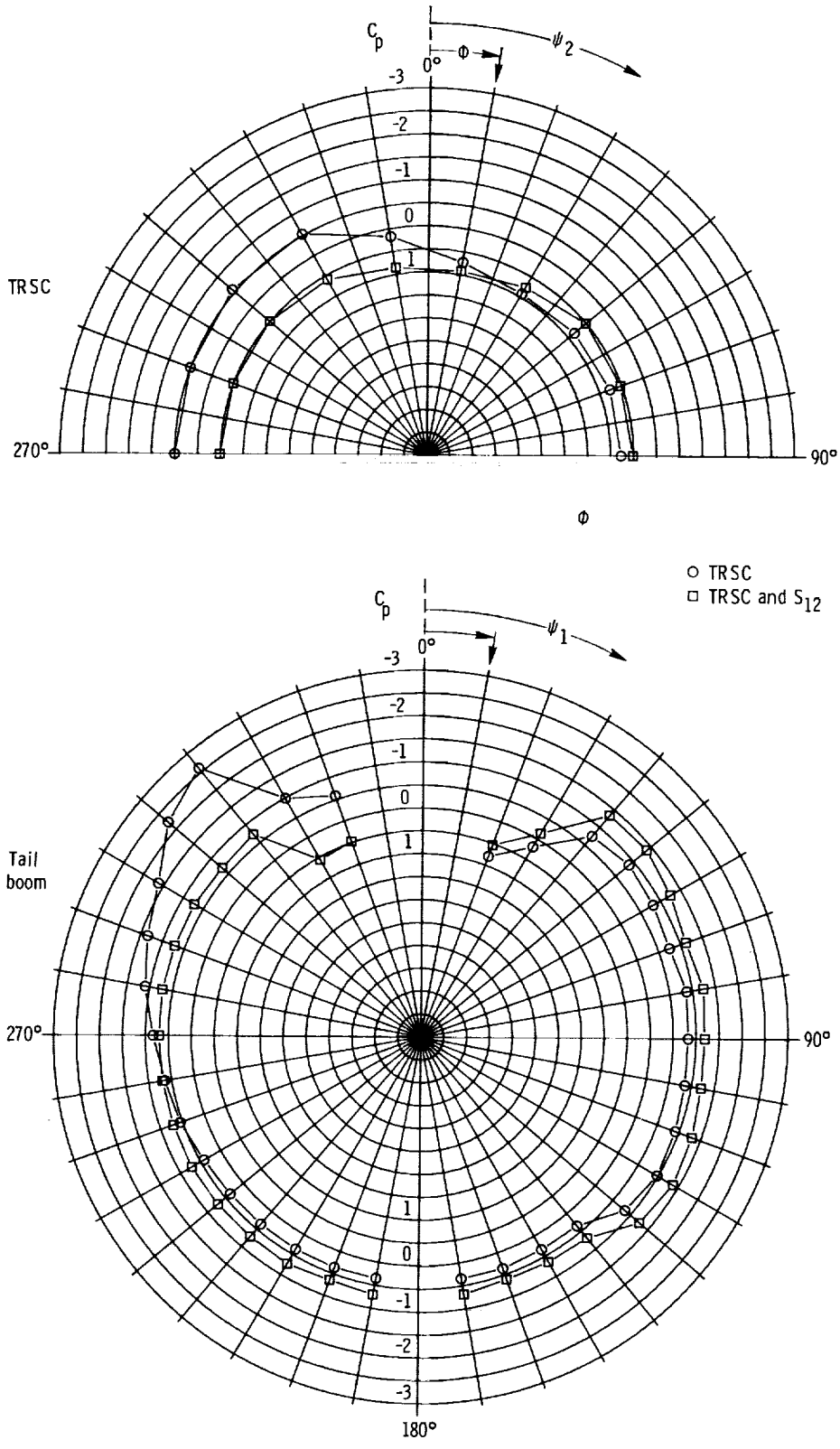

(f) $\phi = 10°$.

Figure 31. Continued.

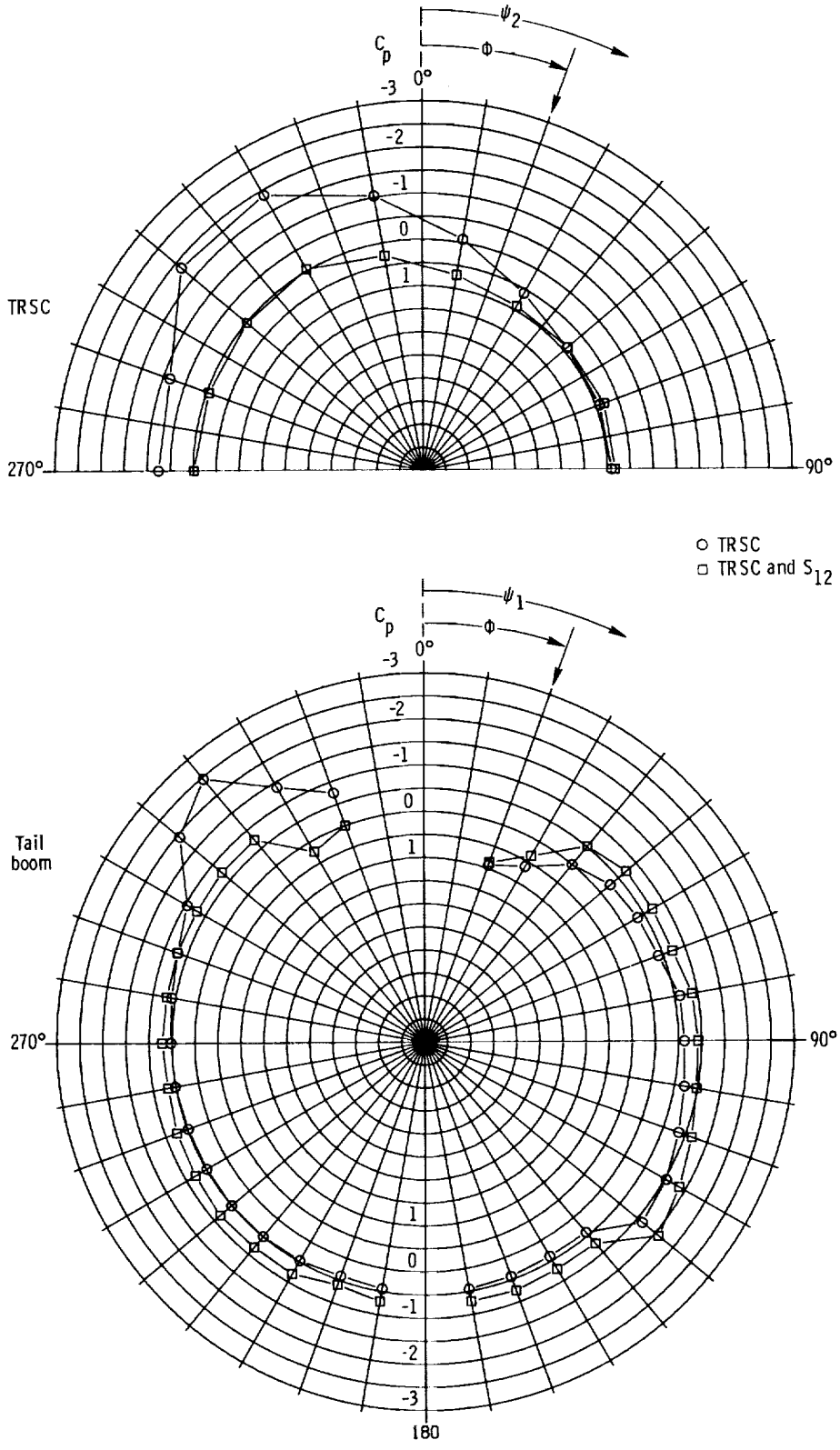

(g) $\phi = 20°$.

Figure 31. Continued.

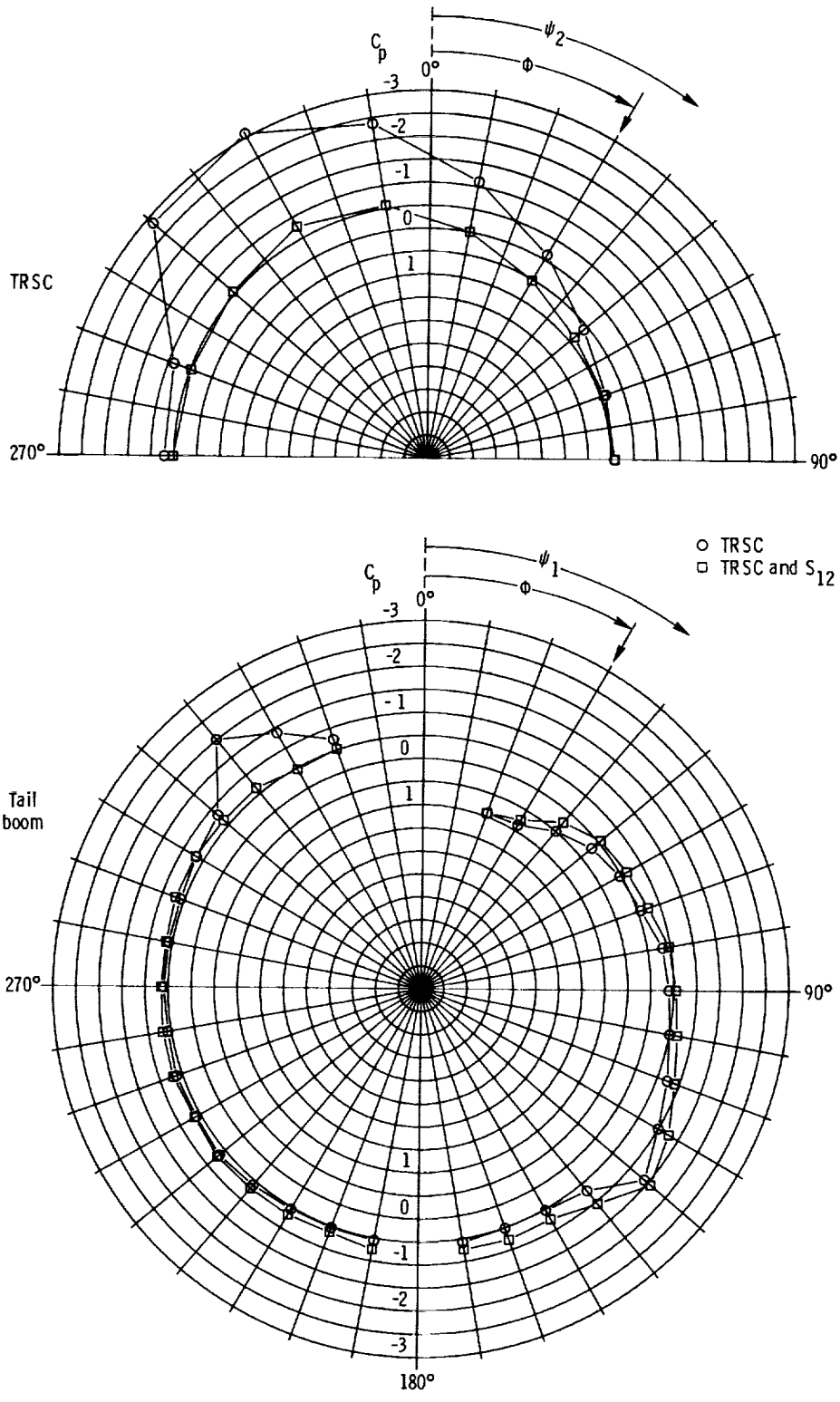

(h) $\phi = 30°$.

Figure 31. Continued.

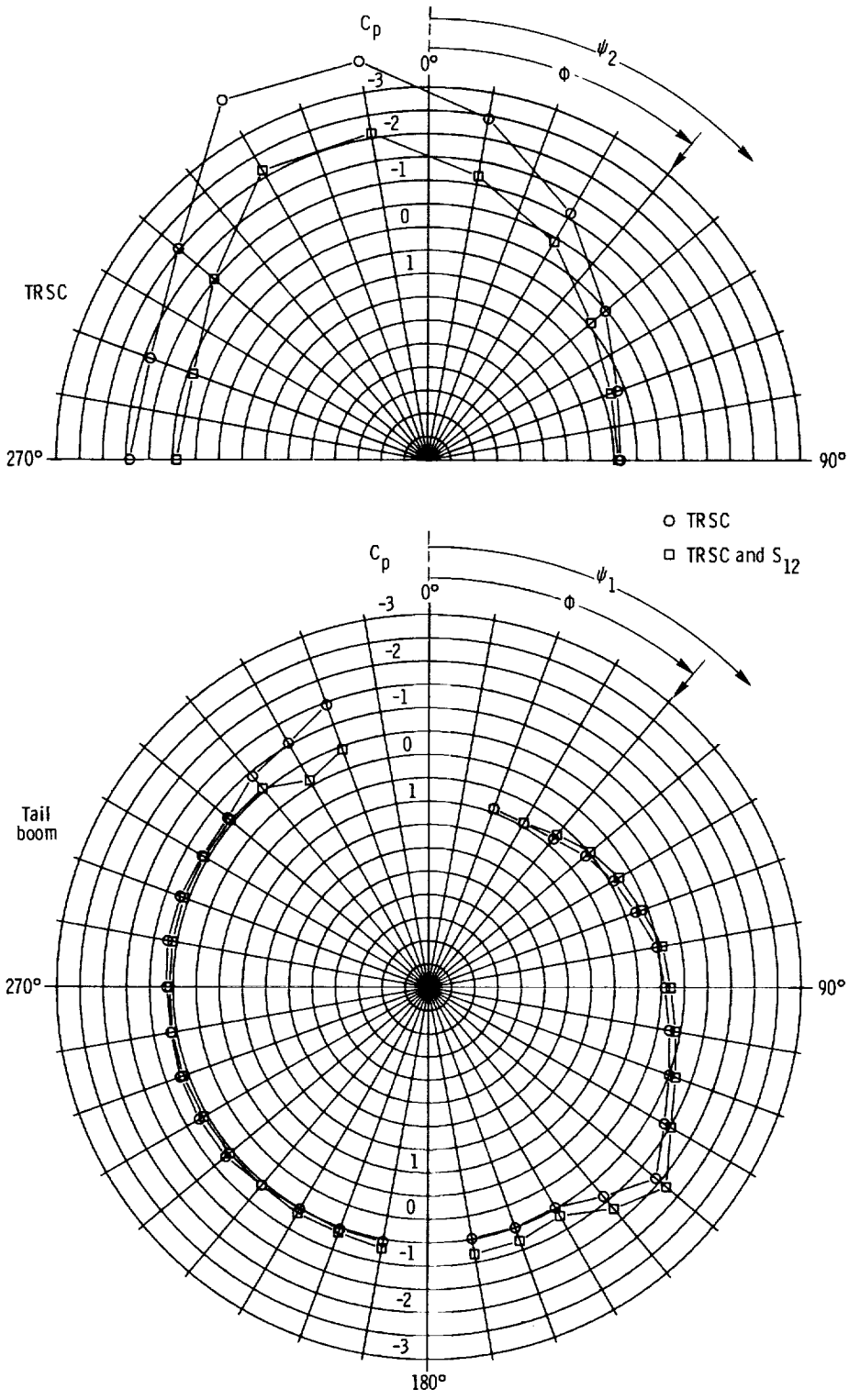

(i) $\phi = 40°$.

Figure 31. Continued.

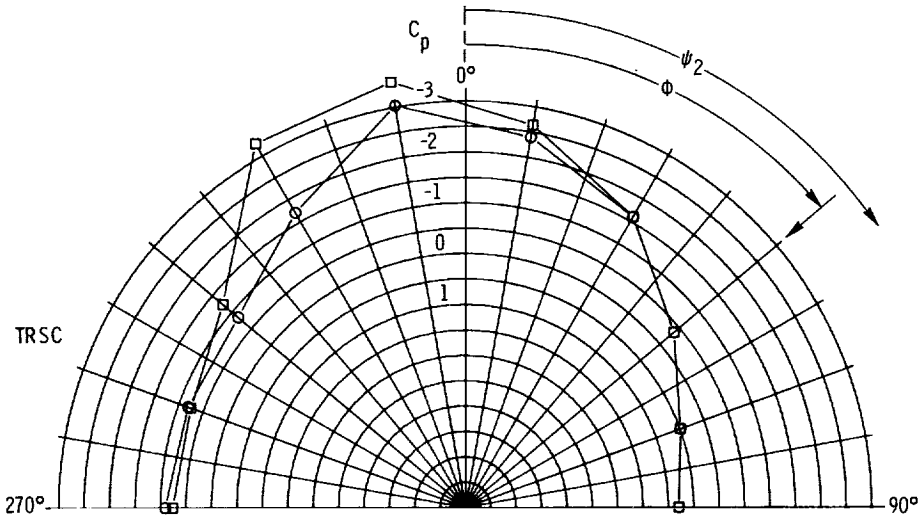

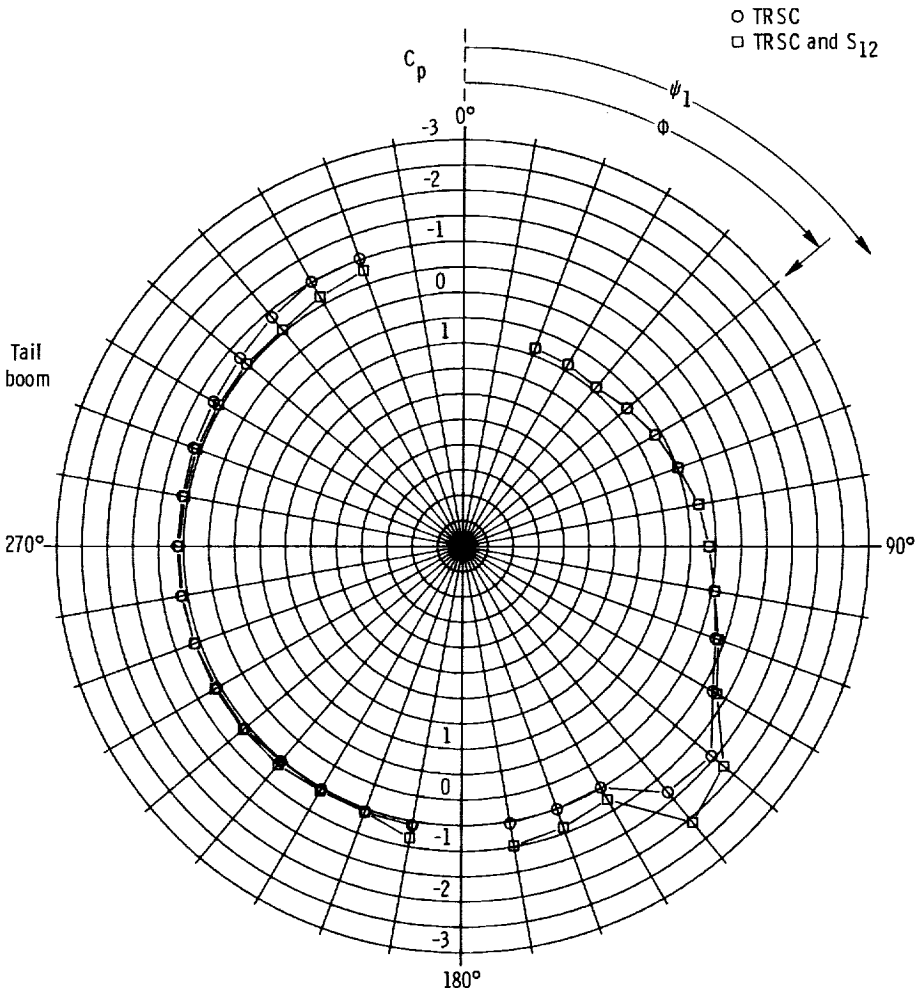

(j) $\phi = 50°$.

Figure 31. Continued.

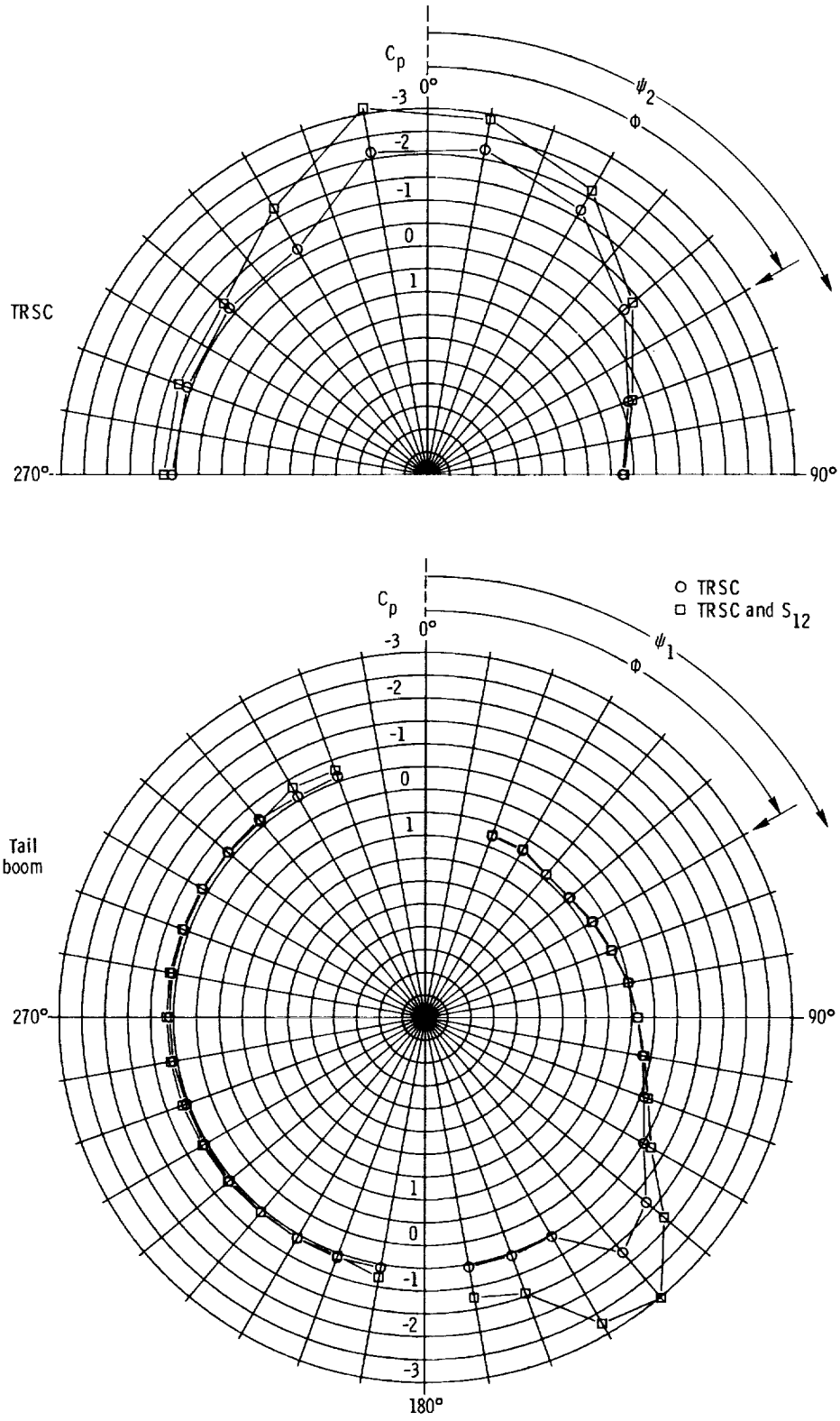

(k) $\phi = 60°$.

Figure 31. Concluded.

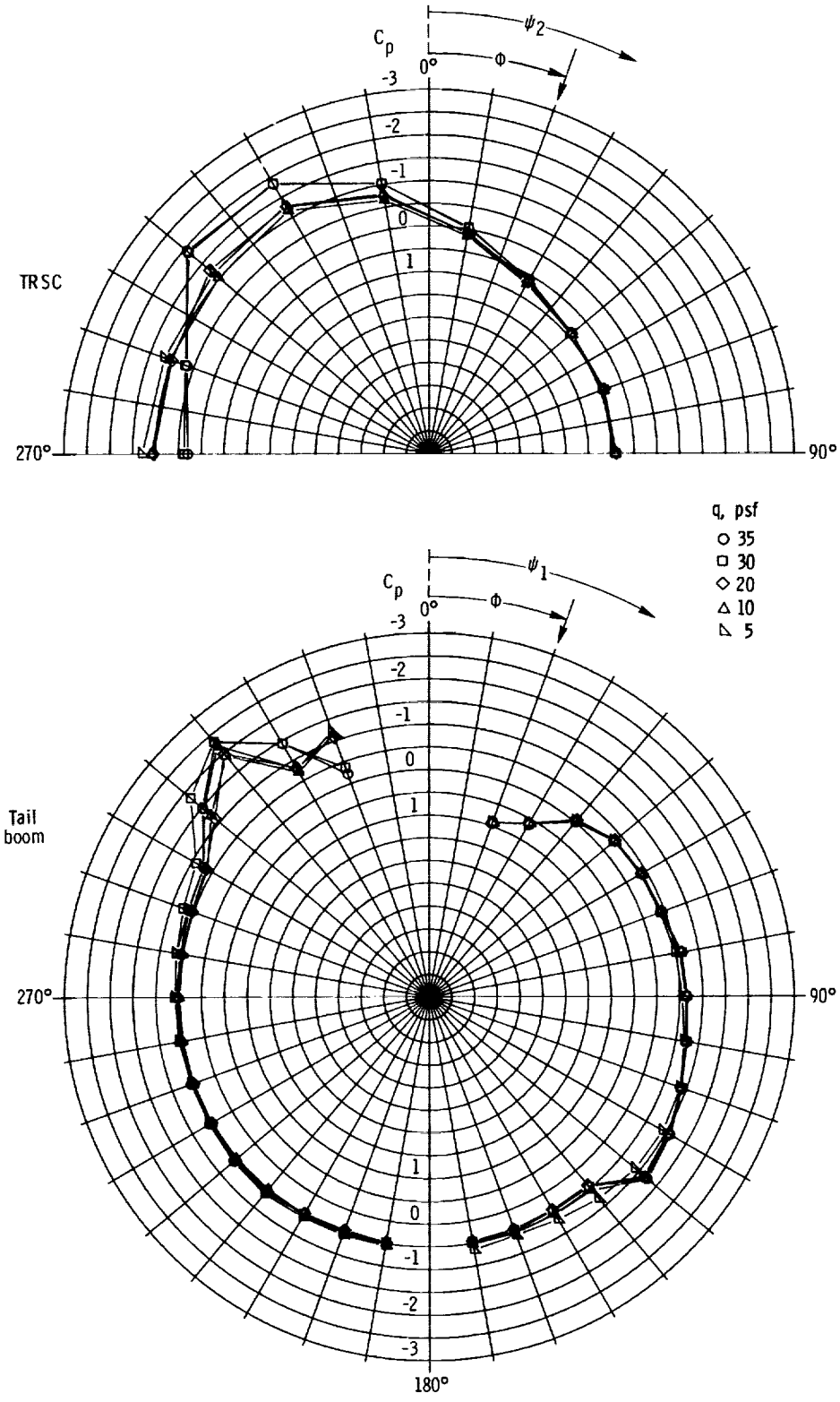

Figure 32. Effects of dynamic pressure on pressure distributions on UH-1H shape with TRSC at $\phi = 20°$.

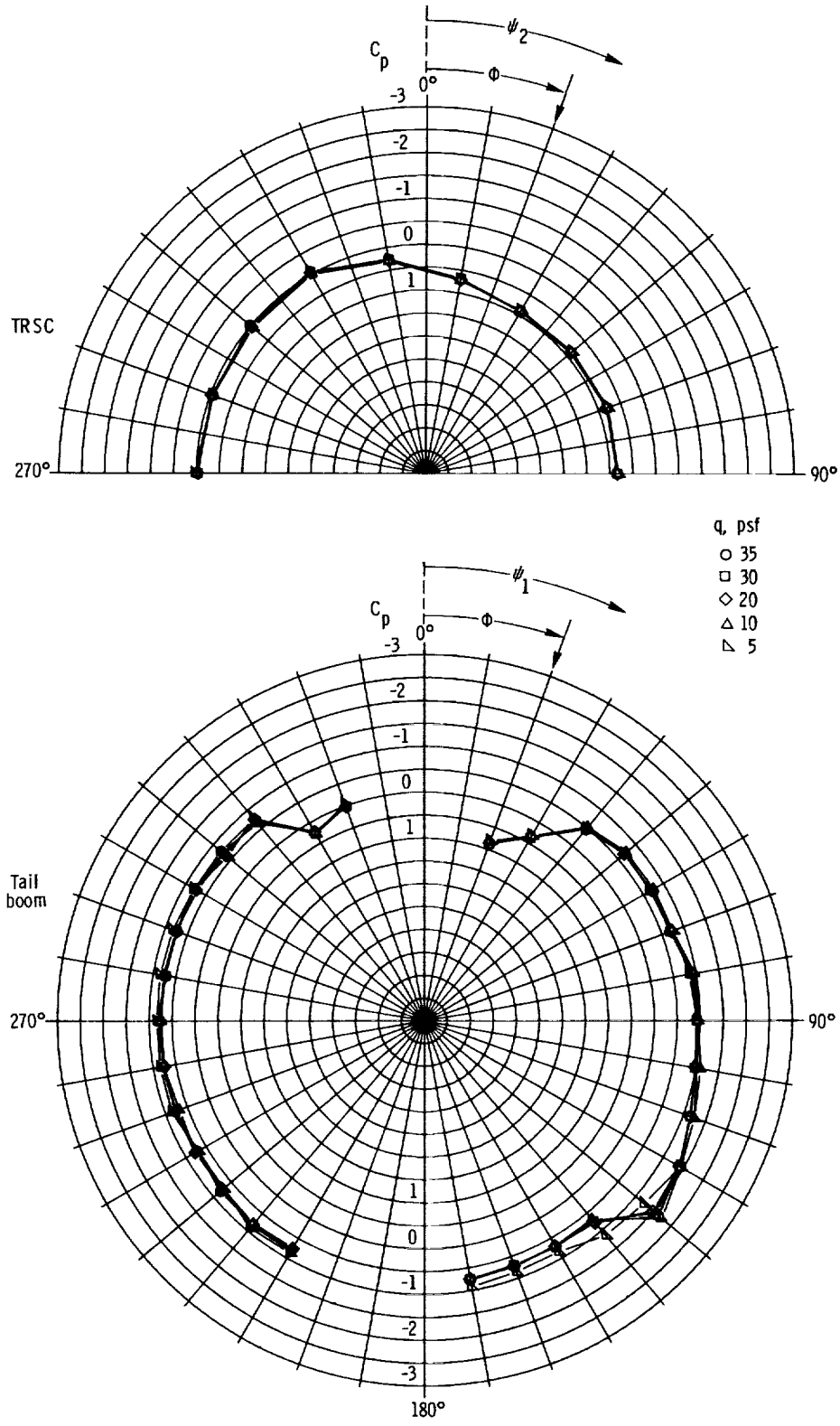

Figure 33. Effects of dynamic pressure on pressure distributions on UH-1H shape with TRSC and spoiler S_{12} at $\phi = 20°$.

1. Report No.	2. Government Accession No.	3. Recipient's Catalog No.
NASA TP-2506 AVSCOM TR 85-B-3		

4. Title and Subtitle	5. Report Date
Aerodynamic Characteristics of Several Current Helicopter Tail Boom Cross Sections Including the Effect of Spoilers	January 1986
	6. Performing Organization Code: 505-42-23-09
7. Author(s): John C. Wilson and Henry L. Kelley	8. Performing Organization Report No.: L-15978
9. Performing Organization Name and Address: Aerostructures Directorate, USAARTA-AVSCOM, Langley Research Center, Hampton, VA 23665-5225	10. Work Unit No.
	11. Contract or Grant No.
12. Sponsoring Agency Name and Address: National Aeronautics and Space Administration, Washington, DC 20546-0001 and U.S. Army Aviation Systems Command, St. Louis, MO 63120-1798	13. Type of Report and Period Covered: Technical Paper
	14. Army Project No.: 1L161102AH45

15. Supplementary Notes

John C. Wilson and Henry L. Kelley: Aerostructures Directorate, USAARTA-AVSCOM.

16. Abstract

Aerodynamic characteristics were determined of three cylindrical shapes representative of tail boom cross sections of the U.S. Army AH-64, UH-60, and UH-1H helicopters. Forces and pressures were measured in a wind-tunnel investigation at the Langley Research Center. Data were obtained for a flow incidence range from $-45°$ to $90°$ and a dynamic pressure range from 1.5 to 50 psf. These ranges provided data representative of full-scale Reynolds numbers and the full range of flow incidence to which these helicopter tail boom shapes would be subjected at low flight speeds. The effects of protuberances such as tail rotor drive-shaft covers and spoilers were evaluated. The data indicate that significant side loads on tail booms of helicopters can be generated and that the addition of spoilers can beneficially alter the side loads. Although an increase in vertical drag occurs, the net effect through reduction of tail rotor thrust required can be an improvement in helicopter performance.

17. Key Words (Suggested by Authors(s))	18. Distribution Statement
Rotorcraft Aerodynamics Stability and control Helicopters Tail booms	Unclassified—Unlimited Subject Category 02

19. Security Classif.(of this report)	20. Security Classif.(of this page)	21. No. of Pages	22. Price
Unclassified	Unclassified	72	A04

For sale by the National Technical Information Service, Springfield, Virginia 22161

NASA-Langley, 1986